Brigham Young University
BYU ScholarsArchive

All Theses and Dissertations

2009-07-13

Visualizing and Modeling Mining-Induced Surface Subsidence

Marcor Gibbons Platt
Brigham Young University - Provo

Follow this and additional works at: https://scholarsarchive.byu.edu/etd

 Part of the Civil and Environmental Engineering Commons

BYU ScholarsArchive Citation

Platt, Marcor Gibbons, "Visualizing and Modeling Mining-Induced Surface Subsidence" (2009). *All Theses and Dissertations*. 2223.
https://scholarsarchive.byu.edu/etd/2223

This Thesis is brought to you for free and open access by BYU ScholarsArchive. It has been accepted for inclusion in All Theses and Dissertations by an authorized administrator of BYU ScholarsArchive. For more information, please contact scholarsarchive@byu.edu, ellen_amatangelo@byu.edu.

VISUALIZING AND MODELING MINING-INDUCED SURFACE SUBSIDENCE

by

Marcor G. Platt

A thesis submitted to the faculty of

Brigham Young University

in partial fulfillment of the requirements for the degree of

Master of Science

Department of Civil and Environmental Engineering

Brigham Young University

August 2009

BRIGHAM YOUNG UNIVERSITY

GRADUATE COMMITTEE APPROVAL

of a thesis submitted by

Marcor G. Platt

This thesis has been read by each member of the following graduate committee and by majority vote has been found to be satisfactory.

Date	Paul W. Richards, Chair
Date	Steven E. Benzley
Date	Kyle M. Rollins

BRIGHAM YOUNG UNIVERSITY

As chair of the candidate's graduate committee, I have read the thesis of Marcor G. Platt in its final form and have found that (1) its format, citations, and bibliographical style are consistent and acceptable and fulfill university and department style requirements; (2) its illustrative materials including figures, tables, and charts are in place; and (3) the final manuscript is satisfactory to the graduate committee and is ready for submission to the university library.

Date

Paul W. Richards
Chair, Graduate Committee

Accepted for the Department

E. James Nelson
Graduate Coordinator

Accepted for the College

Alan R. Parkinson
Dean, Ira A. Fulton College of Engineering and Technology

ABSTRACT

VISUALIZING AND MODELING MINING-INDUCED

SURFACE SUBSIDENCE

Marcor G. Platt

Department of Civil and Environmental Engineering

Master of Science

Ground subsidence due to underground coal mining is a complex, narrowly-understood phenomenon. Due to the complicated physical processes involved and the lack of a complete knowledge of the characteristics of overlying strata, the reliability of current prediction techniques varies widely. Furthermore, the accuracy of any given prediction technique is largely dependent upon the accuracy of field measurements and surveys which provide input data for the technique.

A valuable resource available for predicting and modeling subsidence is aerial survey technology. This technology produces yearly datasets with a high density of survey points. The following study introduces a method wherein these survey points are converted into elevation plots and subsidence plots using GIS.

This study also presents a method, titled the Type-Xi Integration method (TXI method), which improves upon a previous subsidence prediction technique. This method

differs from the previous technique in that it incorporates accurate surface topography and considers irregular mine geometry, as well as seam thickness and overburden variations in its predictions. The TXI method also involves comparing predicted subsidence directly to measured subsidence from subsidence plots. In summary, this study illustrates a method of combining data from aerial survey points and mine geometry with subsidence models in order to improve the accuracy of the models.

ACKNOWLEDGMENTS

I would like to acknowledge the many individuals who have had important roles in this work. First of all, I thank Dr. Paul W. Richards and Dr. Steven E. Benzley for selecting me to perform this research, as well as Dr. Kyle M. Rollins for his assistance. I also thank Dr. Richards for mentoring and advising me throughout it. Additionally, I thank the US Bureau of Land Management for helping to sponsor this project; I thank the Utah Division of Oil, Gas, and Mining for providing the mine survey data used in my research; and I thank the Energy West Mining Company for providing me with additional Deer Creek Mine data. All conclusions and recommendations presented herein are solely those of the author, and not necessarily of the aforementioned organizations.

Finally, I thank my family—my wife, parents, and other members—for their support and encouragement, which were essential to the production of this thesis.

.

TABLE OF CONTENTS

LIST OF TABLES

LIST OF FIGURES

1 Introduction

An effective and relatively recent development in the field of coal mining is a practice known as longwall mining. Longwall mining consists of a mining machine called a shear, which snakes back and forth as it cuts coal from the face of a coal seam block, which can be as wide as 1000 ft, and several miles long. As the shear cuts coal from and moves along the face of the block, hydraulic supports holding up the coal seam roof move forward. The coal and rock from the seam roof then fall into the void space behind the supports. This process is illustrated in Figure 1-1 (image courtesy of [1]).

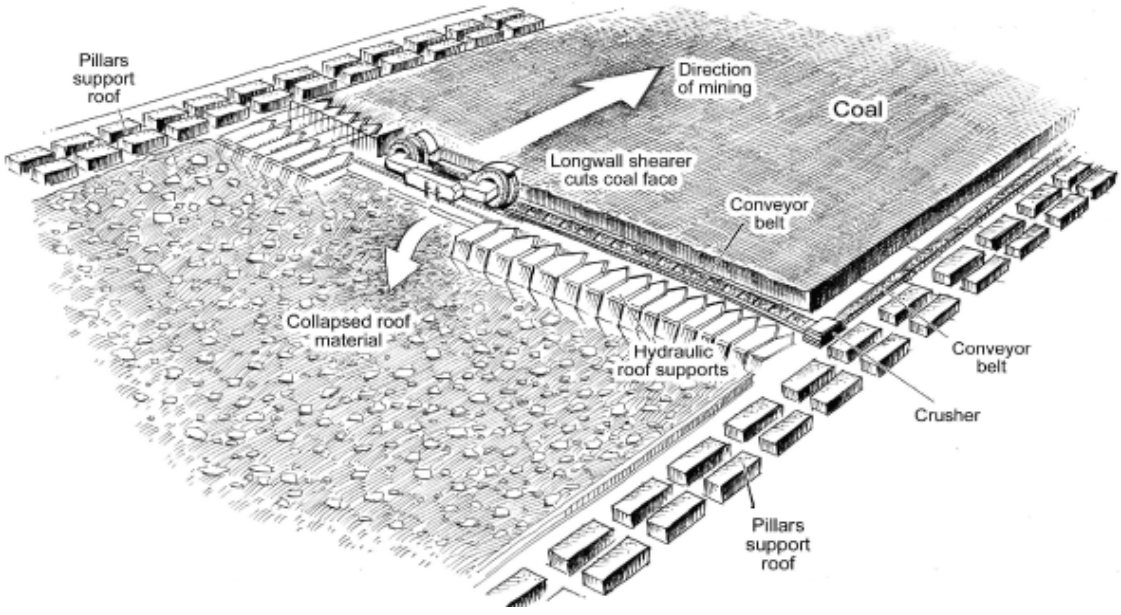

Figure 1-1 Diagram of a Typical Longwall Operation

The area behind the shearing machine consisting of collapsed roof material is known as the "caved area" or simply "cave." As the material collapses and forms the cave, the strata above the mine will be affected. An above stratum will respond by either collapsing itself or redistributing the load from the overburden to nearby strata. Often, depending on the rock strength, depth of overburden, etc., the collapse will propagate to the ground surface. Subsidence occurs when this propagation results in vertical and horizontal movement of the surface directly above and around the cave.

1.1 Subsidence Theory

The phenomenon of mining-induced subsidence has been studied for over a century, and began in the European coal fields. According to C. R. Dunrud [2] the initial perception of subsidence was that the overburden above the cave would fracture along vertical planes corresponding to cave boundaries (see Figure 1-2). Accordingly, the area of surface subsidence would closely resemble the area of the cave.

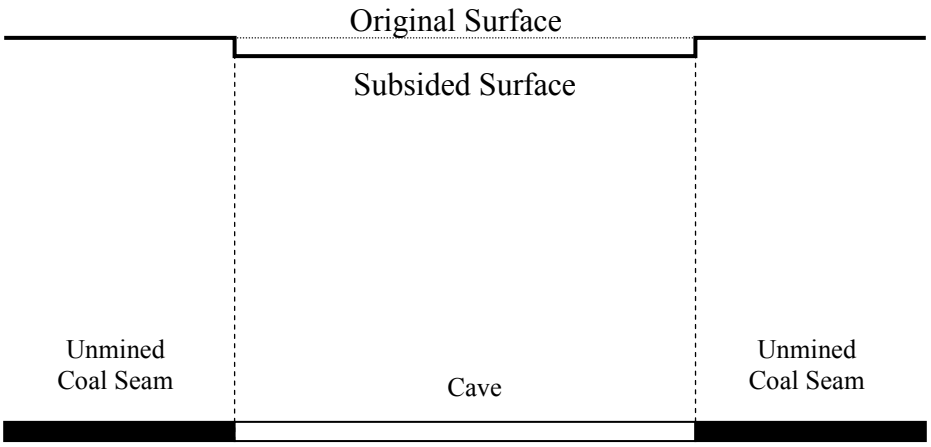

Figure 1-2 Initial Perceptions of Subsidence

Later developments in subsidence theory indicate that rock and material collapse propagates not only vertically, but horizontally as well. Thus, the area of subsidence above the mine will usually differ from the area of the cave, depending on geological conditions of the mining site. Typically, the subsidence area extends beyond the edges of the cave in all directions [3], and the area limits are defined by the limit angle γ as shown in Figure 1-3 (not to scale).

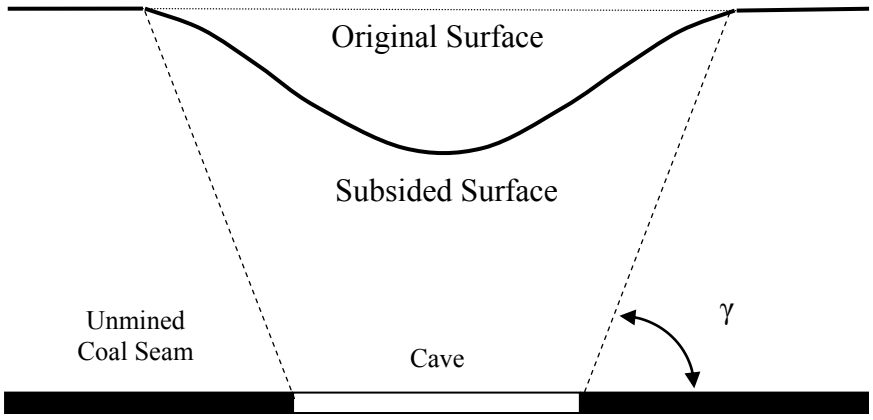

Figure 1-3 Actual Behavior of Subsidence

An additional development in subsidence theory indicates that vertical ground movement is nonuniform; the vertical subsidence reaches a maximum in the center of the cave and diminishes radially until the limit angle is reached. At the limit angle, the subsidence phenomenon may actually include a slight rise in the ground elevation. The entire subsidence profile consisting of both positive and negative elevation changes is known as the subsidence trough.

Ground subsidence due to underground mining can occasionally result in significant changes to the hydrological conditions in the surrounding areas. In addition,

manmade structures in the vicinity of the subsidence trough can experience significant damage due to differential ground movement. These adverse effects of subsidence have led to the passage of longwall mining regulations. For example, the Surface Mining Control and Reclamation Act of 1977 requires a subsidence control plan as part of the permitting process [4]. The continually increasing demands for energy coupled with such regulations have prompted a large number of studies aimed at predicting ground subsidence.

1.2 Literature Survey

Within the last 40 years, a substantial amount of literature on the subject of subsidence due to underground mining has been written. Much of this literature focuses on the various methods which are currently employed to predict and model ground subsidence. Typically, these methods yield results which are at best accurate to within 10 percent [5-6].

The prediction methods can be divided into two general categories: geometric methods and analytical methods [4]. Both methods are found extensively in the literature (see, for example, [7-10]). Geometric methods do not directly consider the geological characteristics of overlying strata, and focus on cases of measured subsidence. Brauner [3] presents such a method developed in the British Coalfields. This method uses measured maximum subsidence, coal seam thickness, angle of draw, and other parameters as input to form a subsidence profile. This subsidence profile is used to predict subsidence in areas with similar geological characteristics.

Another procedure using the geometric method is based on probability. In this approach, geologic factors are accounted for by assuming that they are randomly arranged, and thus subject to the laws of probability. For example, Goel and Page [6] use Gumbel's theory of extremes [11] to model chimney caving, which is a localized form of ground subsidence. In addition, Kim et al. [12] model subsidence using a frequency ratio and logistic regression.

The analytical approach, which mainly consists of the finite element method (FEM), requires knowledge of the in-situ rock properties, including the bedding of planes and orientation of strata. In practice, these characteristics are approximated by "idealizing the rock mass by a continuous medium…that satisfies compatibility and equilibrium considerations" [13]. Generally, FEMs do not rely as heavily on empirical data (i.e. data obtained from subsidence of similar mines), and thus can be more site-specific than geometric methods [14].

The accuracy of the various prediction methods depends heavily upon the geological assumptions, as well as the quality of subsidence measurements. Ground subsidence is measured using survey points, and thus much of the subsidence research is also focused on improving the current survey methods and accuracy. The US Bureau of Mines, for example has conducted several studies in this field [15-16], and as of this writing, the University of Utah is researching using INSAR satellite technology to monitor subsidence.

1.3 Objectives

Two main objectives comprise this study. The first objective is to visualize ground subsidence from longwall coal mining using aerial survey points. A corollary to this objective is to emphasize the importance of accurate and consistent survey data in measuring subsidence. The second objective is to demonstrate how the information provided by subsidence plots can be incorporated into a subsidence prediction model. This objective includes improving upon previous prediction models and quantifying the improvement using a statistical analysis.

2 Visualizing Subsidence

The visualization of mining-induced surface subsidence requires information about the topography and geography of the ground over a mine. In this study, such information is obtained from aerial and/or ground surveys, which are conducted annually by the mine. The following methods developed by the author to visualize subsidence rely heavily on the surveys' completeness and accuracy, which depend on at least two quality control factors: consistency and density. Generally, a more consistent annual survey (with respect to time of year, aerial photogrammetry, etc) will yield more complete comparison plots. Similarly, a greater density of survey points per unit area will result in plots of higher accuracy.

2.1 GIS Mapping

Geographic Information Systems (GIS) provide an effective means for converting raw survey data into meaningful subsidence models. ArcGIS Desktop, Version 9.3, is the main tool used in this study to this end. The models created in ArcGIS enable imaging of the subsidence process, and also provide a basis of comparison as well as input for the Type-Xi Integration method discussed in Chapter 4.

ArcGIS facilitates the visualization of the mine workings, subsidence models, terrain, and other layers in various combinations and overlays. Each layer, however, must be correctly referenced in relation to every other layer, using a common coordinate system. The aerial survey points reference a coordinate system whose coordinate values are mapped from real locations on the surface of the Earth. The system is constructed in the following manner.

The Earth's slightly elliptical shape is first approximated with a spheroid, which in this case is the Clarke 1866 spheroid. A geographic coordinate system (GCS) is then imposed on the spheroid. The GCS references a datum defining the spheroid's position relative to the center of the Earth using spherical coordinates. This datum determines the location the Equator and Prime Meridian (through Greenwich, England) from which latitudes and longitudes respectively are measured. The datum used in this study is the North American Datum, which is based on a 1927 survey. Thus, the geographic coordinate system used in this study is the GCS North American 1927.

The GCS is then converted by a mathematical transformation from a spheroid to a flat surface, called a projection. The projection used in this study is titled the Lambert Conformal Conic, which projection is widely used for middle latitudes with strong East-West orientations. The projection forms the datum for the state plane coordinate systems (SPCS) used by the mines. Unlike a GCS, a SPCS identifies points using Easting, Northing, and Elevation values, which correspond to x, y, and z values respectively in the Cartesian coordinate system. The mines studied in this report lie in the Utah Central zone. Thus, the points for each mine are referenced using the Central Utah 1927 SPCS.

2.2 GIS Modeling

The main purpose of this method is to produce plots which show ground subsidence from one year to the next. There are three main components in the creation of subsidence plots with ArcGIS:

1. Data format (raster or vector)
2. Interpolation scheme
3. Map algebra method

The parameters associated with each component are selected according to their appropriateness for a given model, as described in the following sections.

2.2.1 Data Format

The first component of the plotting process involves converting the data points into either a raster or vector format. Each of these formats uses a unique philosophy to form and represent a surface and features in ArcGIS. A vector dataset consists of points, lines, and polygons. A raster dataset is an array of equally spaced cells (commonly called pixels). Data is analyzed in both formats in this method.

2.2.1.1 Vector Format

The feature is the basic unit of a vector dataset. Points, lines, and polygons are examples of features, each of which are referenced in a Cartesian coordinate system. Features that share the same type (e.g. point type) and attributes form a feature class. Features classes that are located within a common geographic extent form a vector data model. Thus, each vector data model may be made up of single or multiple feature types.

The survey data provided by the mines is transformed into point feature classes in ArcGIS. The mines typically furnish the yearly Easting, Northing, and Elevation values of survey points in a table, which is copied into Microsoft Excel. The data is then imported from Excell into ArcGIS, where it is converted to a point feature class. This feature class may then be further developed into a vector surface.

A vector surface is represented by a Triangulated Irregular Network (TIN). A TIN is set of non-overlapping, bordering triangles. It is derived from a point dataset according to two criteria. First, the data points make up the triangle nodes. Second, the triangles are constructed in such a way that a circle circumscribed about any triangle will contain the nodes of only that triangle in its interior (see Figure 2-1). Such triangles are known as Delaunay triangles; thus, a TIN is a collection of Delaunay triangles.

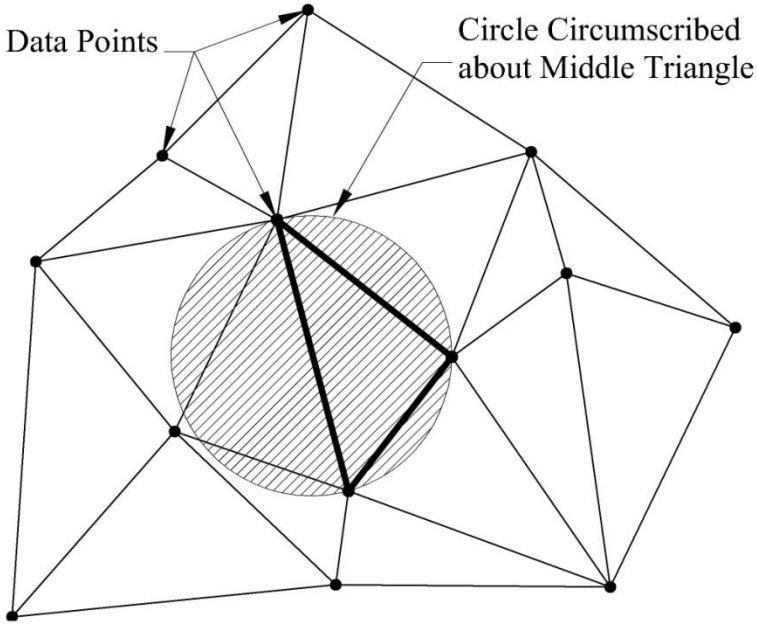

Figure 2-1 Layout of Delaunay Triangles

2.2.1.2 Raster Format

A raster dataset stores the location and characteristics of each cell in an array. The array is oriented in a Cartesian coordinate system such that the cell edges are parallel to the x and y axes. Each cell's location may be identified with respect to either the raster's array or the coordinate system in which it is placed. When a raster is isolated, it is convenient to reference each cell according to its place in the array, such that the reference consists of the cell's row number and the column number. However, because multiple rasters are often analyzed together in a geographic dataset, each cell is referenced in this case using x and y coordinates, similar to vector data.

The characteristics of a raster dataset consist of the size of the cells, as well as the attribute value associated with each cell. All cells are equally sized in an array, so a raster dataset will have a single cell size value. Attribute values, however, may vary from cell to cell in a given raster dataset. Each cell is assigned a single attribute value, which is represented by a real number. Thus, cells with the same value share the same attribute, and are considered equal. In geographic data, a cell's attribute often represents a physical phenomenon, such as elevation or slope. Assigning a cell's attribute according to these criteria leads to spatial autocorrelation, or the tendency of equal attribute cells to be grouped together in zones. The interpolation schemes in ArcGIS take advantage of the fact that cells with the same or similar attribute values are often in the vicinity of one another.

2.2.2 Interpolation

Several raster interpolation schemes are available in ArcGIS, including Inverse Distance Weighted (IDW), Kriging, Spline, and Natural Neighbor. Though all four schemes were investigated, the IDW and Natural Neighbor proved to be most conducive to this study. Thus, only these two schemes will be described. The IDW and Natural Neighbor methods are called deterministic methods, and both follow the same general concept for computing the raster cell values. Values are computed on a cell-by-cell basis using a weighted average of surrounding data point values. The methods differ in how the weighting terms are computed, and how spatial autocorrelation is applied. The general formula for these methods is given in Equation 2-1.

$$z = \sum_{i=1}^{n} \lambda_i z_i \quad \textbf{(2-1)}$$

z = calculated value for a given raster cell

z_i = given value of i^{th} data point

λ_i = weighted term for i^{th} data point

n = number of data points used in calculation

2.2.2.1 Inverse Distance Weighted

In the IDW method, the weighted average of the each point in the vicinity of the cell is based on the inverse of the distance of that point from the cell, raised to a power *p*. Thus, data points closer to the cell have a greater weight, and the weight diminishes with greater distance. The rate of diminishing influence is determined by *p*, which is typically

either 1 (linear) or 2 (quadratic). Also, because points relatively far from the raster cell have minimal influence, the number of data points, *n*, often is limited to the points nearest the cell. This method has the advantage of being the simplest, and requiring the least computation time. The weighting term for IDW is calculated according to Equation 2-2.

$$\lambda_i = \frac{d_i^{-p}}{\sum_{j=1}^{n} d_j^{-p}} \quad \textbf{(2-2)}$$

$d_i =$ linear distance from raster cell to i^{th} data point

$p =$ power term regulating the influence of spatial autocorrelation

2.2.2.2 Natural Neighbor

The Natural Neighbor method, though sharing the same general equation as the IDW method, uses a different approach to calculate the weighting values. First, the interpolation area is subdivided into regions known as Voronoi or Thiessen polygons. A set of Voronoi polygons forms a Voronoi diagram, and each dataset maps to a unique Voronoi diagram. Similarly, each data point in the dataset maps to a single Voronoi polygon in the Voronoi diagram. The diagram is constructed in such a way that every location within a given Voronoi polygon is closer to the data point corresponding to that polygon than to any other data point in the dataset (see Figure 2-2)

After the Voronoi diagram is constructed, the values of each raster cell are computed. First a modified Voronoi diagram is constructed from the original dataset plus an additional point, which point's x and y coordinates correspond to the center of the raster cell. The modified diagram is then superimposed on the original diagram. New

polygons are formed by the intersection of the raster cell's Voronoi polygon from the modified diagram, and the surrounding points' Voronoi polygons from the original diagram (see Figure 2-3). The weighting terms for the surrounding points are calculated according to Equation 2-3. Finally, the value of the raster cell is calculated according to Equation 2-1 and the procedure repeats for the next cell in the raster.

$$\lambda_i = \frac{A_i}{A} \quad \textbf{(2-3)}$$

A = area of a given raster cell's Voronoi polygon

A_i = area of the intersection formed by the i^{th} point's Voronoi polygon and A

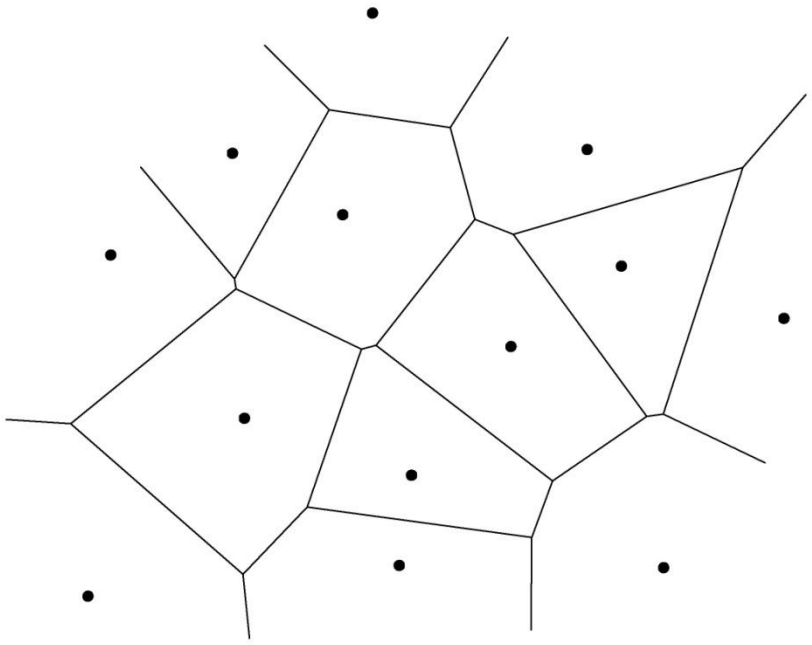

Figure 2-2 Original Voronoi Diagram

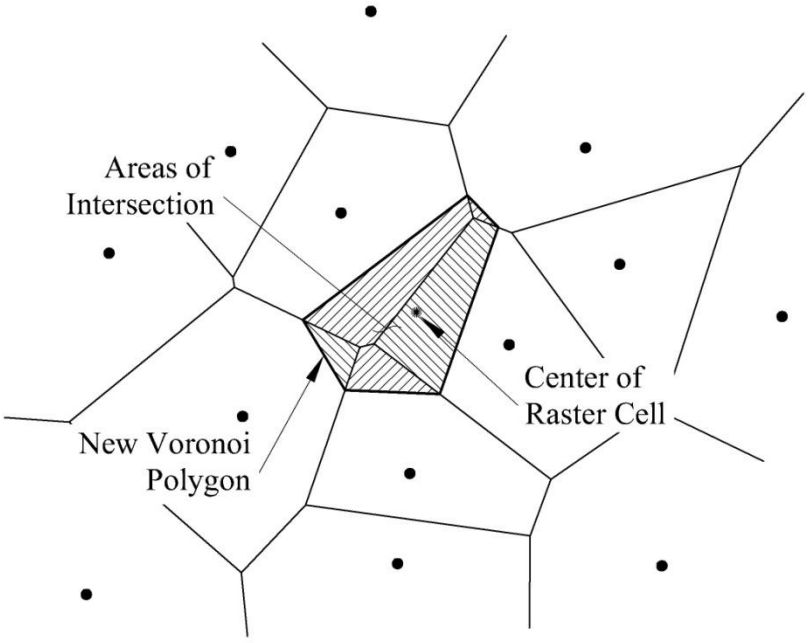

Figure 2-3 Modified Voronoi Diagram

The Natural Neighbor method has the advantage of requiring fewer input parameters, and of forming a generally smoother surface plot. Thus, cross sections taken from a Natural Neighbor surface are generally easier to curve fit than those taken from IDW surfaces.

2.2.2.3 Statistical Analysis

The appropriate interpolation scheme for a set of subsidence plots is determined based on a statistical procedure called validation. In validation, a given dataset is divided into two sets, called the training and test datasets. The training dataset contains 90% of the data points, while the test dataset contains the remaining 10%. The interpolation scheme in question is executed on the training dataset. A statistical analysis is then performed on the resulting raster, which analysis predicts values for the test dataset,

compares them with the actual test dataset values, and calculates the root mean square (RMS) error according to

$$\mathrm{RMS} = \sqrt{\frac{\sum_{i=1}^{n} e_i^{\,2}}{n}} \qquad \textbf{(2-4)}$$

$\mathrm{RMS} =$ root mean square

$n =$ total number of data points in test dataset

$e_i =$ difference between i^{th} data point's predicted and actual values

The RMS adds a quantitative basis of comparison to the qualitative bases discussed for the two interpolation schemes in Section 2.2.2.

Three statistical analysis tools are used in this study, which are Radial Basis Functions, Local Polynomials, and Kriging. These tools are similar to the IDW and Natural Neighbor interpolation schemes, in that they interpolate measured data. The difference is that the statistical analysis tools compare predicted values (training dataset) with measured values (test dataset) which are not included in the original interpolation.

Radial Basis Functions and Local Polynomials are deterministic tools (see Section 2.2.2). The Radial Basis Functions (e.g. Splines) tool is an exact interpolator, meaning that the predicted surface passes through all data points, while the Local Polynomial tool is an inexact interpolator. Kriging, on the other hand, is a geostatistical tool, meaning that it utilizes the inherent statistical properties of the measured points in its interpolation. The application of these statistical methods is described in Section 3.2.2.

2.2.3 Map Algebra Method

In order to produce year-to-year subsidence plots, a consistent and general method was developed. Yearly survey data provided by the mines typically includes base year elevations, in addition to current year elevations, for each data point. Typically, all years refer to the same base year, with a few exceptions. In this method, elevation differences between the current year and base year data points are computed in a spreadsheet.

Two primary sets of output data are created for each year. The first, called a current elevation dataset (CED), contains the Eastings, Northings, and current elevations for that year. The second, called an elevation difference dataset (EDD) contains the Eastings, Northings, and elevation differences from either the base year or the preceding year. The primary roles of each dataset are described below.

2.2.3.1 Current Elevation Dataset

The CEDs are mainly used to construct a TIN surface, though they can also be used to construct subsidence plots. However, due to the mountainous terrain typically above coal mines, when CEDs are interpolated they result in subsidence plots with significant errors in areas with few data points. For example, validation performed on CEDs typically returns a RMS error of approximately 50 feet (see Section 2.2.2.3). This error propagates when an interpolated CED surface from the current year is subtracted from that of the previous year, resulting in a plot with excessive yearly rises and falls in elevation.

As previously mentioned the CEDs are, however, effective in forming a vector surface. The vector surface created from a CED is a specialized TIN called a Terrain.

The Terrain is able to take thousands of points as input, generating a surface that will display differently at various scales. The Terrain has several important functions in this method, one of which is to provide a reference to correctly align Digital Elevation Models with subsidence data.

2.2.3.2 Digital Elevation Model

Several Digital Elevation Models (DEMs) are added as map layers in order to visualize the subsidence areas according to their topography. The DEMs used in this report were imported from the National Map Seamless Server website, provided by the United States Geological Survey [17]. The imagery for the DEMs was obtained from the National Agriculture Imagery Program (NAIP), which consists of arrays of one to two meter resolution aerial photographs. The NAIP DEMs reference the Universal Transverse Mercator coordinate system, and are spatially correlated to form a seamless map when imported together. DEMs comprising the area of subsidence were imported into ArcGIS, where their coordinate system was converted to the Utah Central 1927 SPCS (see Section 2.1)

2.2.3.3 Elevation Difference Dataset

The EDDs produce subsidence rasters with higher accuracy than those from corresponding CEDs. The possibility of error in areas with fewer data points is minimized in EDD subsidence rasters, due to the small variation in raster values. Typically, the RMS error from validation analysis is on the order of one to two feet.

2.2.4 Subsidence Algorithm

In order to facilitate the construction of subsidence plots, the process of converting, interpolating, and subtracting datasets—as well as formatting the final plots—is automated using the ArcGIS model builder. Generally, each of the three elements discussed in Sections 2.2.1 to 2.2.3 can be described as a process in which new data is derived from existing data (e.g. interpolation schemes create an array of values from a few data values). The new data is often used as input for another process, and so on until a satisfactory subsidence plot is created. The ArcGIS model builder allows for these intermediate processes to be linked together such that the initial input data is converted to a subsidence plot in one algorithm.

Two methods were developed which use EDDs in the ArcGIS model builder to produce a subsidence plot. The methods differ only as to the step where the actual subtracting of the data occurs. The first method involves subtracting the data in a spreadsheet. Two EDDs representing consecutive years are input to the spreadsheet, and the Easting and Northing values of each data point from one EDD are compared with those of each data point from the other EDD. If the Northings and Eastings match, the elevation difference between the data points is computed. The resulting EDD contains elevation changes with respect to the previous year.

In the second method, the subsidence surface is created by subtracting two EDD rasters in ArcGIS. The EDDs in this method contain elevation changes with respect to a common base year. An interpolation scheme is applied to each EDD creating corresponding EDD rasters. The EDD raster values are subtracted in ArcGIS according to Equation 2-5 resulting in a yearly subsidence raster.

$$(y_p - y_c) = (y_p - y_b) - (y_c - y_b) \quad \textbf{(2-5)}$$

$y_c =$ Elevation of current year

$y_p =$ Elevation of previous year

$y_b =$ Elevation of base year

$y_p - y_b =$ EDD raster for previous year

$y_c - y_b =$ EDD raster for current year

$y_p - y_c =$ Resulting yearly subsidence raster

Two models were assembled corresponding to the respective subtraction methods described above. The first model requires only a single EDD, which is first interpolated to form a raster dataset. The model then splits the raster according to positive and negative elevation changes, resulting in two new rasters. The subsidence raster is split into two additional rasters which show large and small amounts of subsidence, while the rise raster is reclassified to only show small rises in elevation. The specific classification of the large-subsidence raster is outlined in Chapter 3.

The second model adds an extra step to the first. Two EDD's which reference a common base year are required as input. After the interpolation of these EDD's, the previous year EDD raster is subtracted from the current year EDD raster using map algebra. The resulting output rasters are then split and classified according to the same criteria used in the first model. The two models are represented by the flow charts displayed as Figure 2-4 and Figure 2-5.

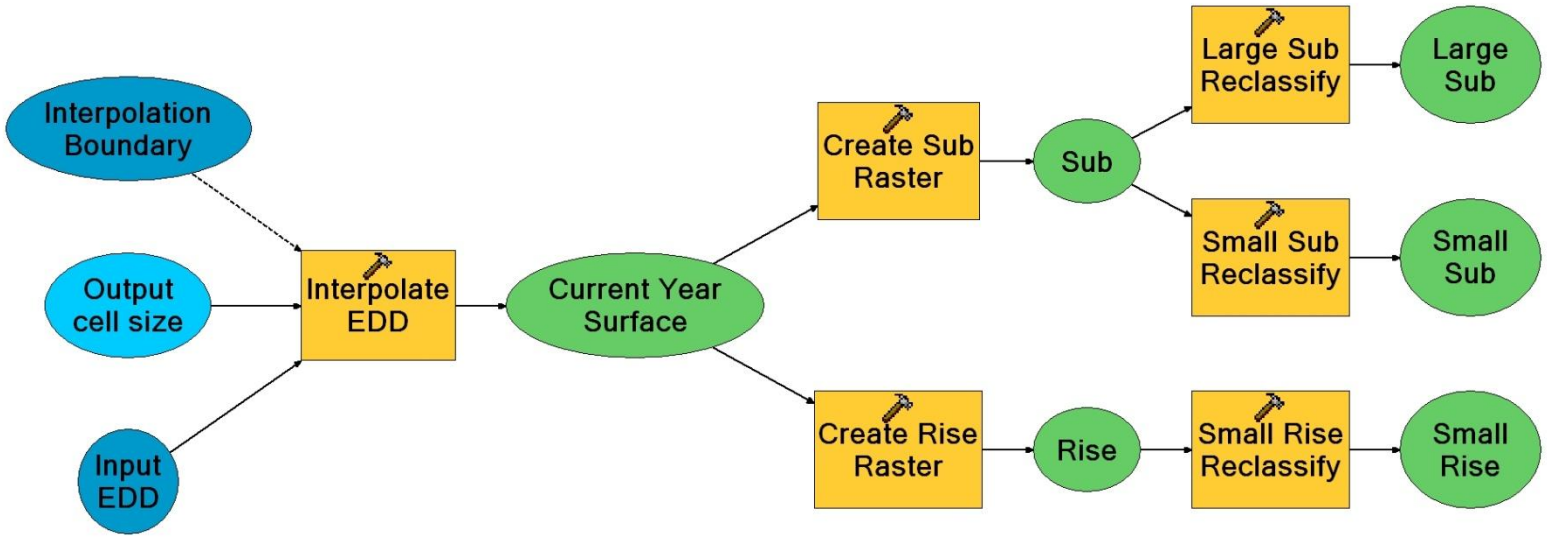

Figure 2-4 Single EDD Model Flowchart

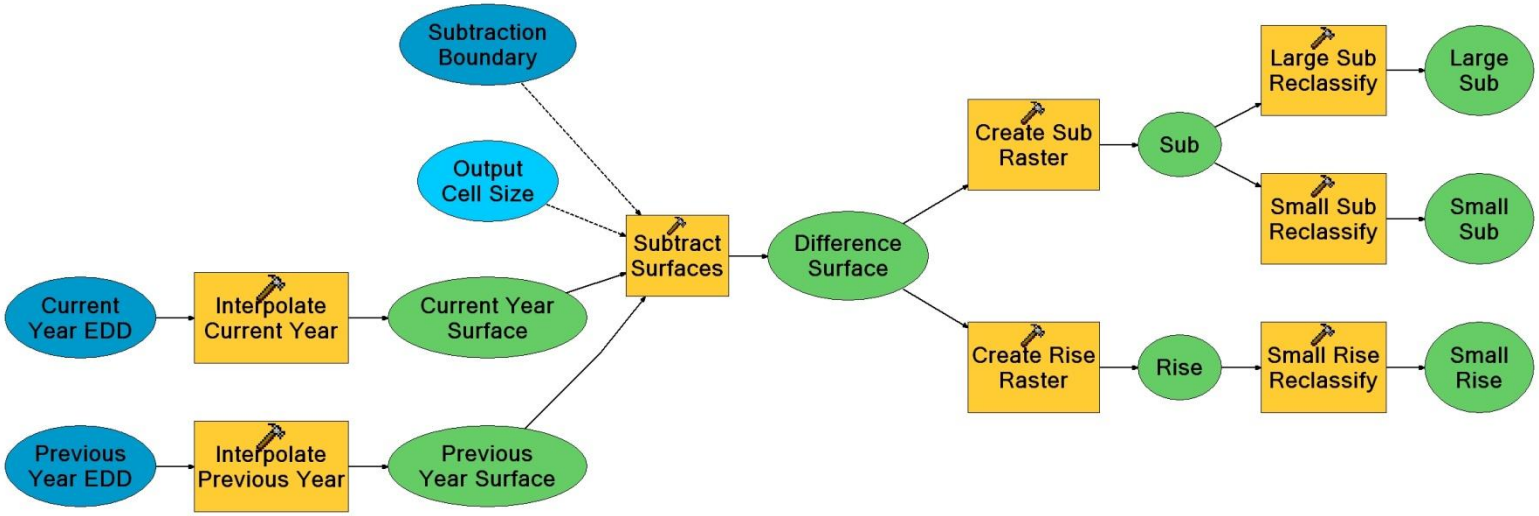

Figure 2-5 Multiple EDD Model Flowchart

3 Mines

Survey datasets from three separate coal mines were used in this study. These mines are Deer Creek, Crandall Canyon, and Aberdeen (also known as Centennial). Deer Creek and Crandall Canyon mines are surveyed using aerial photography, while Aberdeen mine is surveyed using ground techniques. The data from the surveys and mine workings are organized into layers, which function as the basis for the resulting subsidence plots.

3.1 Data Layers

Several layers of data are presented for each mine. The layers are arranged and overlain to form subsidence and elevation plots corresponding to survey data and mine activity. The principle layers which make up these plots are:

1. Mine layouts
2. DEMs (see Section 2.2.3.2)
3. Subsidence plots

The mine layouts are constructed in AutoCAD 2009, and imported into ArcGIS. The layouts consist of vector features (see Section 2.2.1.1) and are classified according to the time between aerial surveys, which typically take place in September or October.

Thus, the years in the following plots refer to mining which begins in October of the previous year, rather than January of the current year.

The subsidence plots consist of filled subsidence contours. The main purpose of the subsidence plots is to provide a comparison of subsidence from one year to the next, and to identify areas wherein subsidence from one year does not coincide with the mine workings for that year. Thus, the filled subsidence contours are limited to three ranges of subsidence values, facilitating visualization of relative yearly subsidence and identification of subsidence inconsistent with mining activity.

A subsidence plot is created by reclassifying the interpolated large-subsidence raster (see Section 2.2.4) into three classes. The classes represent subsidence ranges of 1 to 2 feet, 2 to 3 feet, and greater than 3 feet. The year-to-year subsidence plots can be compared to one another by overlaying the plots on transparency sheets. Appendix A contains copies of the transparency layers for every mine.

3.2 Deer Creek Mine

Deer Creek Mine is located in central Utah about 12 miles west of Huntington, near the mouth of Huntington Canyon, in Emery County. It is owned and operated by Energy West Mining Company, a subsidiary of Pacific Corp. Only part of the mine is used in this study, which part is located under an area known as Rilda Canyon. Thus, in this report, “Deer Creek Mine” and “Deer Creek” refer exclusively to the Rilda Canyon portion of the mining area. The geography of Deer Creek is made up of cliffs, mountains, and canyons. Geologically, the overburden consists of alternating layers of sandstone and mudstone. Figure 3-1 is a DEM of the Deer Creek mining area.

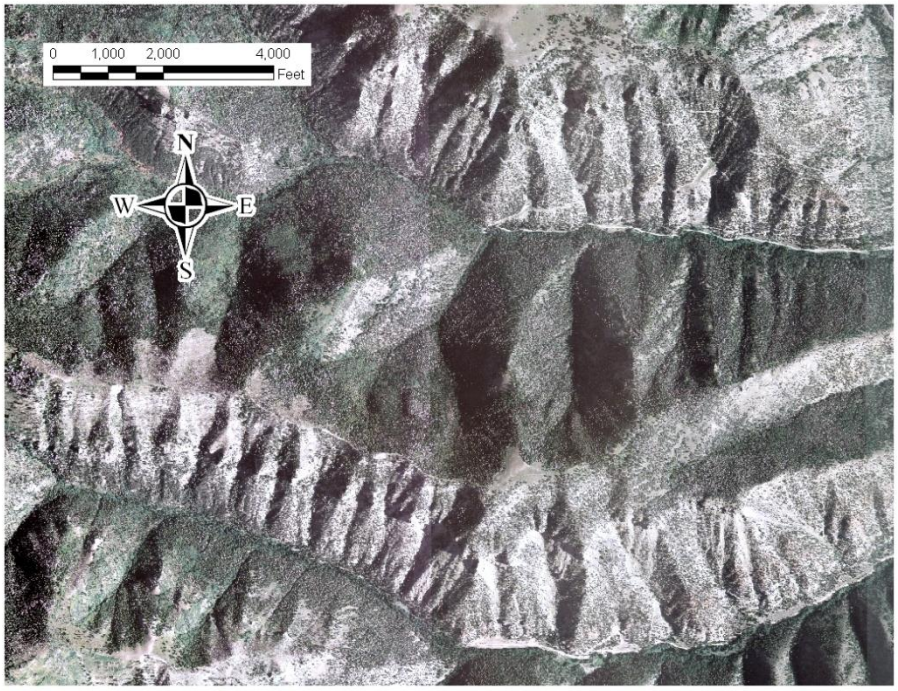

Figure 3-1 DEM of Deer Creek Mining Area

3.2.1 Mine Layout

Deer Creek Mine consists of two separate coal seams, known as the Hiawatha and Blind Canyon seams. The seams run basically horizontally, and are assumed at constant elevations in this study. The Hiawatha seam is at an elevation of approximately 7600 feet above sea level, with the Blind Canyon seam 80 feet above it. The overburden above the Hiawatha seam ranges from under 400 to over 1700 feet. The Blind Canyon seam was mined first from April 1999 to December 2001. Mining in the Hiawatha seam followed, beginning February 2002 and ending August 2004. The mine layout for both seams is illustrated in Figure 3-2 and Figure 3-3.

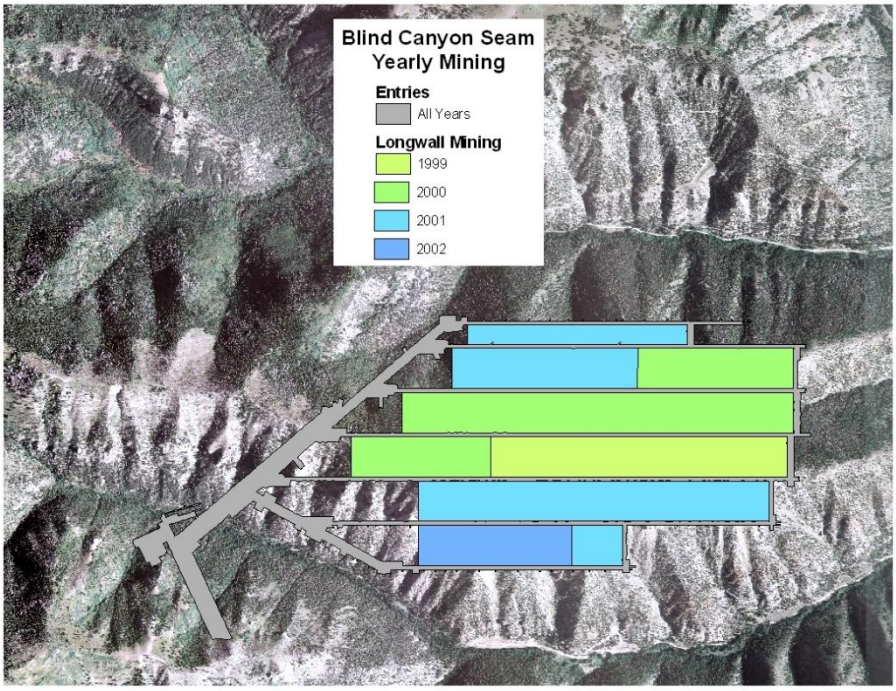

Figure 3-2 Deer Creek Yearly Mine Workings: Blind Canyon Seam

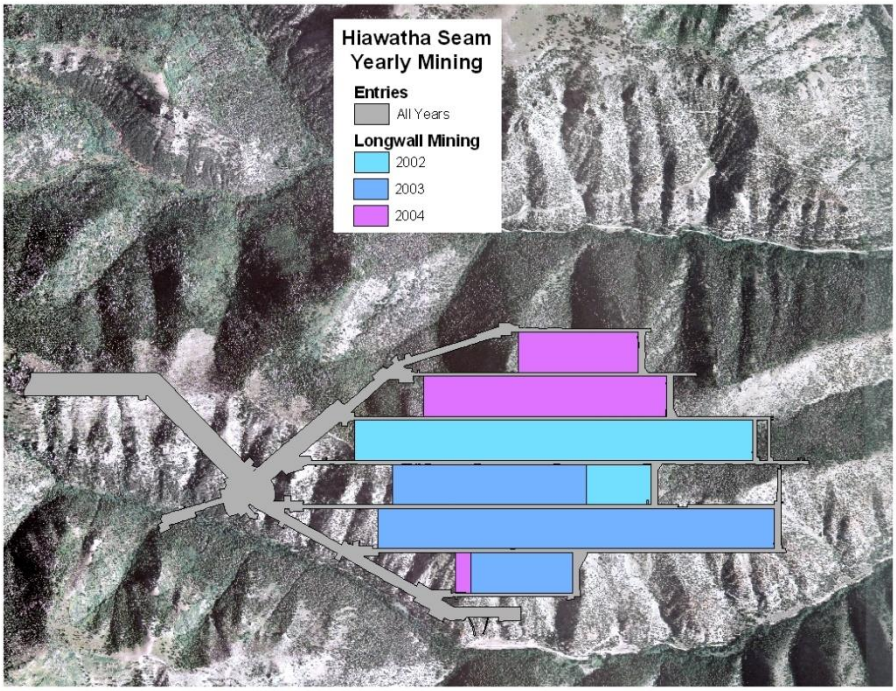

Figure 3-3 Deer Creek Yearly Mine Workings: Hiawatha Seam

3.2.2 Subsidence Plots

The annual aerial survey datasets provided by Energy West for this area correspond to the years 2001 to 2006. Each dataset references the 1999 base year; thus the subsidence plots were created using the multiple EDD model (see Figure 2-5). An EDD representing 1999 to 2006 was selected as input for the statistical process described in Section 2.2.2.3. The resulting RMS error values from the IDW and Natural Neighbor interpolation schemes for three separate statistical analyses is given in Table 3-1.

Table 3-1. RMS Error Values from Validation Analysis

Method:	Radial Basis Functions	Local Polynomial	Kriging
IDW:	1.432	1.433	1.432
Natural Neighbor:	1.496	1.621	1.498
Percent Difference:	**4.47%**	**13.12%**	**4.61%**

Table 3-1 indicates that the IDW scheme is slightly more accurate than the Natural Neighbor scheme. While the difference in accuracy using the Local Polynomials technique is significant, the RMS error is less than five percent using the Kriging and Radial Basis Function techniques. However, in light of quality considerations the Natural Neighbor scheme outperforms the IDW scheme (see Section 2.2.2.2), and the small quantitative difference in RMS error may be overruled. The Natural Neighbor scheme is thus used to interpolate the Deer Creek Mine EDDs. Year-to-year subsidence plots overlying each seam separately are given in Figure 3-4 to Figure 3-13.

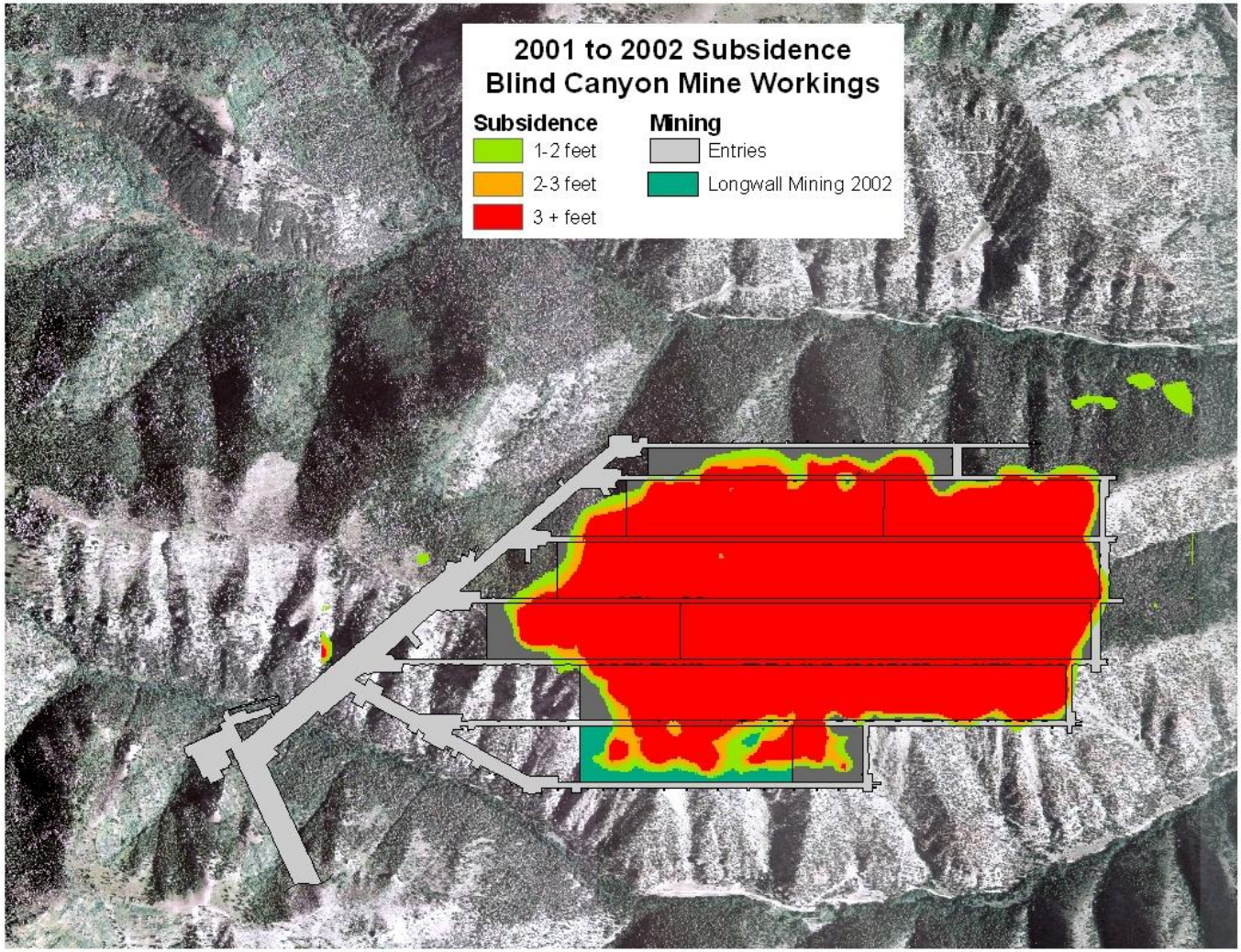

Figure 3-4 Deer Creek Subsidence: Blind Canyon Seam 2002

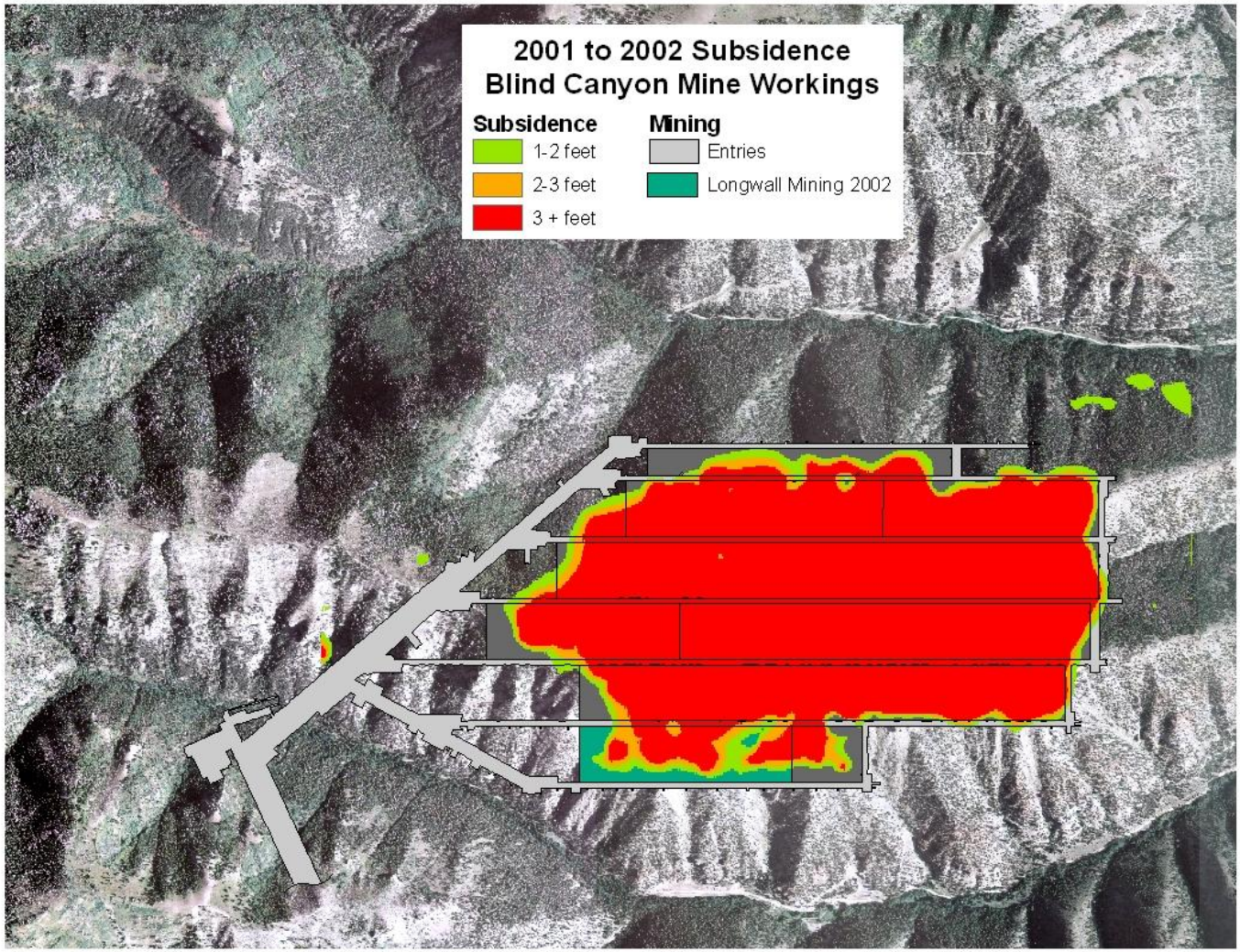

Figure 3-5 Deer Creek Subsidence: Hiawatha Seam 2002

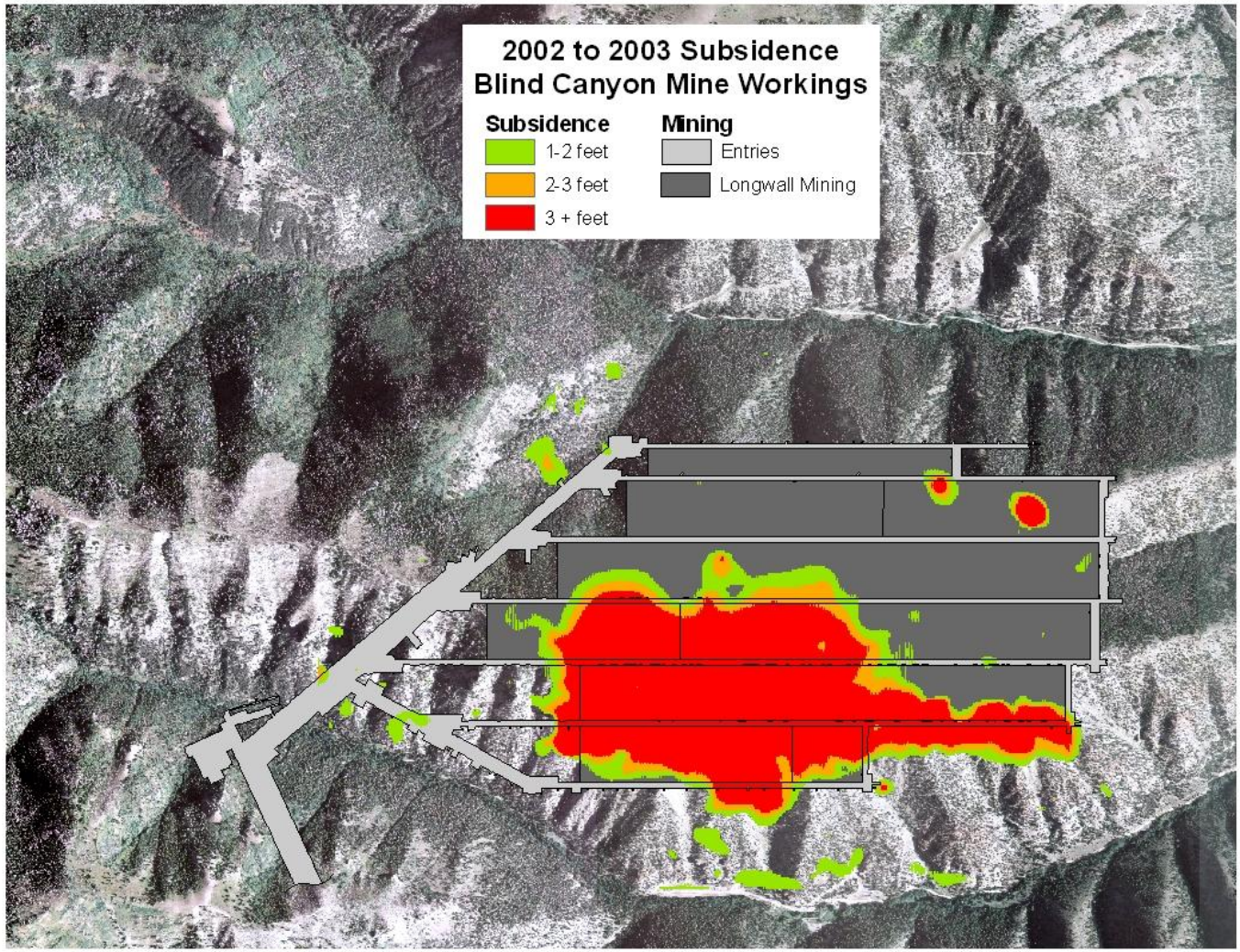

Figure 3-6 Deer Creek Subsidence: Blind Canyon Seam 2003

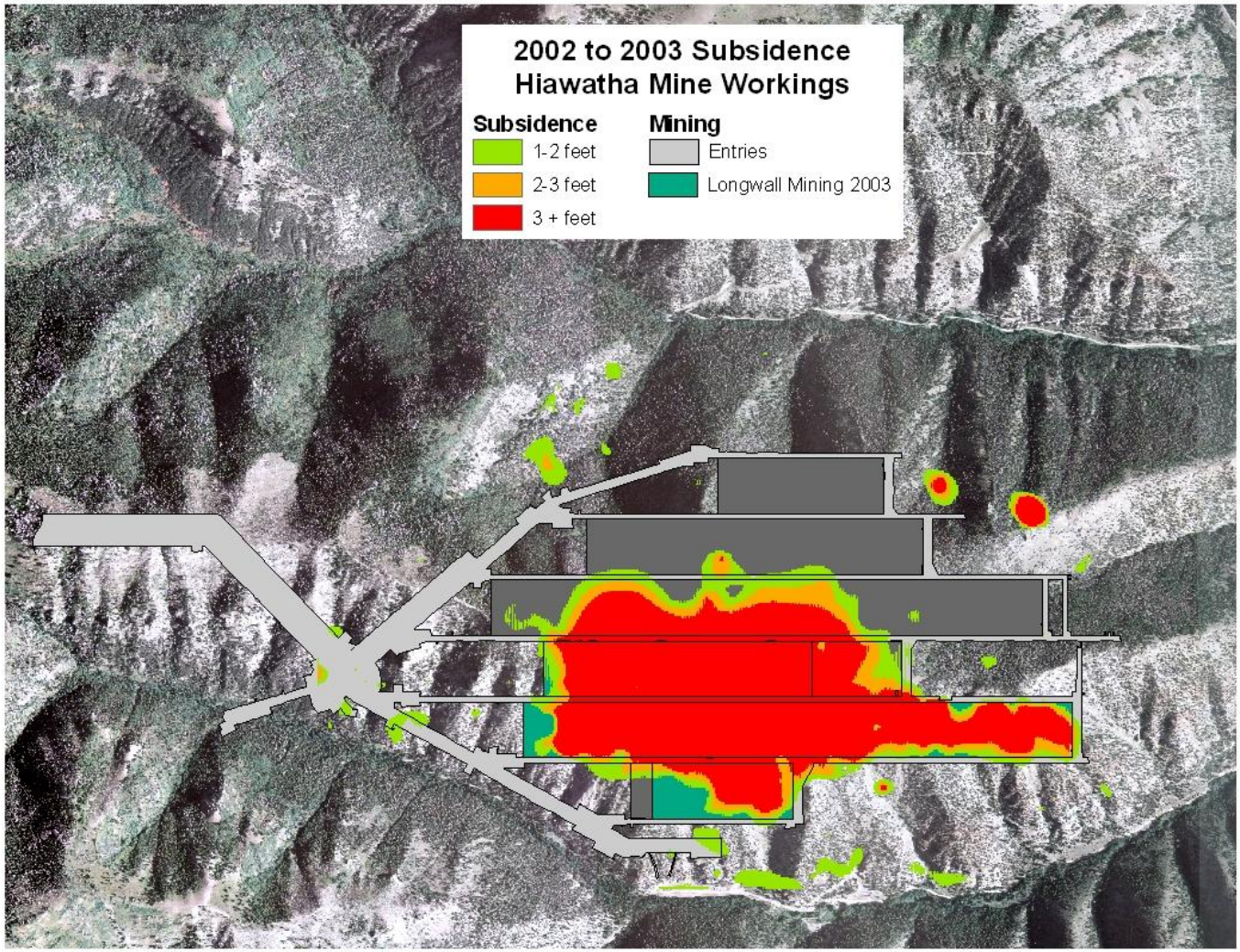

Figure 3-7 Deer Creek Subsidence: Hiawatha Seam 2003

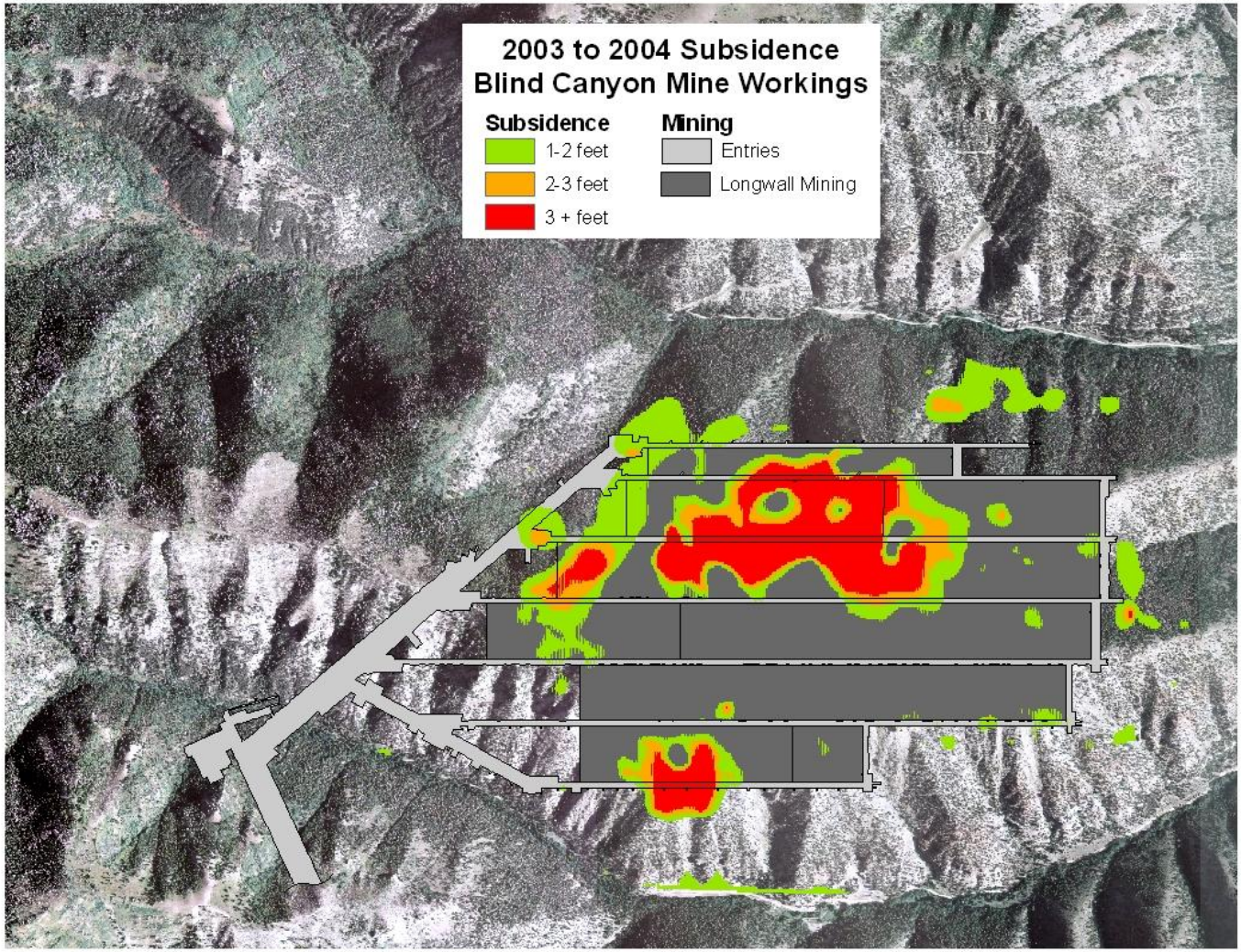

Figure 3-8 Deer Creek Subsidence: Blind Canyon Seam 2004

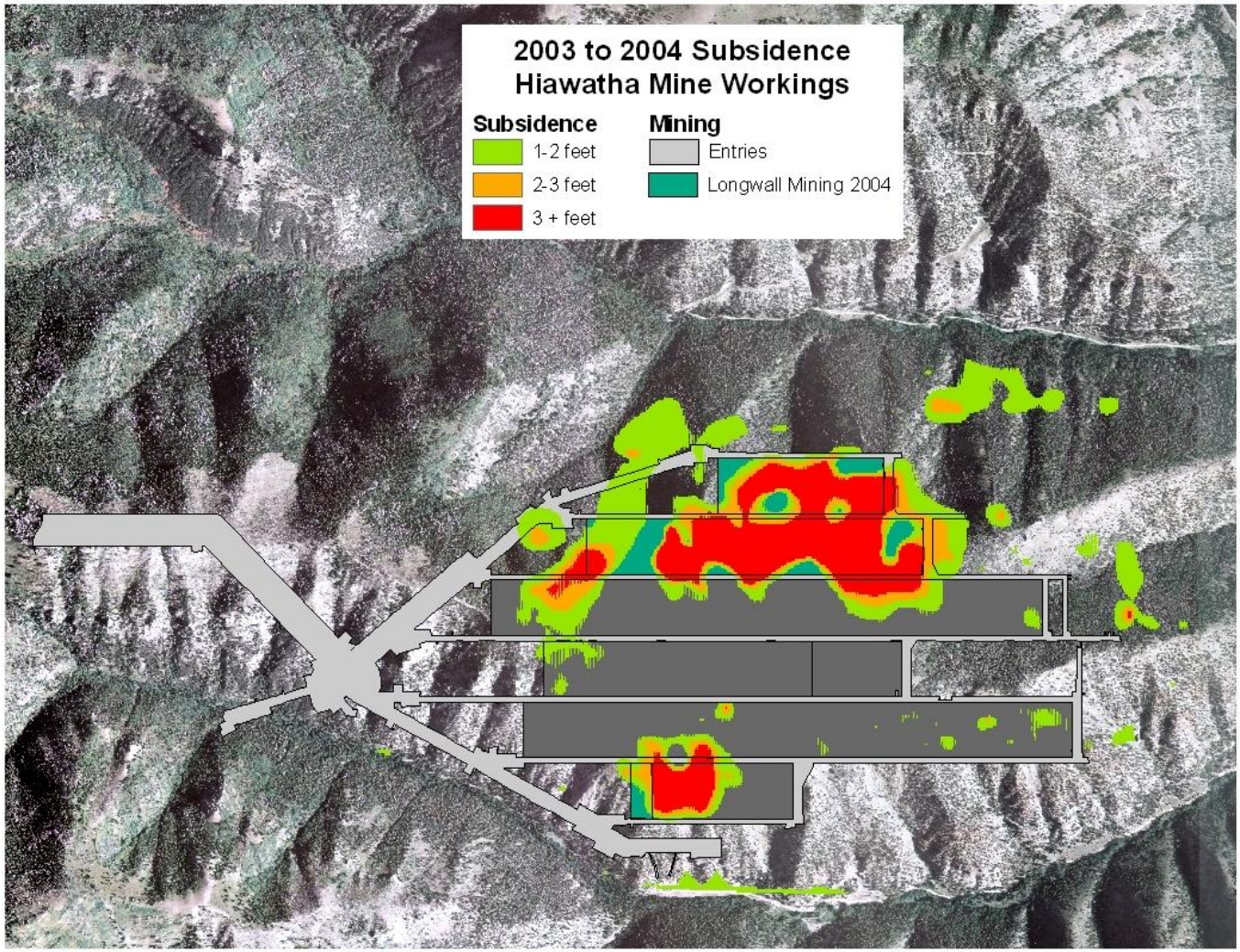

Figure 3-9 Deer Creek Subsidence: Hiawatha Seam 2004

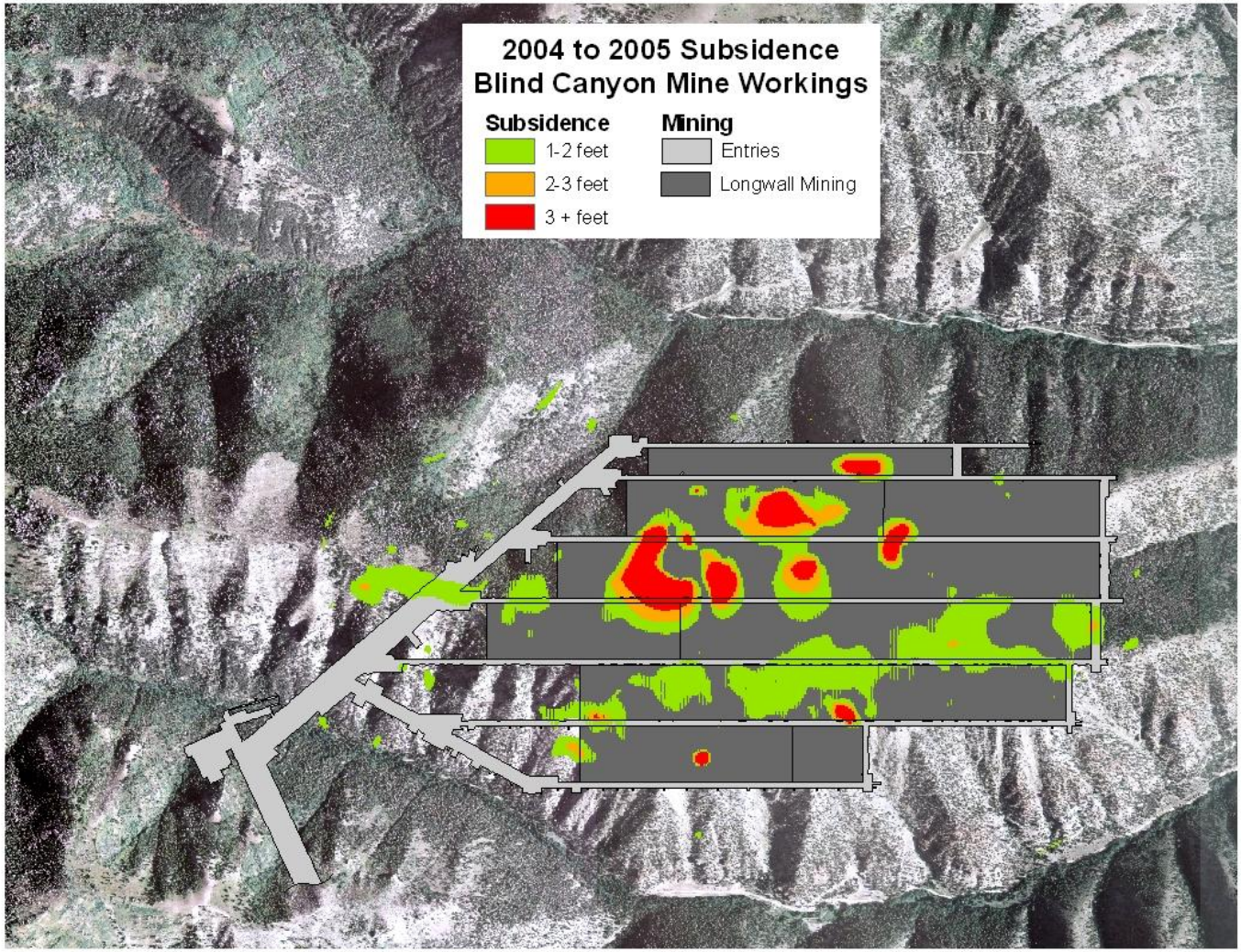

Figure 3-10 Deer Creek Subsidence: Blind Canyon Seam 2005

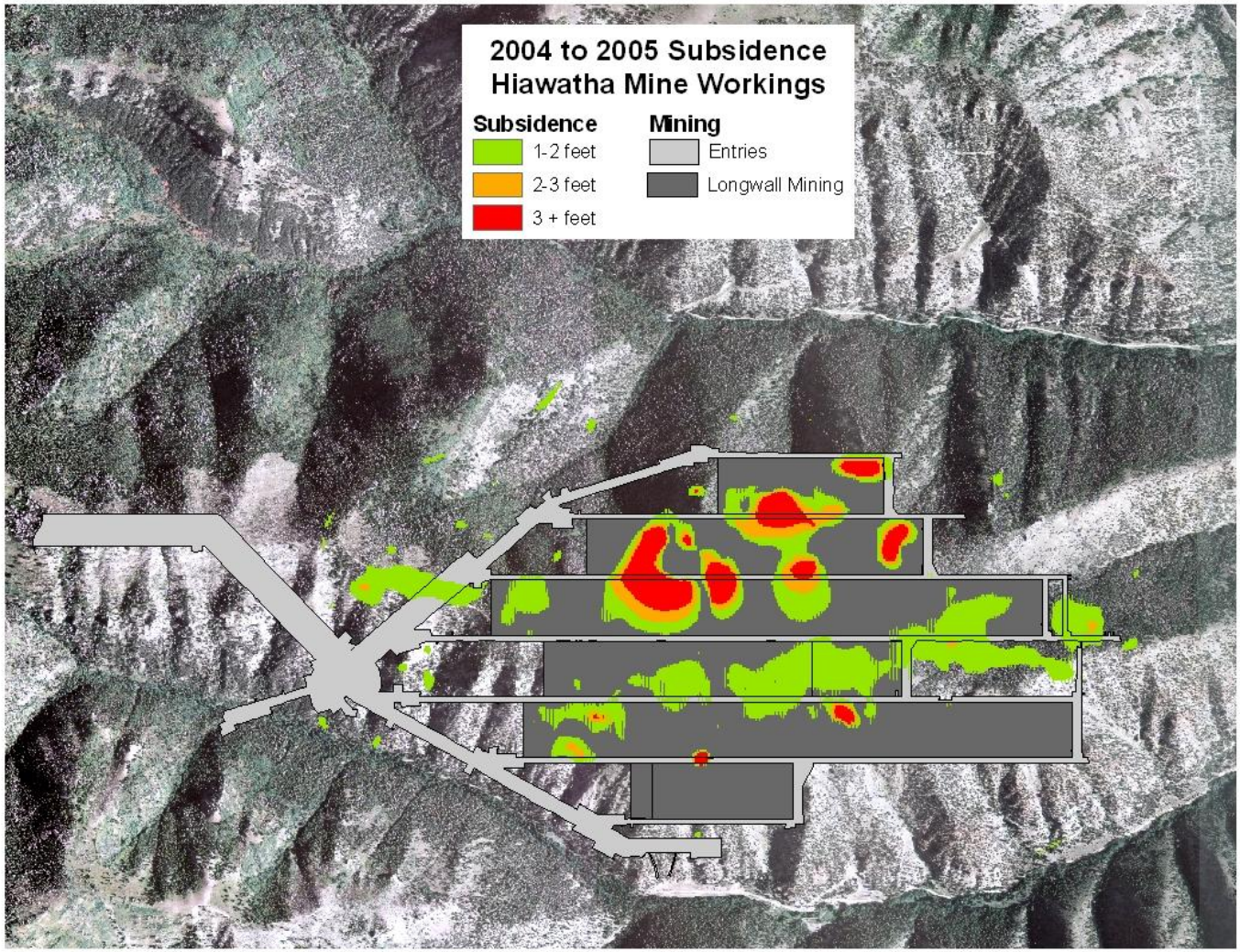

Figure 3-11 Deer Creek Subsidence: Hiawatha Seam 2005

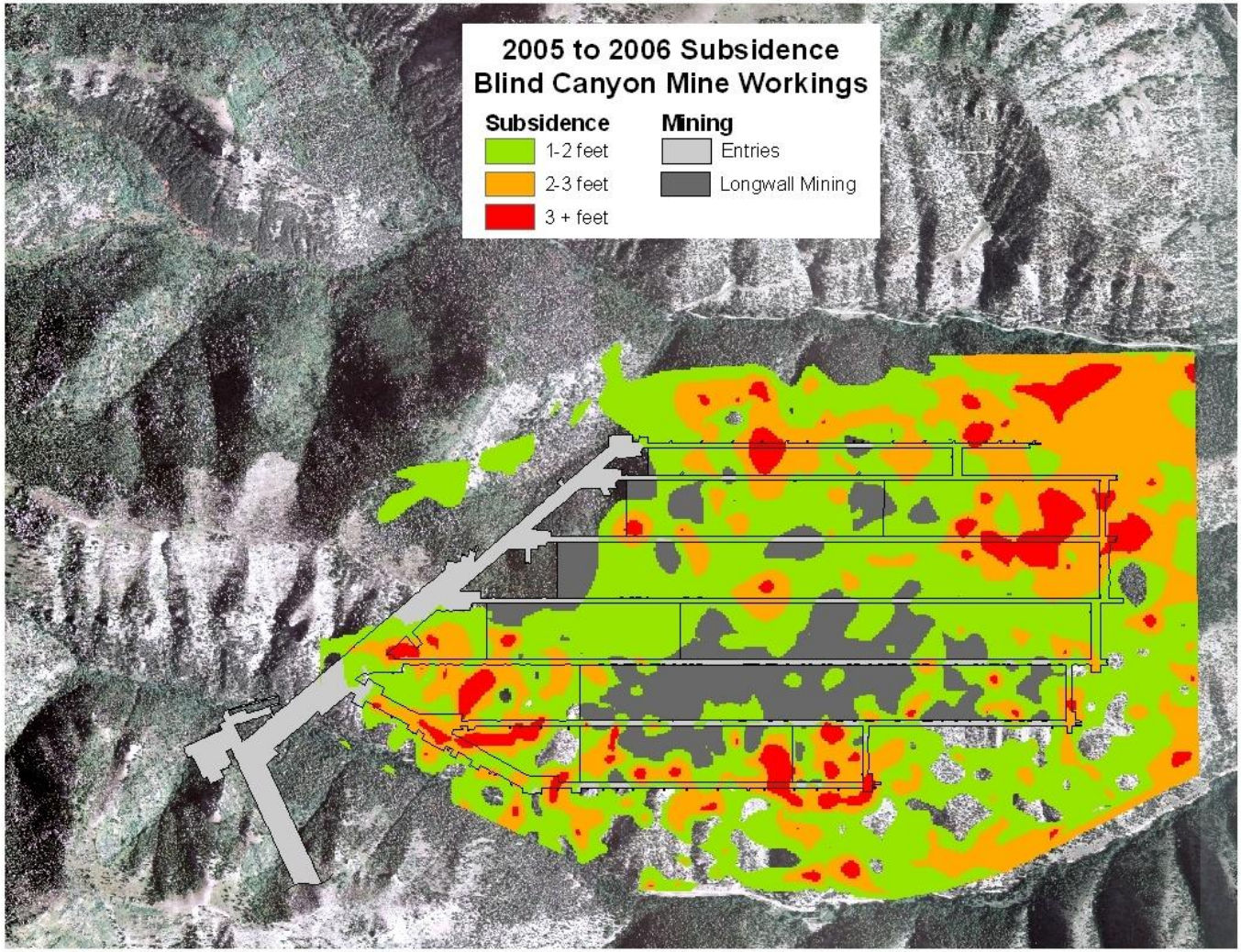

Figure 3-12 Deer Creek Subsidence: Blind Canyon Seam 2006

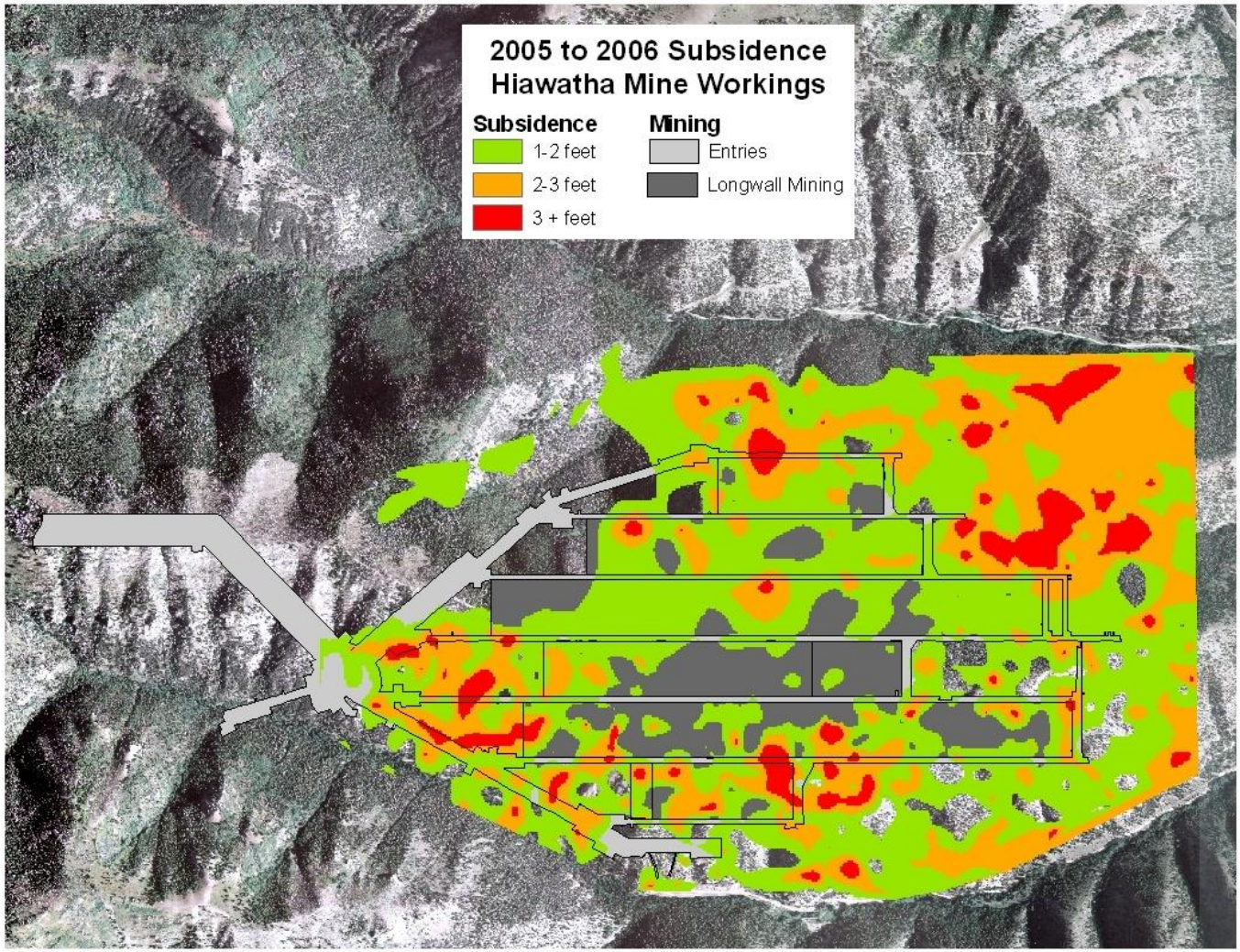

Figure 3-13 Deer Creek Subsidence: Hiawatha Seam 2006

3.3 Crandall Canyon Mine

Crandall Canyon Mine is located about five miles north of Deer Creek Mine, in Huntington Canyon. The mine, owned by Genwal Resources Inc. (a subsidiary of Intermountain Power Agency and Murray Energy Corporation), .is now idle due to two related fatal accidents in August 2007 [18]. Subsidence plots for this mine were created for the entire range of available aerial survey data. The geography and geology of this mine are similar to those of Deer Creek Mine. Figure 3-14 is a DEM of the Crandall Canyon mining area.

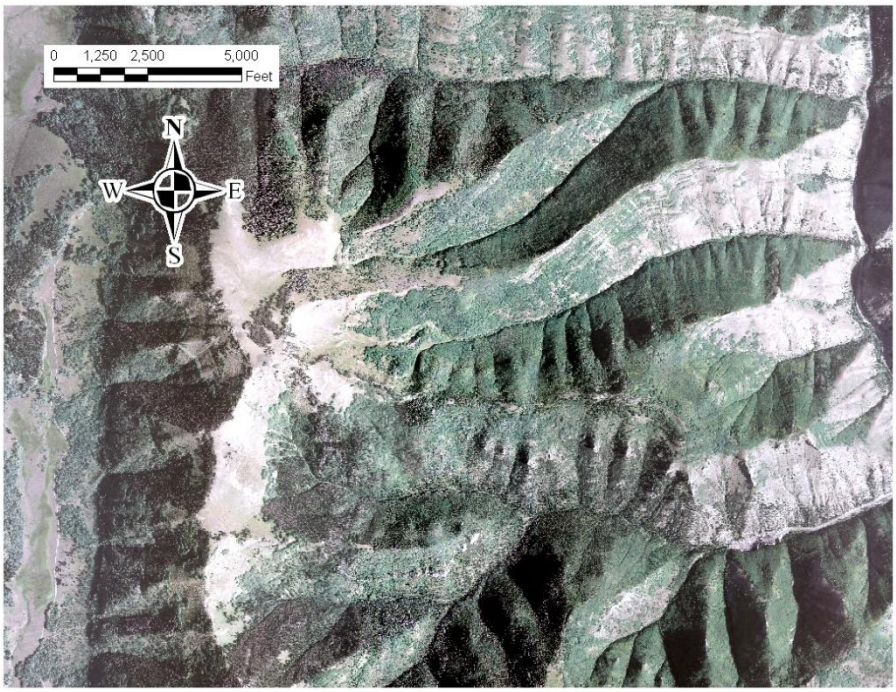

Figure 3-14 DEM of Crandall Canyon Mining Area

3.3.1 Mine Layout

In contrast to the Deer Creek Mine, the Crandall Canyon Mine operated on only a single coal seam, namely the Hiawatha coal seam. Longwall mining began in 1995 and continued until 2005. From 2005 to 2007 mining was done through pillar extraction, a practice of systematically removing the coal pillars originally left to support the entries. The first of the August 2007 accidents occurred during pillar extraction, and mining in Crandall Canyon ceased shortly thereafter [18]. Figure 3-15 shows the Crandall Canyon Mine layout and workings prior to closure.

3.3.2 Subsidence Plots

The Natural Neighbor interpolation scheme was used for the Crandall Canyon mine subsidence plots in order to be consistent with the Deer Creek Mine plots, as well as for visual quality purposes (see Section 2.2.2.2). These plots comprise the years 2001, 2002, 2003, 2005 and 2007. The 2004 and 2006 datasets are not available, and thus the last two plots manifest two years of activity and subsidence. Each yearly (or biyearly) subsidence plot also shows the mine workings for the time period indicated. The plots are shown as Figure 3-16 through Figure 3-20.

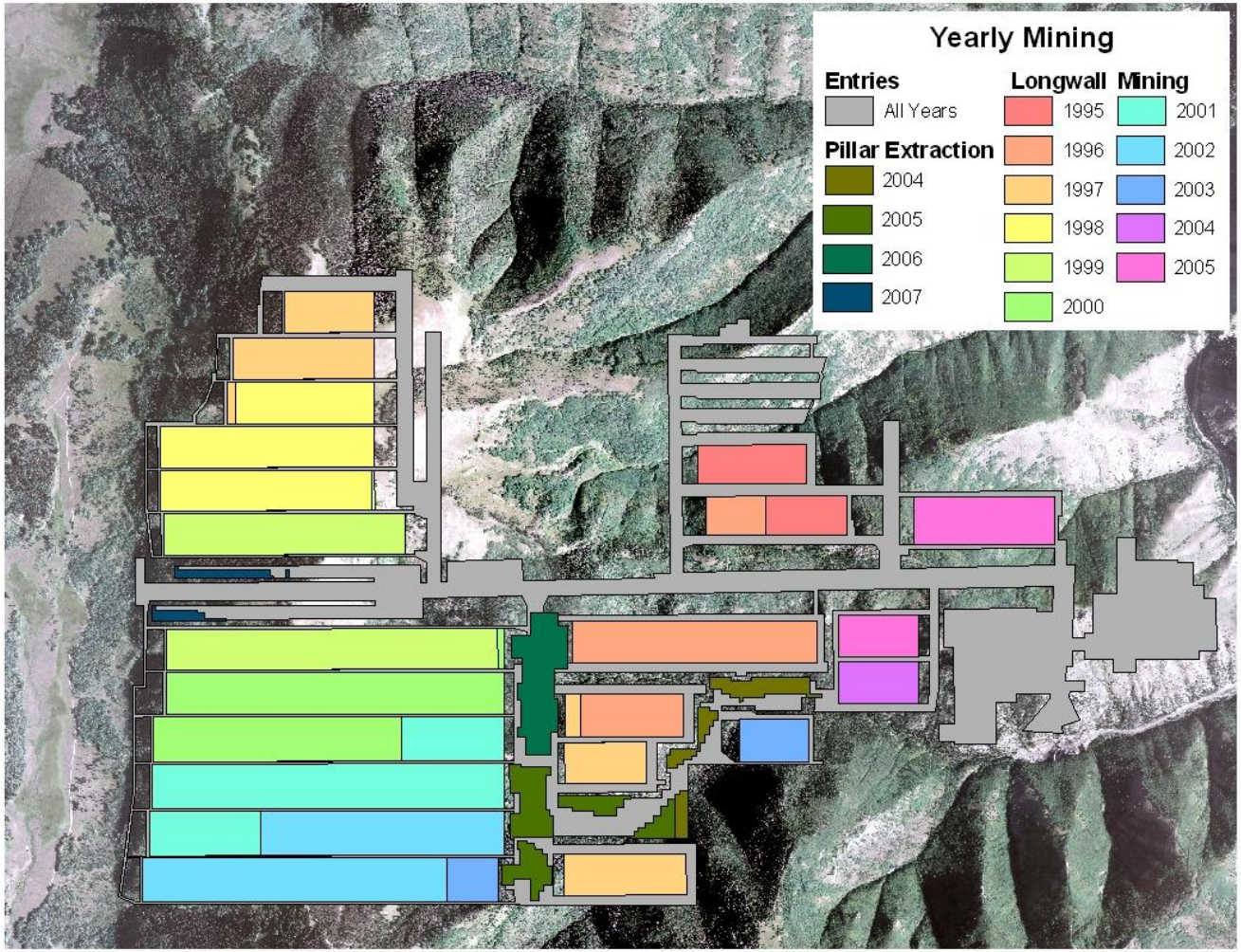

Figure 3-15 Crandall Canyon Yearly Mine Workings

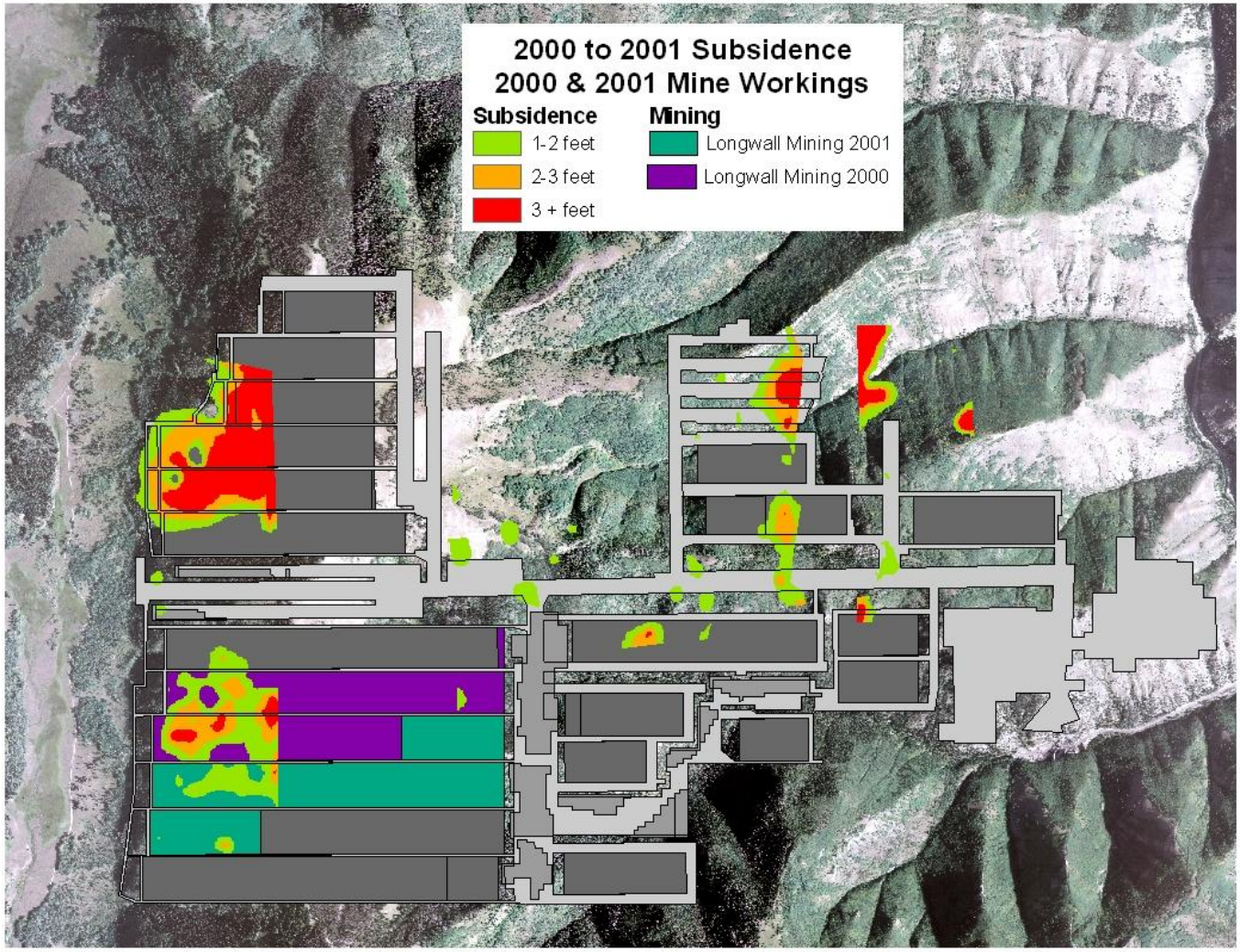

Figure 3-16 Crandall Canyon Subsidence 2001

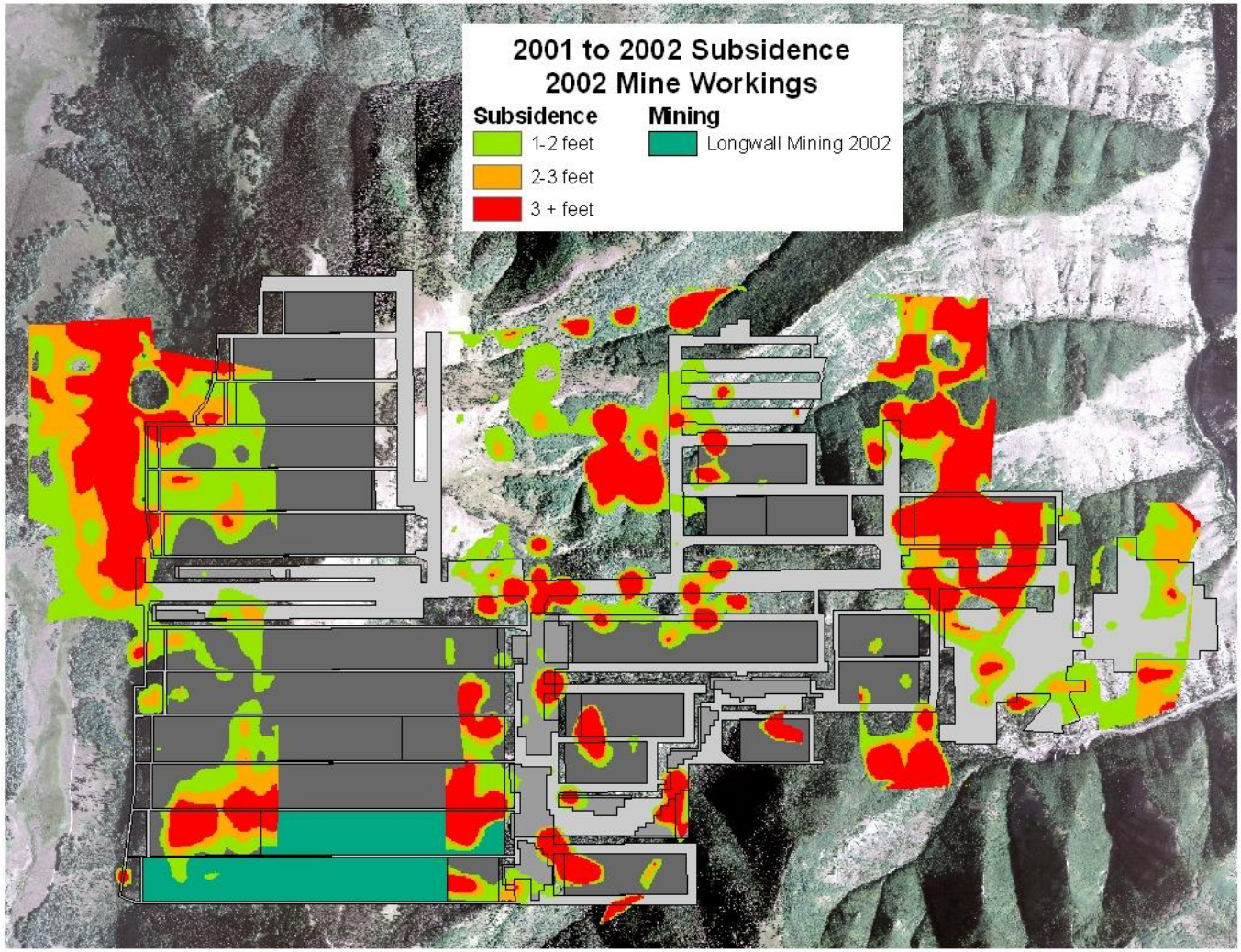

Figure 3-17 Crandall Canyon Subsidence 2002

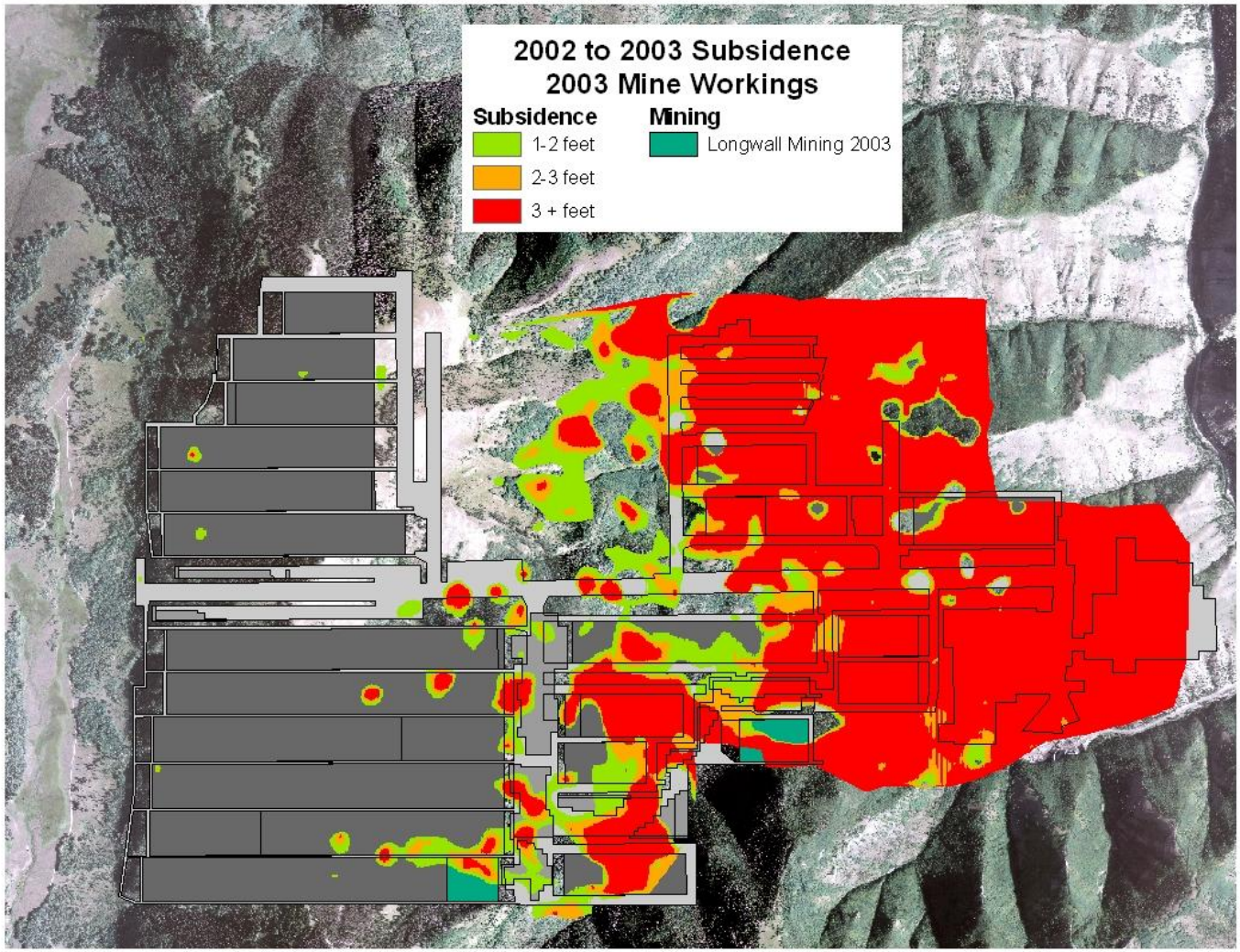

Figure 3-18 Crandall Canyon Subsidence 2003

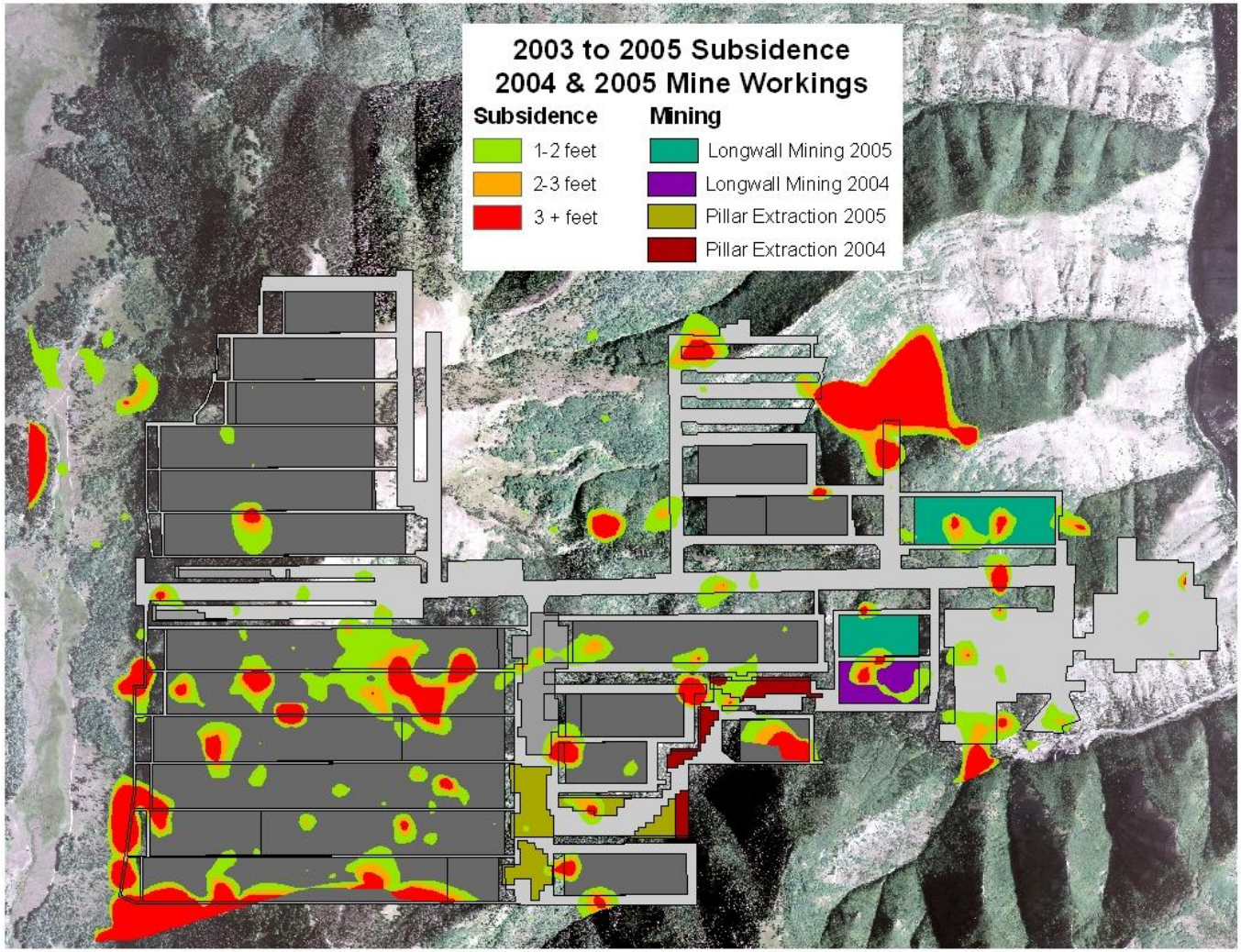

Figure 3-19 Crandall Canyon Subsidence 2004 and 2005

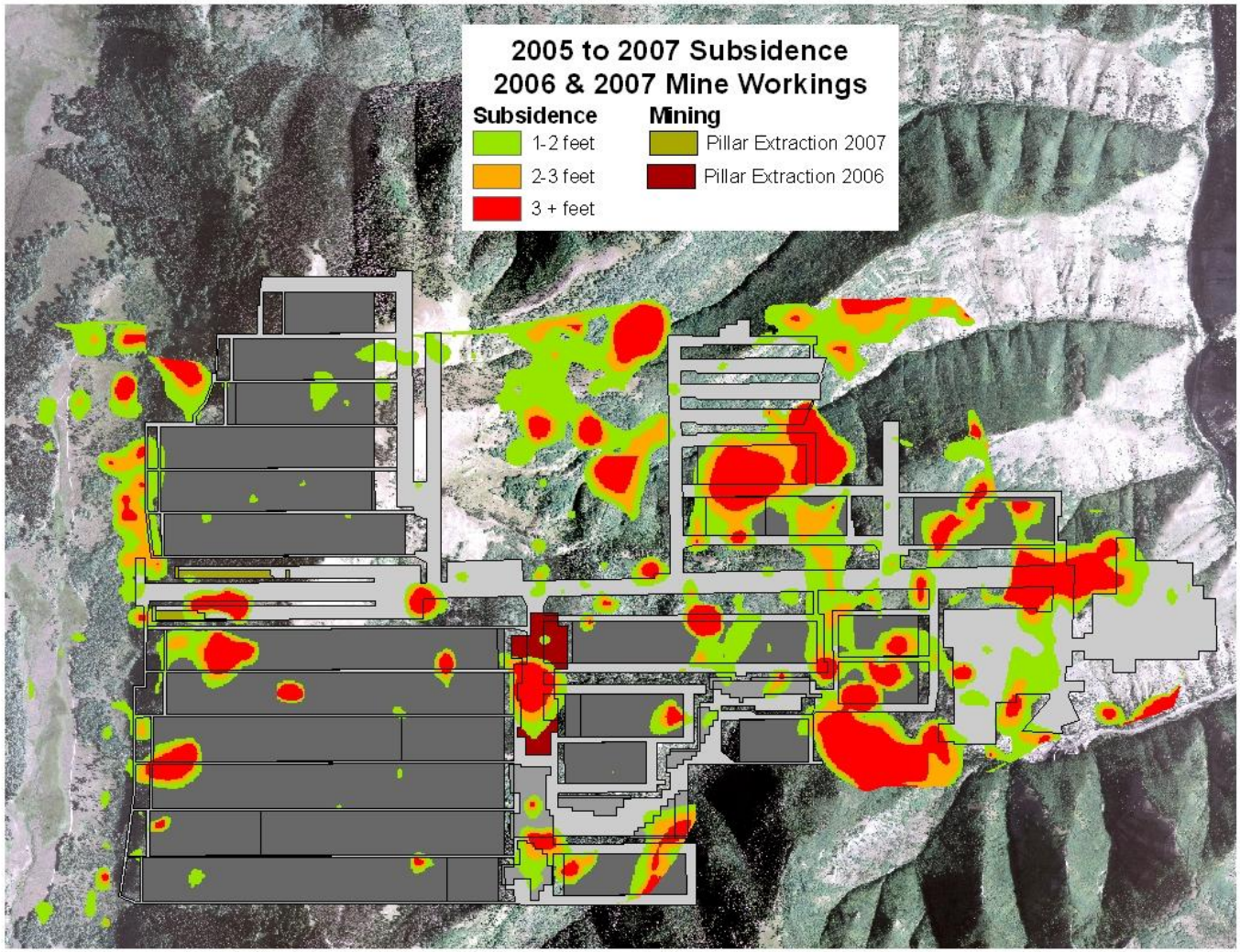

Figure 3-20 Crandall Canyon Subsidence 2006 and 2007

3.4 Aberdeen Mine

Aberdeen Mine is located about 7 miles north of Price in Carbon County, Utah, in an area known as Coal Creek. It is one of the deepest mines in the United States, with overburden exceeding 3,000 feet [19]. Similar to Crandall Canyon Mine, Aberdeen is owned by Genwal Resources Inc. Figure 3-21 is a DEM of the Aberdeen Mining Area.

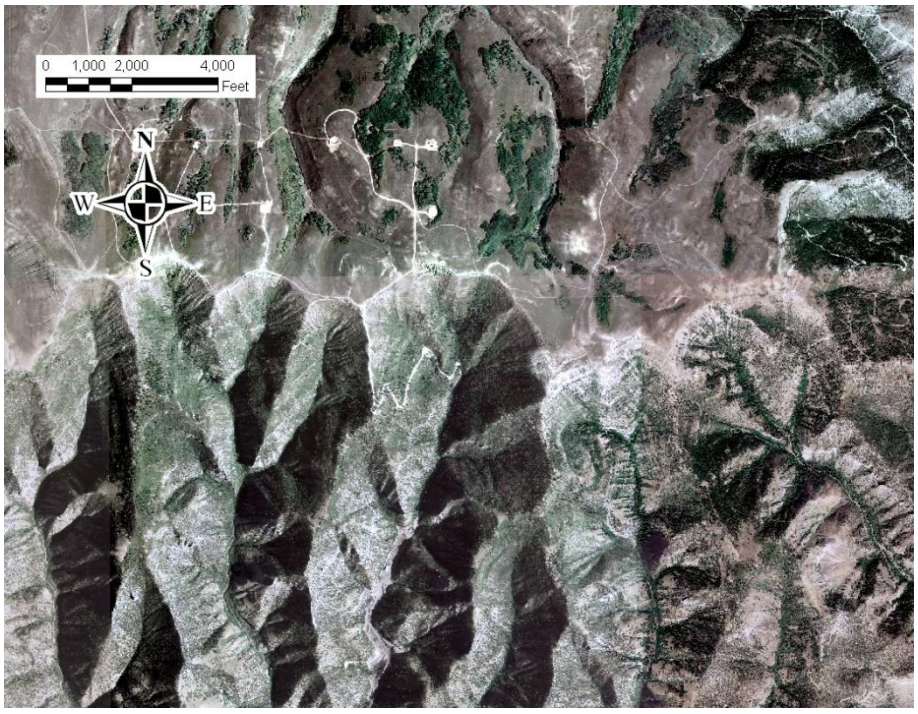

Figure 3-21 DEM of Aberdeen Mining Area

Aberdeen Mine differs significantly from the previous two mines in a number of ways. First of all, the subsidence monitoring for Aberdeen is done using ground survey points rather than aerial survey points. Survey monuments mark the points, and the elevation of each monument is measured annually. Secondly, the longwall panels in

Aberdeen mine are separated by coal barriers, which are almost as wide as the longwall panels themselves (see Figure 3-22). Finally, due to the mine's large overburden, subsidence is an order of magnitude less than that for either Deer Creek or Crandall Canyon. The largest subsidence measured by the data points is about six inches.

3.4.1 Mine Layout

Aberdeen Mine consists of two sections which partially overlap. The main section is referred to as the Aberdeen Mine, while the second section is referred to as the Pinnacle Mine, which is approximately 110 feet above the Aberdeen Mine. Layouts of the Aberdeen and Pinnacle mine sections relative to the surrounding topography are given in Figure 3-22 and Figure 3-23, respectively.

3.4.2 Subsidence Plots

Due to the scarcity of data points, an interpolation scheme is inappropriate for this mine, and thus continuous subsidence plots cannot be created. Instead, subsidence-versus-time graphs were created for each point. Figure 3-24 through Figure 3-29 indicate the locations of the points relative to nearby mine workings, and display the accompanying subsidence graphs. The years where mining took place in the vicinity of each point are highlighted with a vertical line on that point's corresponding graph.

The graphs in the following figures represent consecutive years of measurement. Initially, the point dataset contained gaps of three years in the measurements of points S20 and S21. However, the points' earlier years do not correspond to mining activity, and these years are consequently not considered in the subsidence graphs.

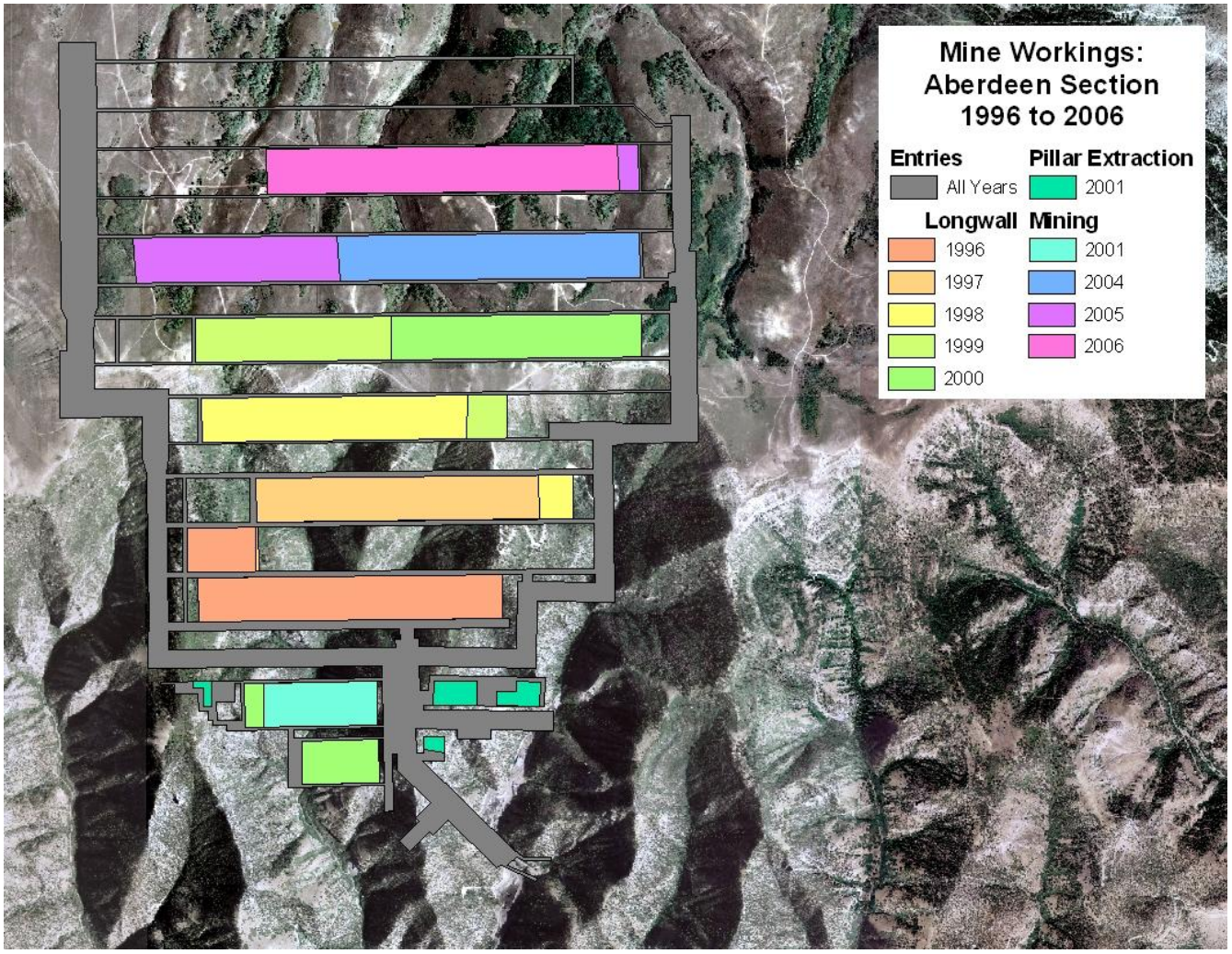

Figure 3-22 Aberdeen Yearly Mine Workings

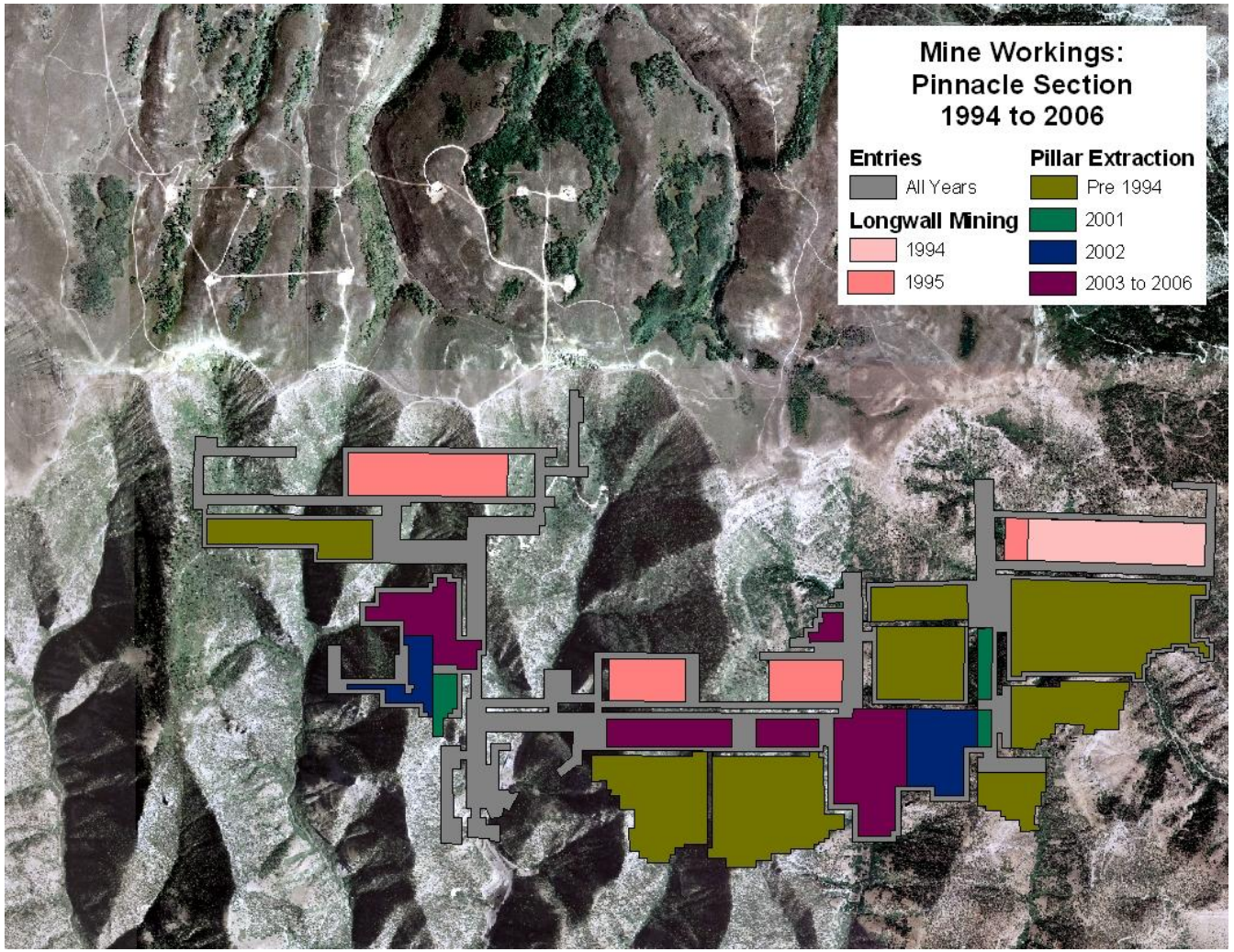

Figure 3-23 Pinnacle Yearly Mine Workings

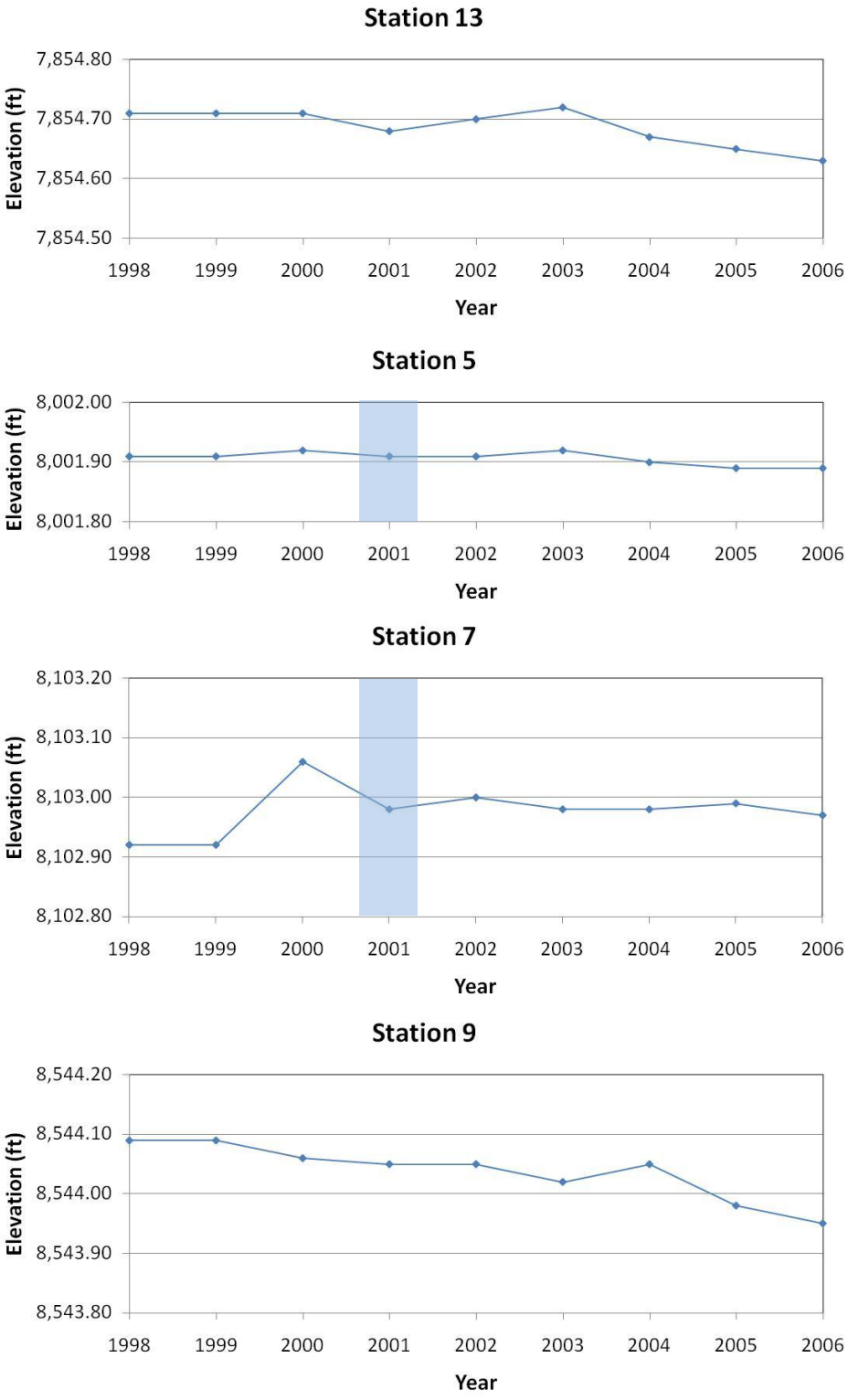

Figure 3-24a Point Elevation Plots

Figure 3-24 Aberdeen Mine Stations 5, 7, 9, & 13

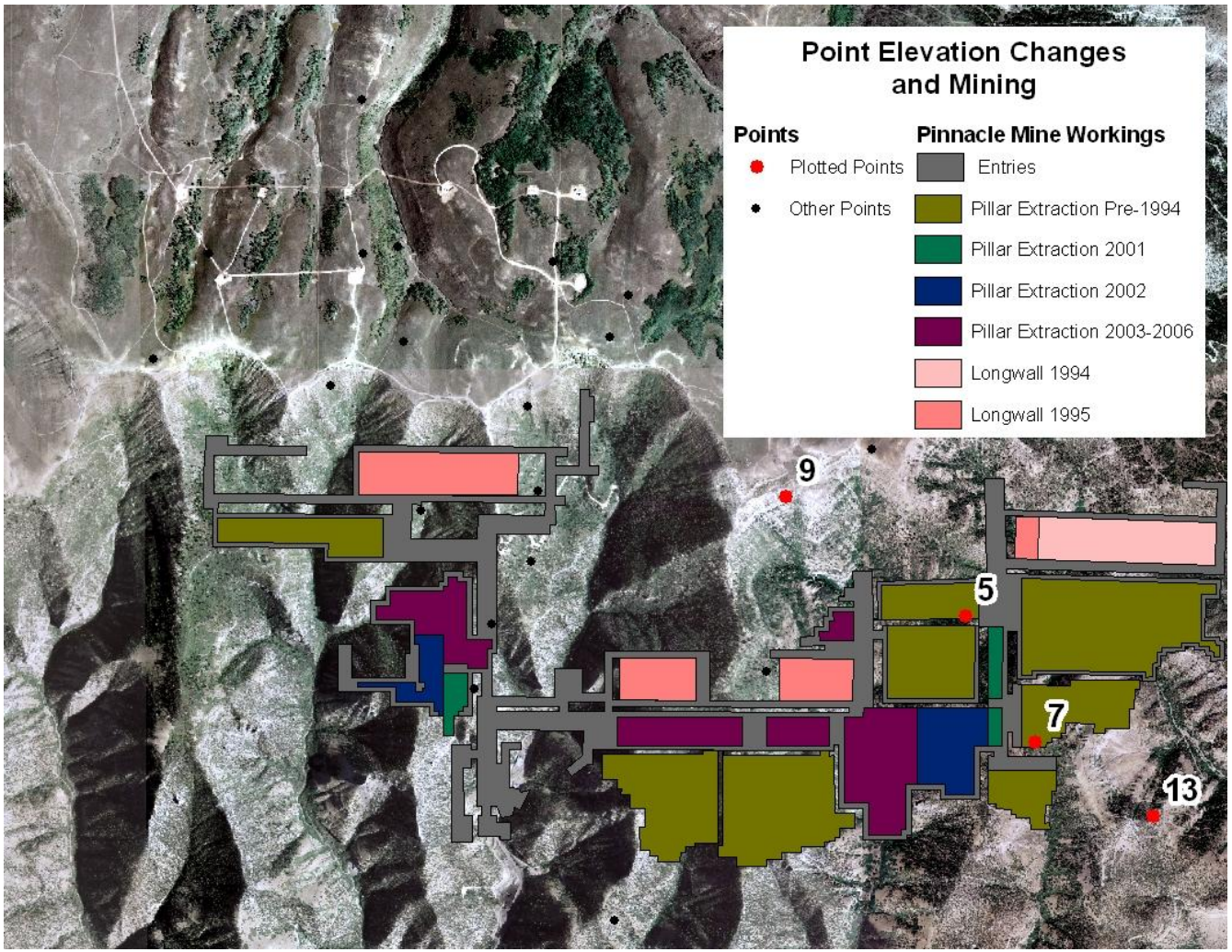

Figure 3-24b Point Locations and Surrounding Mine Workings

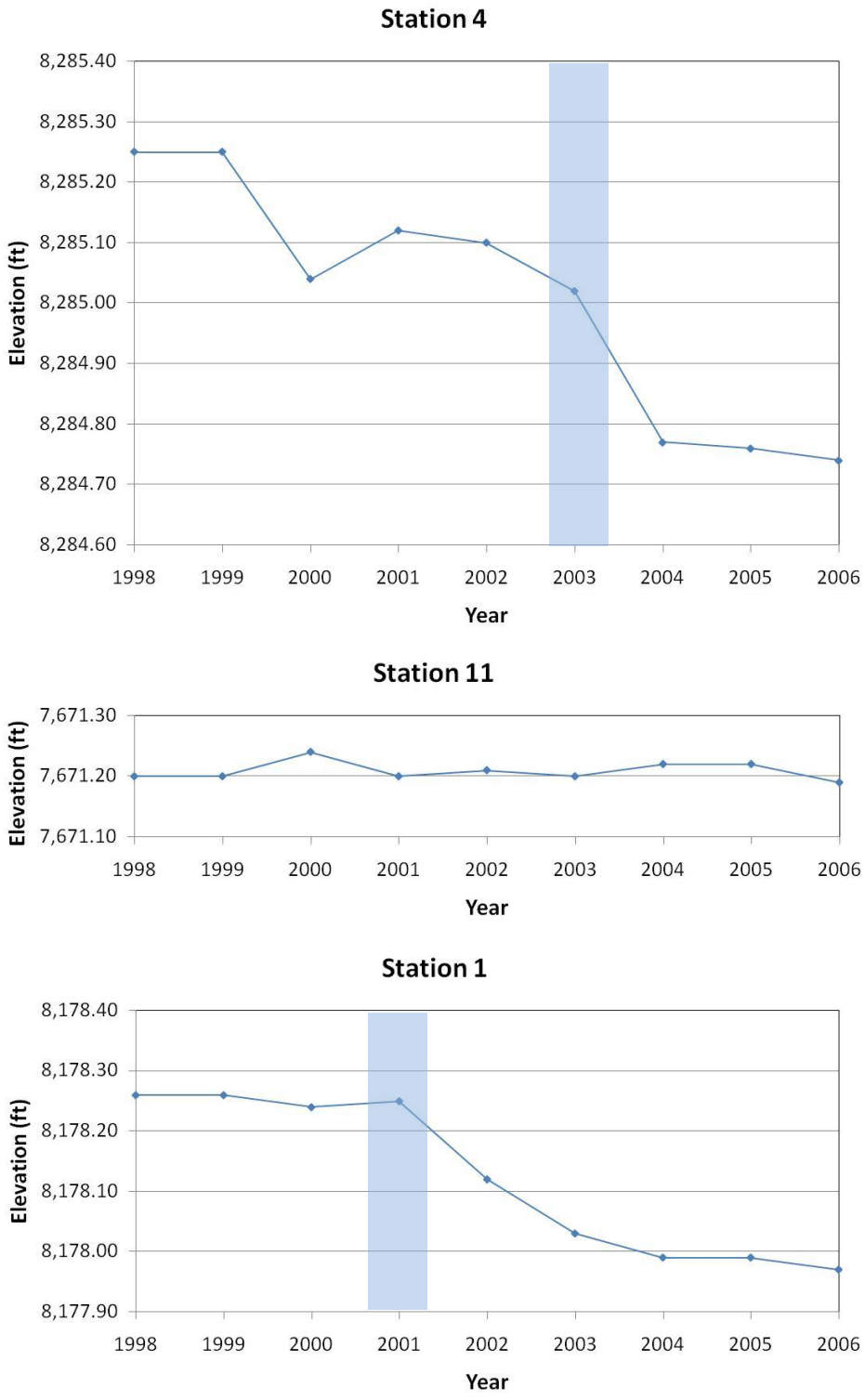

Figure 3-25a Point Elevation Plots

Figure 3-25 Aberdeen Mine Stations 1, 4, & 11

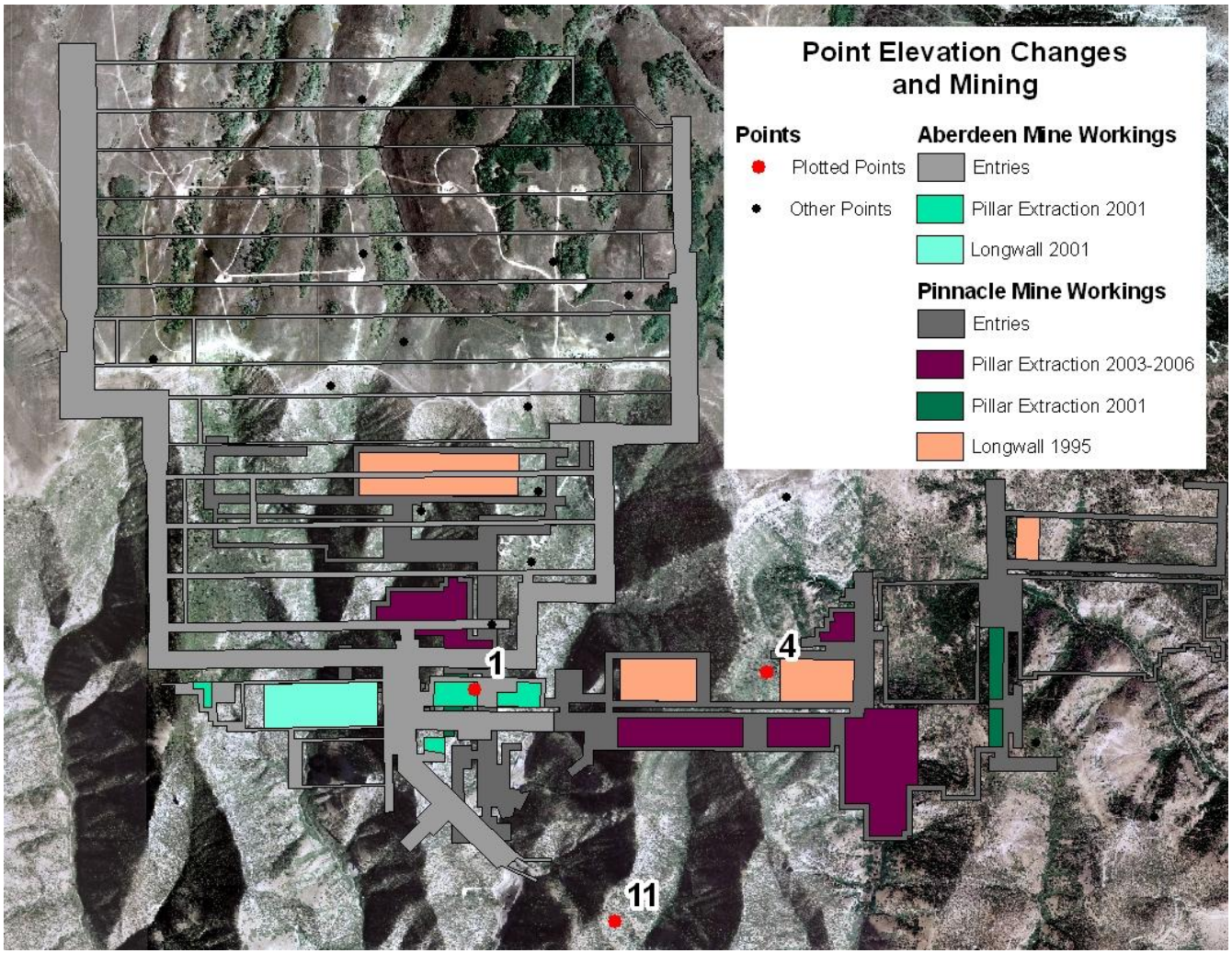

Figure 3-25b Point Locations and Surrounding Mine Workings

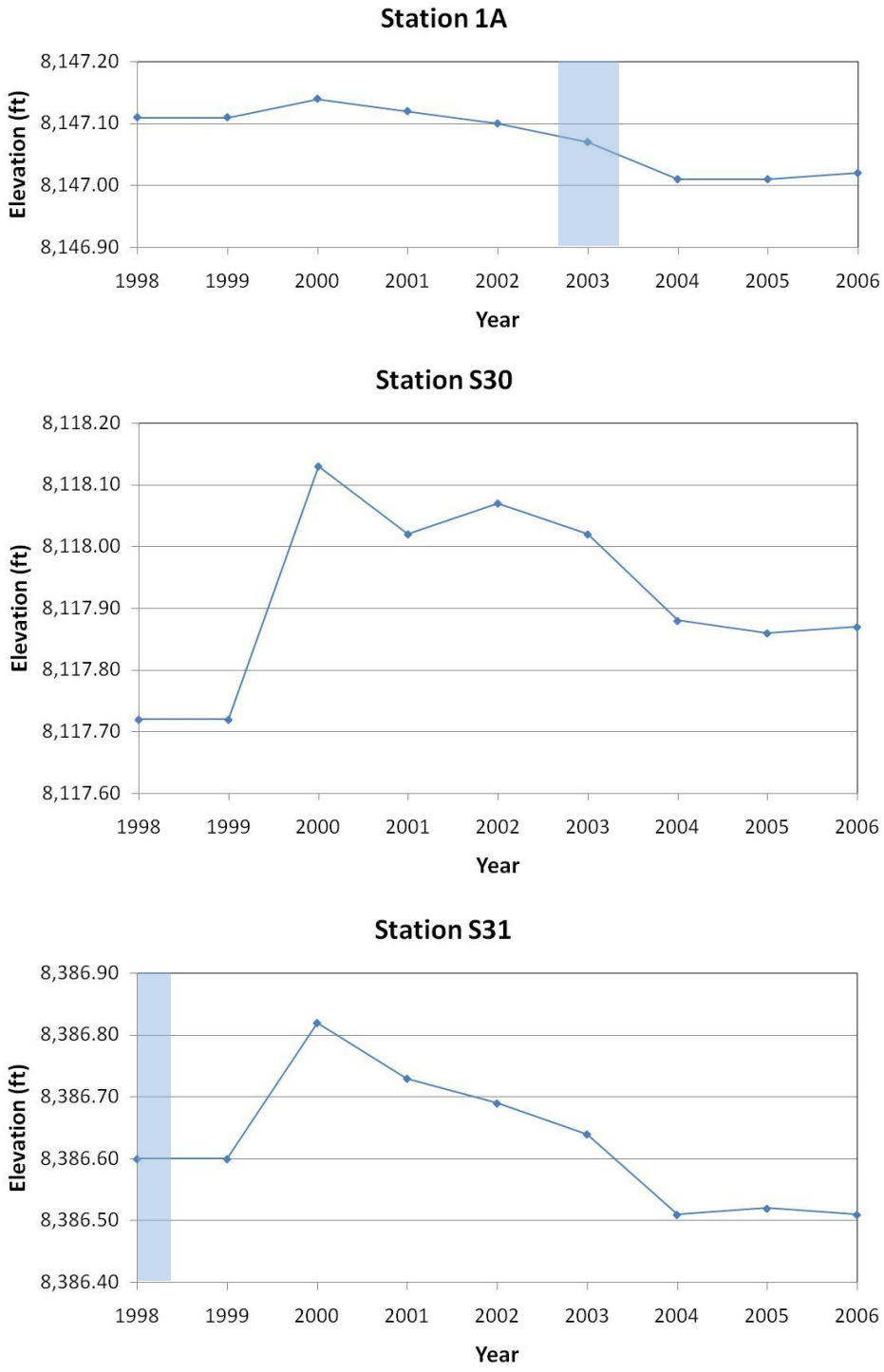

Figure 3-26a Point Elevation Plots

Figure 3-26 Aberdeen Mine Stations 1A, S30, & S31

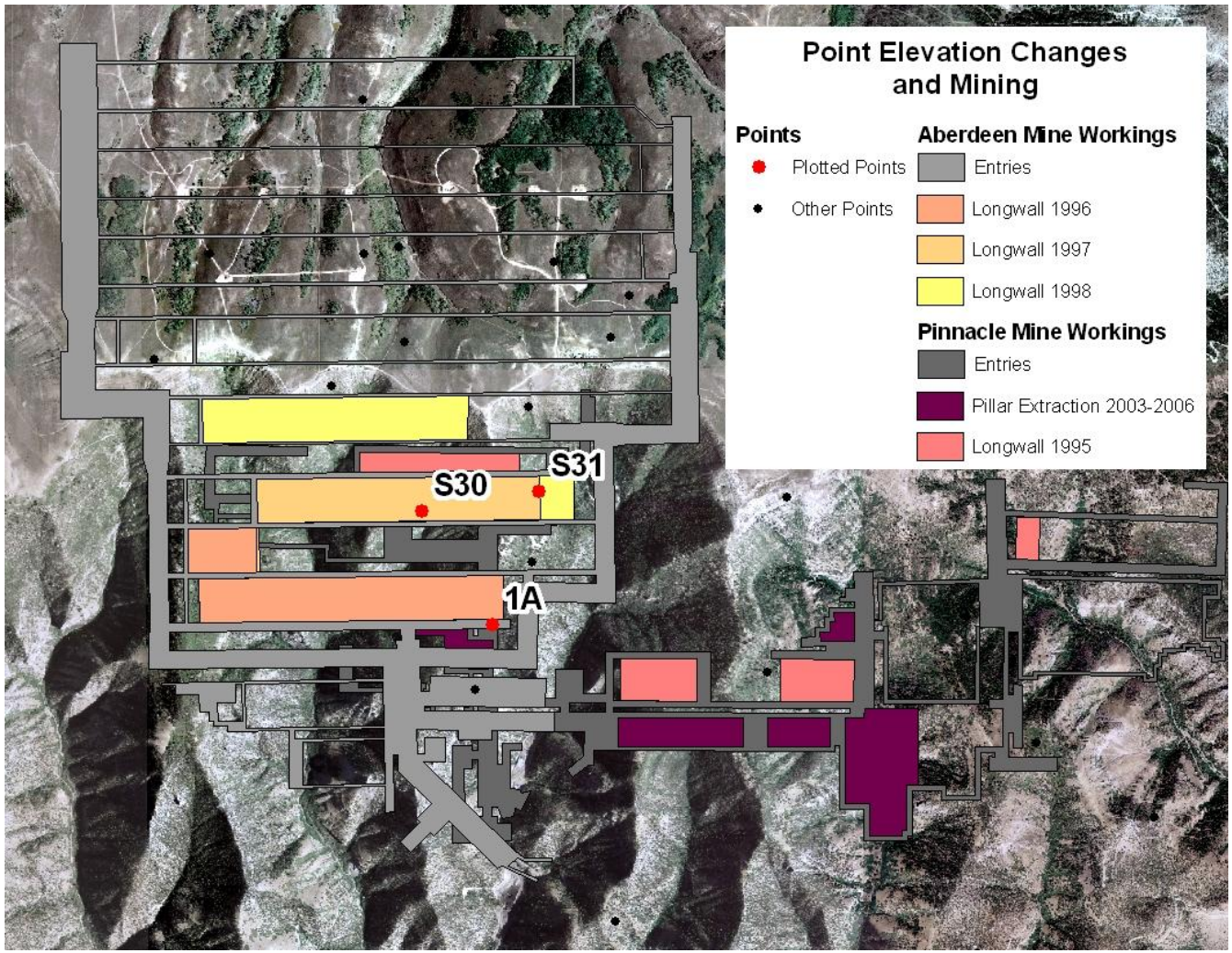

Figure 3-26b Point Locations and Surrounding Mine Workings

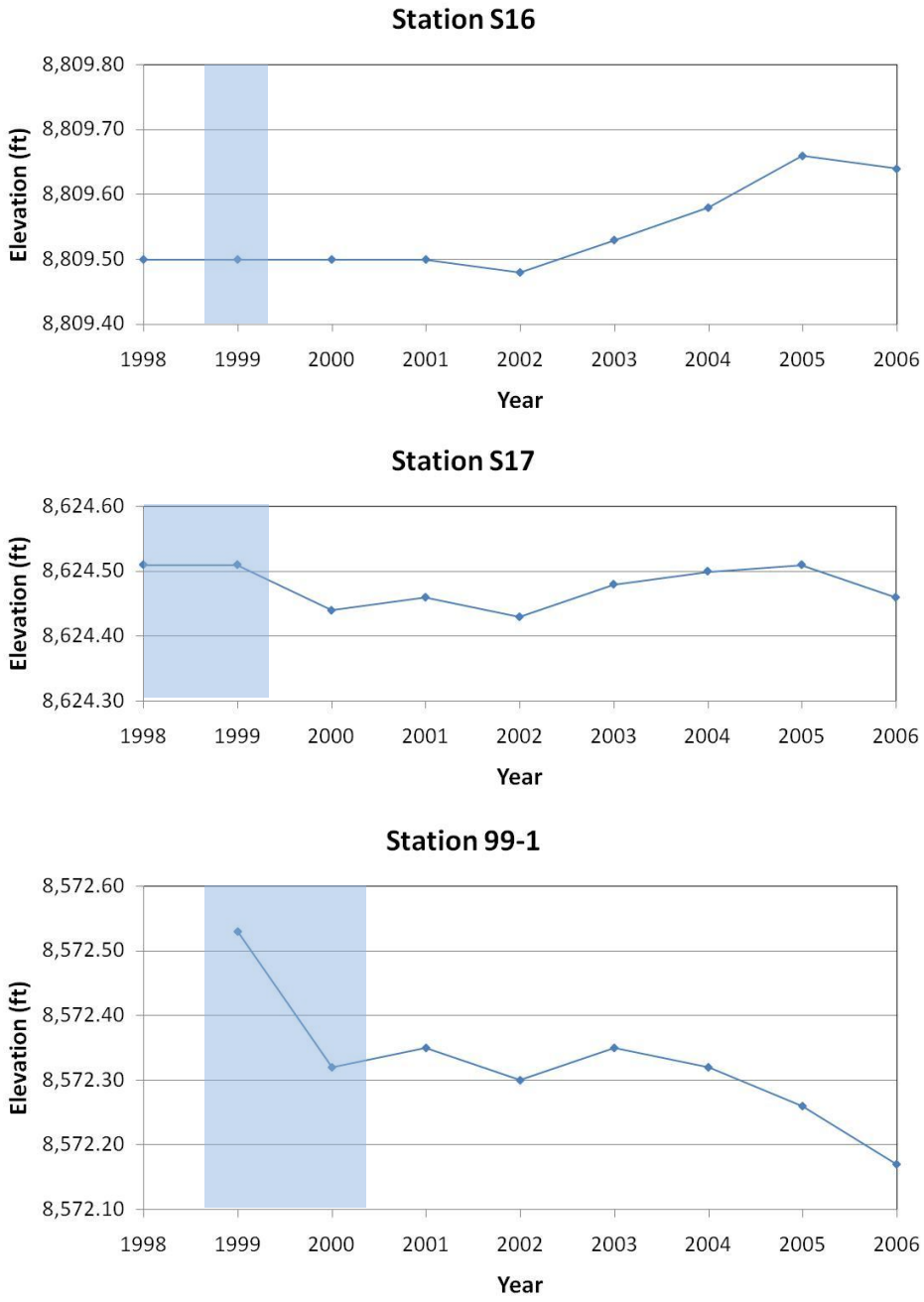

Figure 3-27a Point Elevation Plots

Figure 3-27 Aberdeen Mine Stations S16, S17, & 99-1

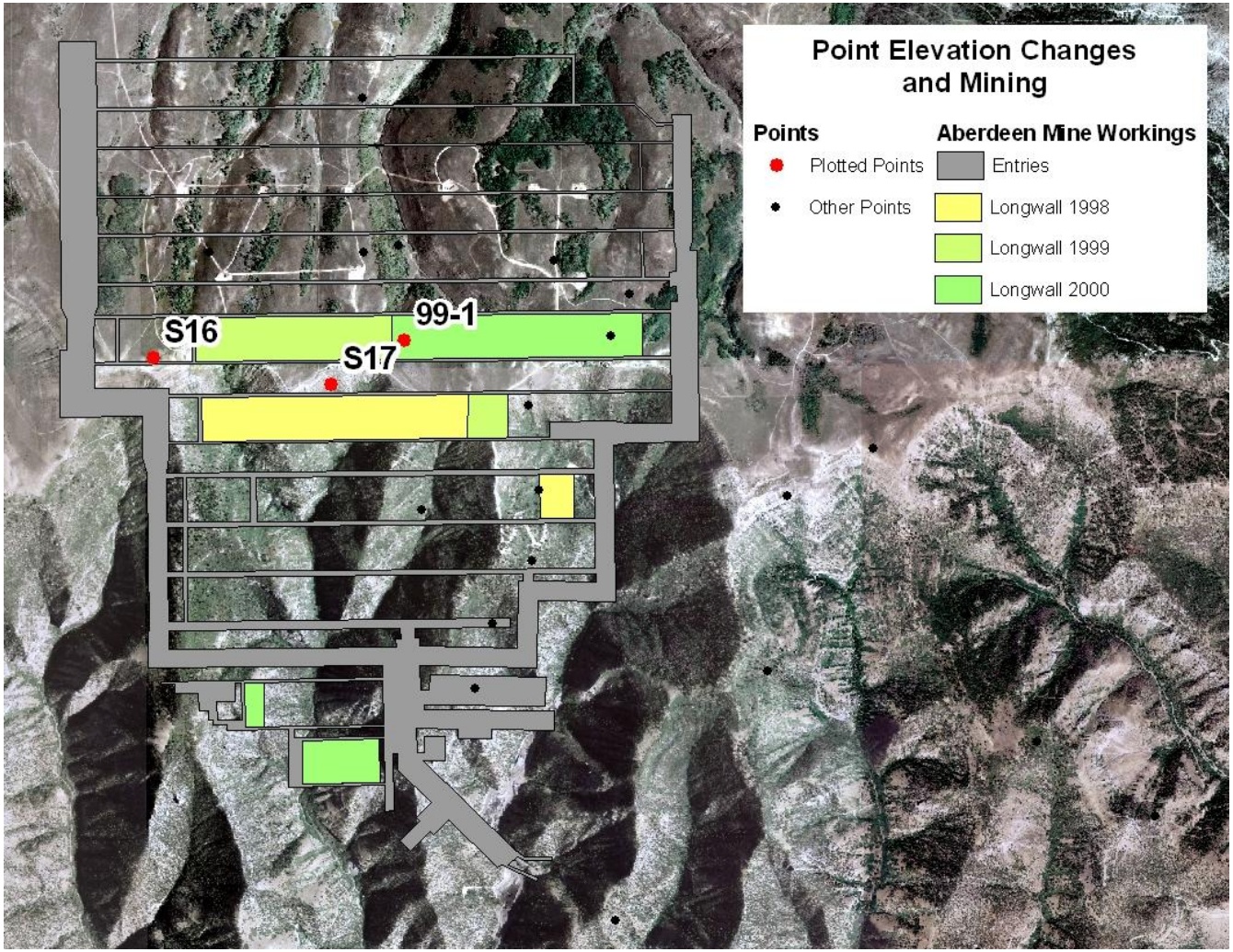

Figure 3-27b Point Locations and Surrounding Mine Workings

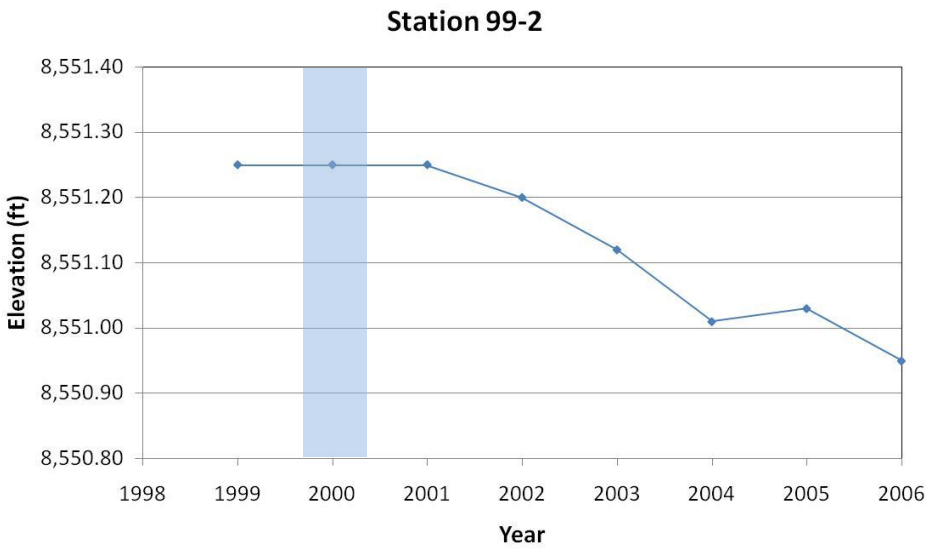

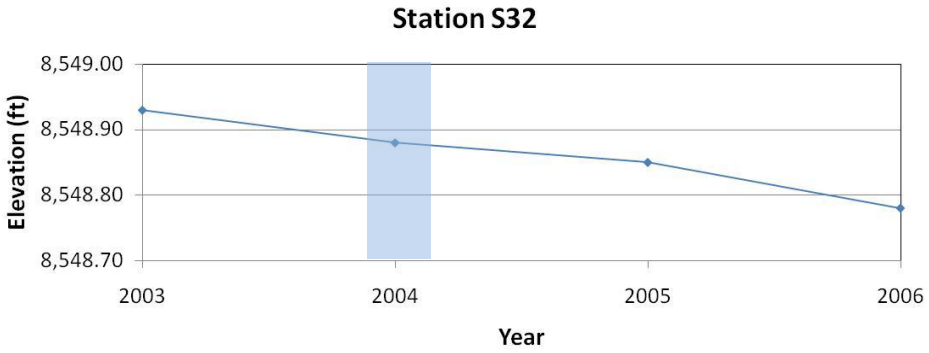

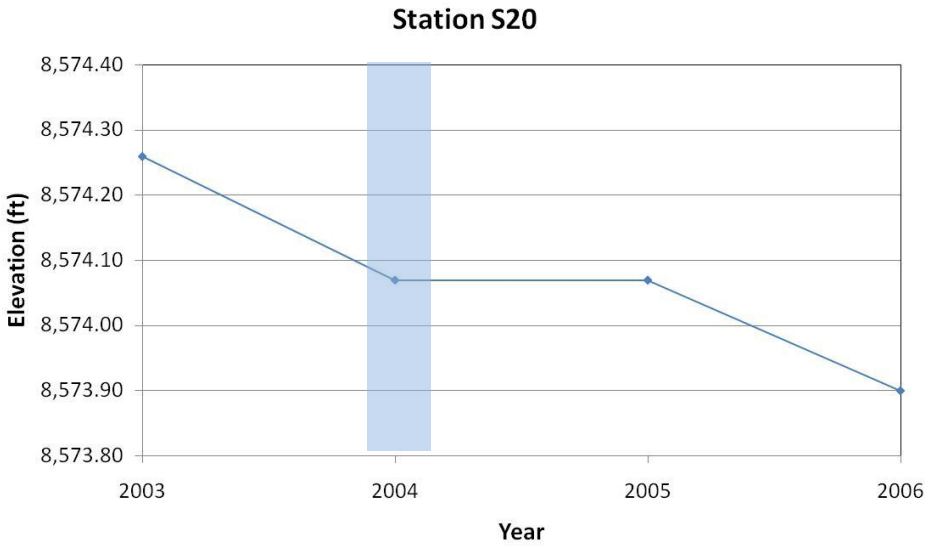

Figure 3-28a Point Elevation Plots

Figure 3-28 Aberdeen Mine Stations 99-2, S32, & S20

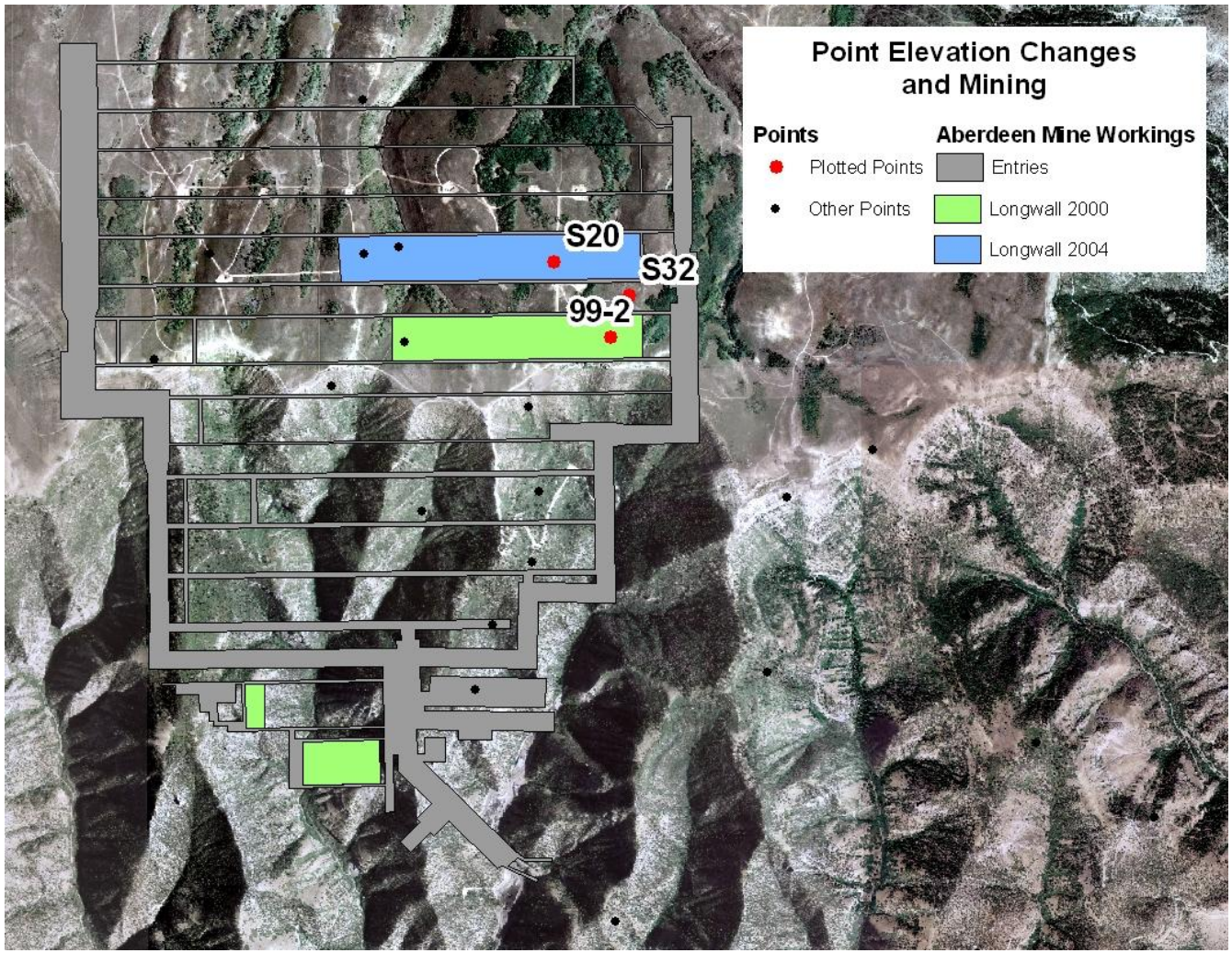

Figure 3-28b Point Locations and Surrounding Mine Workings

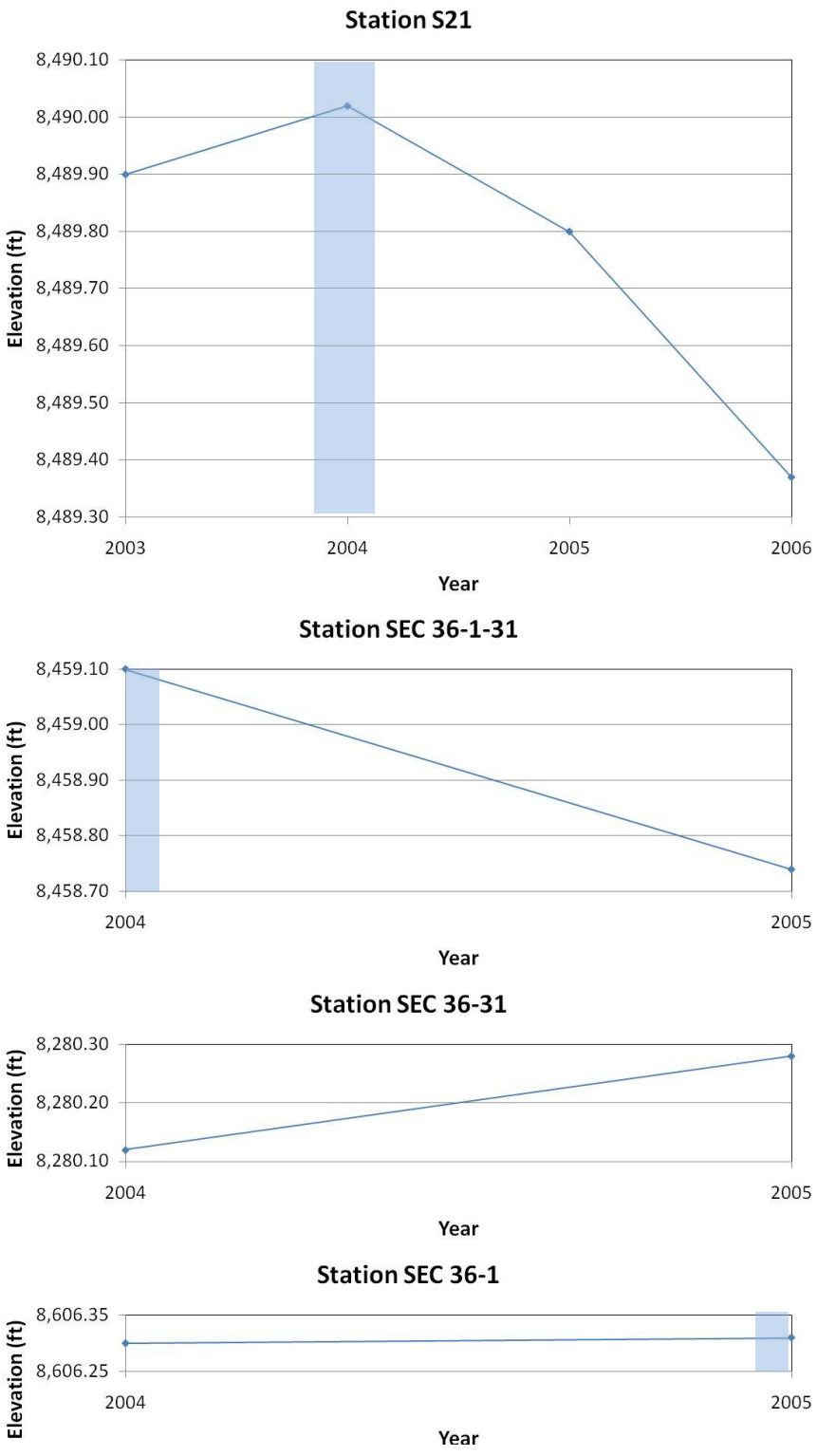

Figure 3-29a Point Elevation Plots

Figure 3-29 Aberdeen Mine Stations S21, SEC 36-1-31, SEC 36-31, & SEC 36-1

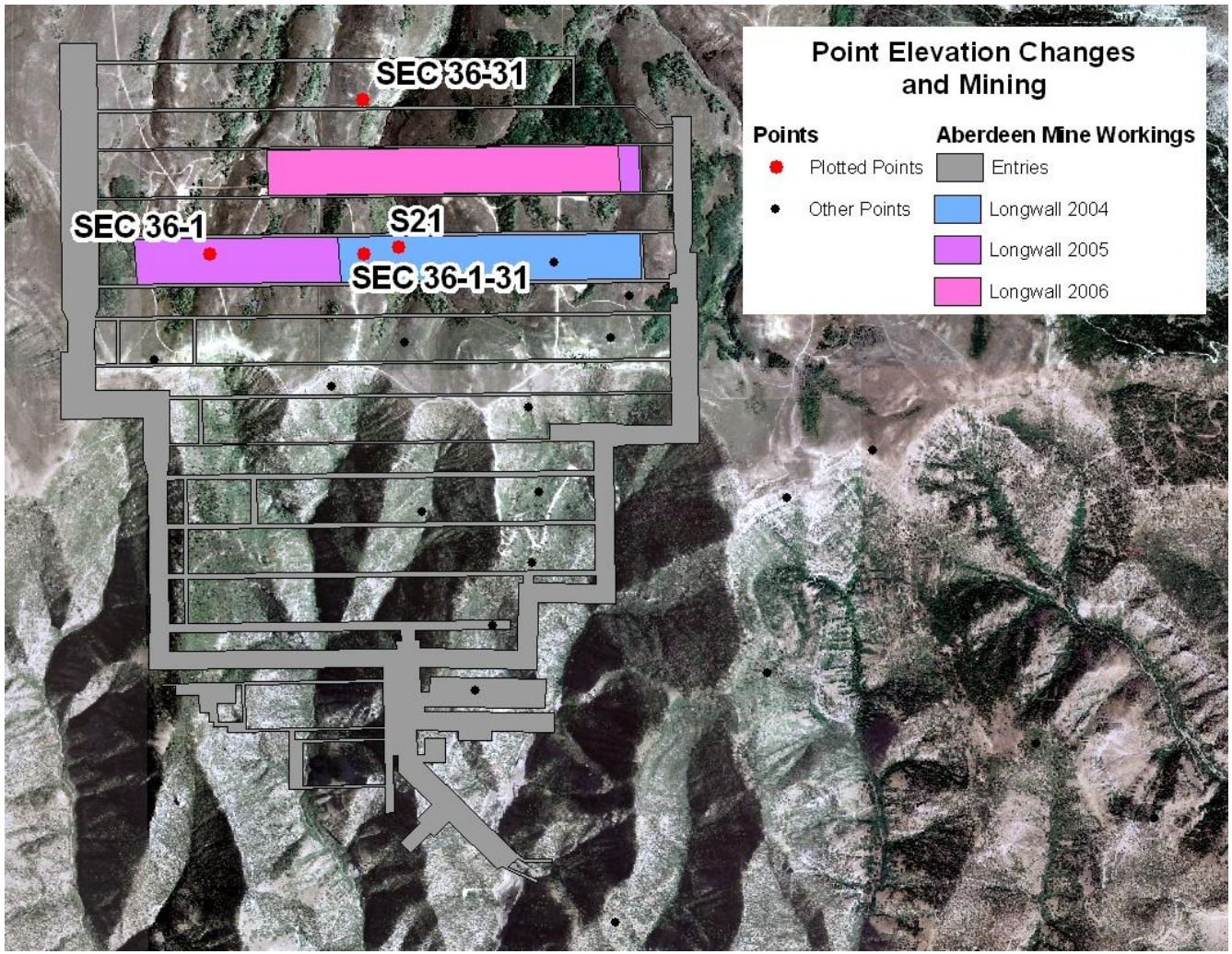

Figure 3-29b Point Locations and Surrounding Mine Workings

4 Modeling Subsidence

The modeling method developed in this study, entitled the Type-Xi Integration method (TXI method), uses subsidence plots to enhance previous subsidence profiling methods, which profiling methods are described in Section 4.1. These profiling methods were developed for the British coal fields, and are taken from an article written by Gerhard Brauner [3].

The TXI method is based on a geometric method which is also given by Brauner in his article. The development and explanation of this previous method is repeated in Section 4.2 of this study. The TXI method developed by the author improves upon the previous method. The TXI method's development and application are described in Section 4.3.

4.1 Subsidence Profiles

A subsidence profile is a function or a set of functions which map the vertical subsidence over a mine. Profiles are typically two-dimensional, and thus correspond to a cross section of the mine. This cross section can be either parallel or perpendicular to the direction of longwall mining. Both cases are considered in this study.

Subsidence profiles are based on a geometric method, and consequently do not receive geological data directly. The geology of the area is captured in several input parameters. Specifically, these parameters are the limit angle (γ), the subsidence factor (a), the height of overburden (h), and the coal seam thickness (m).

The limit angle is measured at the edge of a longwall panel, from a level parallel to the mine roof, to the point where vertical subsidence is no longer discernible on the surface (see Figure 4-1). The subsidence factor relates the maximum subsidence (S_{max}) to the coal seam thickness according to

$$S_{max} = a \cdot m \quad \textbf{(4-1)}$$

The subsidence factor varies among mines, and is usually back-calculated from Equation 4-1. It may be interpreted as representing the ratio of seam thickness to maximum vertical ground movement. The subsidence factor used in predicting maximum subsidence for a new mine typically corresponds to that measured from similar mines which have already subsided.

Another important input parameter is the critical radius (B). The critical radius is calculated using the overburden depth and limit angle, via

$$B = h/\tan(\gamma) \quad \textbf{(4-2)}$$

The critical radius B may be described as one-half of the cave length which will produce the maximum subsidence at one and only one point. Alternatively, it may be described as half the distance from the area where maximum subsidence occurs to the area where no

subsidence occurs. Figure 4-1 illustrates the subsidence profile and associated parameters (not to scale).

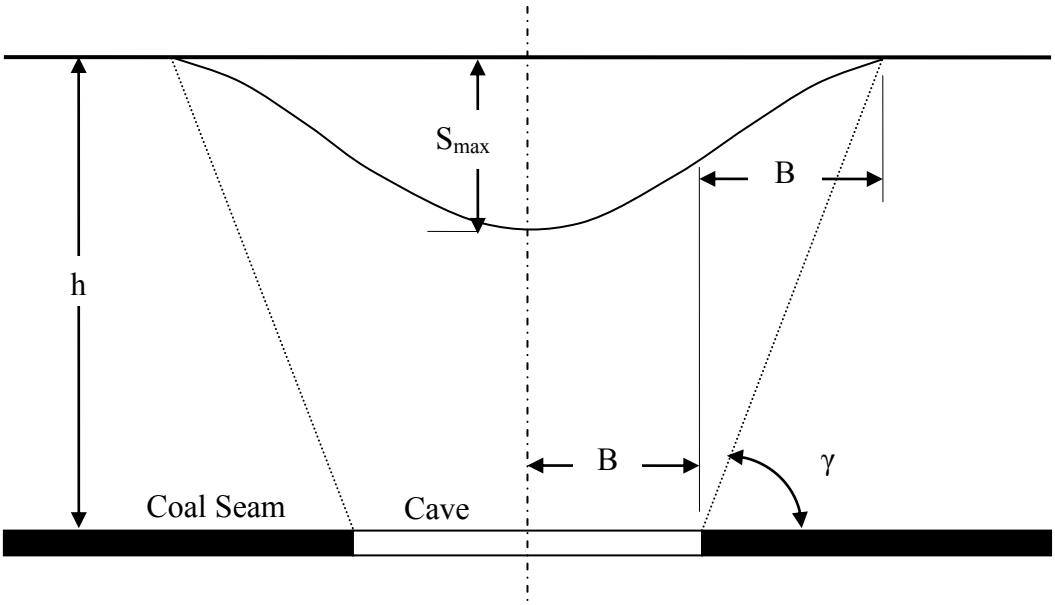

Figure 4-1 Typical Subsidence Profile

In the case of multiple coal seams, the maximum subsidence is determined using the principle of superposition. This principle states that the subsidence at a surface point is equal to the sum of the subsidences calculated considering each seam separately:

$$S_{total} = a \sum_{i=1}^{k} m_i \quad \textbf{(4-3)}$$

where

S_{total} = total subsidence at a given point

k = total number of coal seams

m_i = thickness of i^{th} coal seam

4.2 Function Modeling

This study considers two different approaches to using the geometric method to model subsidence. The first approach is based in profile functions, while the second is based on influence functions. Each method is discussed in the article by Brauner [3] and the relative benefits of each are compared therein. The two methods will be briefly presented in the following sections.

4.2.1 Profile Functions

"A subsidence profile function is an equation of one-half of the subsidence profile" (see [3], p.10). The criteria for this equation are

- The subsidence profile must be equal to or very near zero at the limit angle
- The subsidence profile is at a maximum in the middle of the cave
- Half of the maximum subsidence occurs at the critical radius

Figure 4-2 is an example of a profile function which satisfies the above criteria.

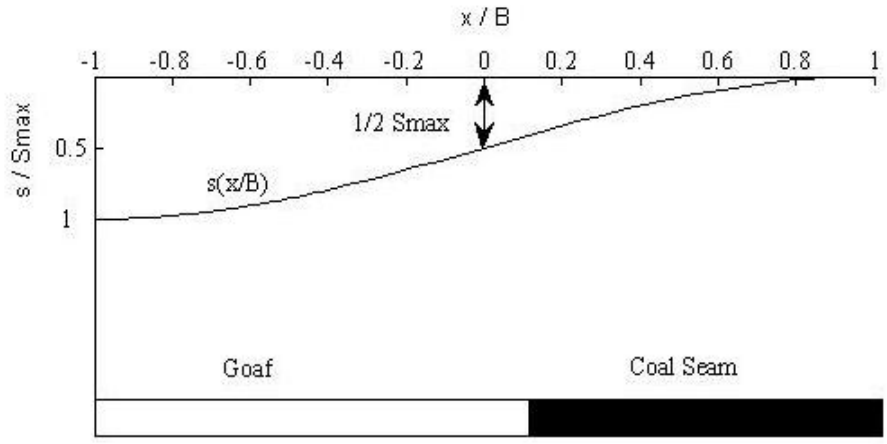

Figure 4-2 Typical Profile Function

As Figure 4-2 illustrates, a profile function is constructed such that the inflection point occurs at the origin.

Profile functions are useful for modeling a single longwall panel that is isolated from other longwall panels by coal barriers left in place during mining. The layout for Aberdeen follows this pattern (see Figure 3-22). Thus, profile functions would be appropriate for modeling this mine. Due to the scarcity of survey data points, however, the benefits of the TXI method cannot be implemented, and thus a subsidence profile for Aberdeen Mine was not created in this study.

4.2.2 Influence Functions

Influence functions are constructed using an application of the principle of superposition (see Section 4.1). This application states that the total subsidence of a given point on the surface results from the superposition of subsidences from "influence areas." The influence areas are all areas of the cave which are within a certain radius of the surface point. It can be shown that this radius is equal to the critical radius, B (see [3], p.17).

The contribution of a particular area within the cave is based on the radial distance (r) of that area to the point of interest. The relationship between relative influence and distance is established by an influence function, P, which is centered with the origin at the point of interest. Influence functions are related to profile functions in that the influence function is a maximum over the point of interest, and zero at and beyond the critical radius. Thus, it can be said that an influence function spans the area

of influence, and is equal to zero outside of this area. The influence function used in this study, obtained from page 19 of [3] is

$$P(r) = \frac{3}{\pi}\frac{S_{max}}{B^2}\left[1 - \left(\frac{r}{B}\right)^2\right]^2 \quad \textbf{(4-4)}$$

This equation is plotted in Figure 4-3.

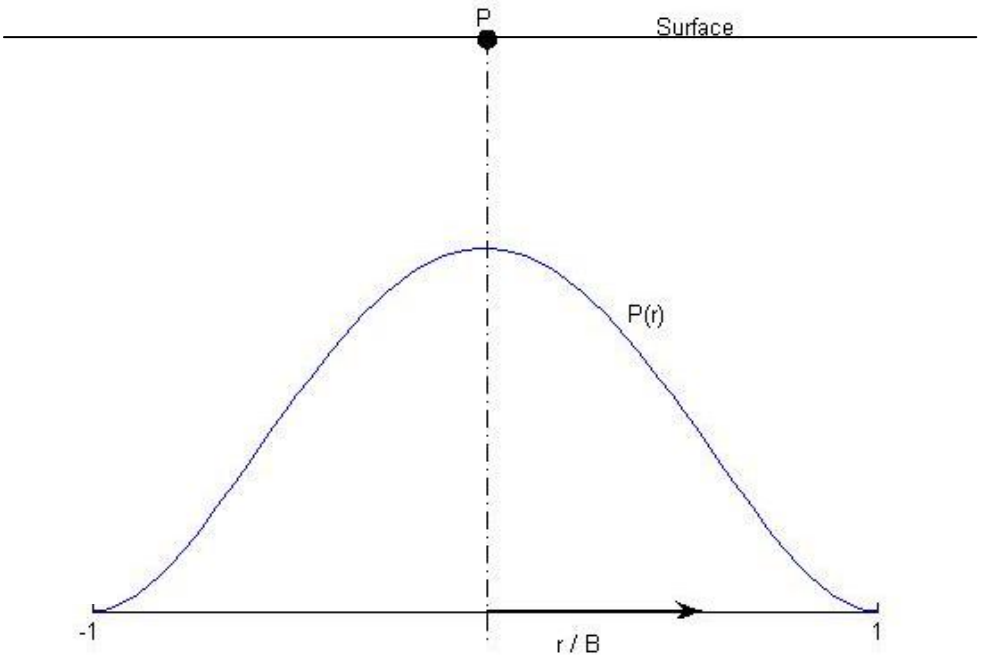

Figure 4-3 Influence Function from Equation 4-4

If we subdivide the influence area into infinitesimal areas dA, then the subsidence (S) at the point of interest is the sum of the influences of all dA. This summation is found by integrating the influence function over the area of influence, according to

$$S = \iint P(r)dA \quad \textbf{(4-5)}$$

This integration may be performed directly using cylindrical coordinates if the area of influence is simply a circle within the cave (i.e. the critical radius does not extend beyond the width or length of the longwall panel). For points near the edge of the longwall length, however, the critical radius extends beyond cave boundaries, and the left or right bounds of the integration area are no longer simply a circle. In this case, the integration is more effectively performed in rectangular coordinates. The radial cylindrical coordinate is thus transformed to rectangular coordinates ξ and η using

$$r^2 = \xi^2 + \eta^2 \tag{4-6}$$

where ξ and η correspond to orthogonal axes parallel and perpendicular, respectively, to the direction of longwall mining.

Substituting Equation 4-6 into Equation 4-4 yields

$$P(\xi,\eta) = \frac{3}{\pi}\frac{S_{max}}{B^2}\left[1 - \left(\frac{\xi}{B}\right)^2 - \left(\frac{\eta}{B}\right)^2\right]^2 \tag{4-7}$$

and substituting Equation 4-7 into Equation 4-5 yields

$$S = \frac{3}{\pi}\frac{S_{max}}{B^2}\iint \left[1 - \left(\frac{\xi}{B}\right)^2 - \left(\frac{\eta}{B}\right)^2\right]^2 d\eta d\xi \tag{4-8}$$

By setting B equal to 1, Equation 4-8 can be simplified to

$$S = \frac{3}{\pi}S_{max}\iint [1 - (\xi)^2 - (\eta)^2]^2 d\eta d\xi \tag{4-9}$$

where values of ξ and η now represent fractions of the critical radius.

4.3 The Type-Xi Integration Method

Equation 4-9 is effective for longwall panels where the critical radius does not extend beyond the panel's width. It also accounts for the ends of the longwall panels, wherein the left or right bound of the first integral corresponds to the face of the panel. However, Equation 4-9 does not account for the presence or absence of adjacent longwall panels. If the crticial radius extends beyond the *width* of the longwall panel into unmined regions, the equation will overpredict subsidence.

The Type-Xi Integration method (TXI method) was developed by the author principally to handle the geometric irregularities caused by presence or absence of adjacent panels within a point's area of influence. These irregularities prevent a direct integration of Equation 4-9; thus, the TXI method uses a modified version of this equation. The TXI method makes several additional modifications to the previous method, which are presented in Table 4-1.

Table 4-1. Comparison of Previous Method to TXI Method

Previous Method	TXI Method
• Does not account for irregular mine geometry	• Accounts for remaining coal pillars and adjacent caves
• Considers a flat surface above the mine	• Considers a sloping surface above the mine
• Uses a constant (average) critical radius	• Uses variable critical radii, measured from overburden
• Uses a constant (average) seam thickness	• Uses variable seam thicknesses, taken from panel measurements

4.3.1 TXI Method Development

As mentioned in the Section 4.2, the critical radius often extends beyond the cave boundaries, either into adjacent caves or into unmined areas. As only the cave contributes to subsidence, Equation 4-9 should be integrated over only the cave areas within the area of influence, as shown in Figure 4-4. The previous integration method discussed in Section 4.2.2, however, integrates over the entire area between the ends of the longwall panels or area of influence, as illustrated in Figure 4-5.

In order to integrate over only the cave areas (shown as hatched areas in Figure 4-4) the cave areas with the area of influence are divided into their respective longwall panels. Each panel's boundaries are defined according to four input parameters, as shown in Figure 4-6 (main panel) and Figure 4-7 (adjacent panels).

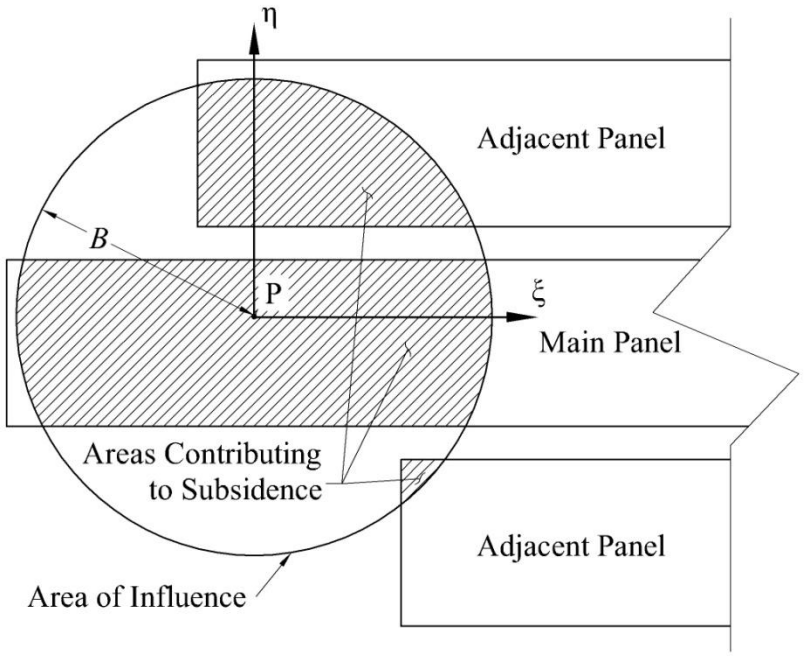

Figure 4-4 Cave Regions within Area of Influence

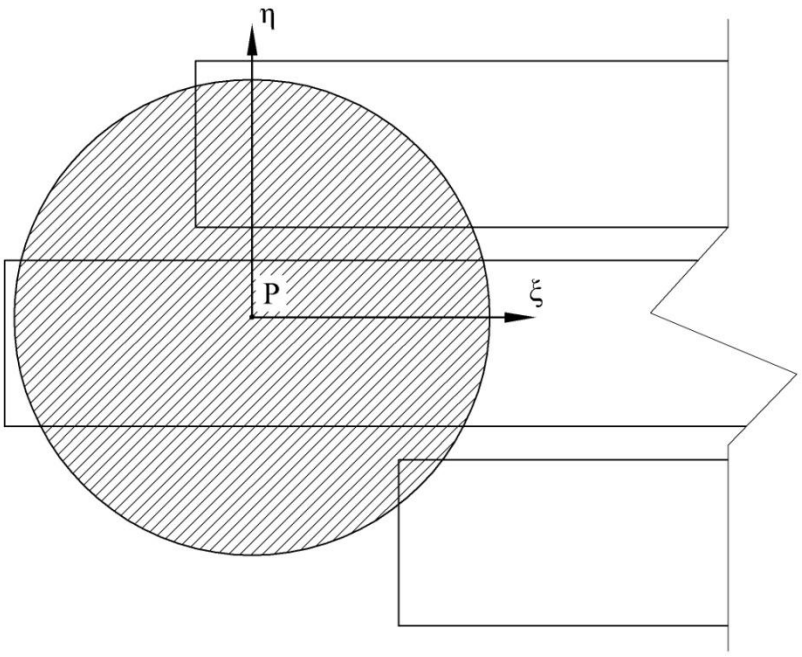

Figure 4-5 Area Integrated in Previous Method

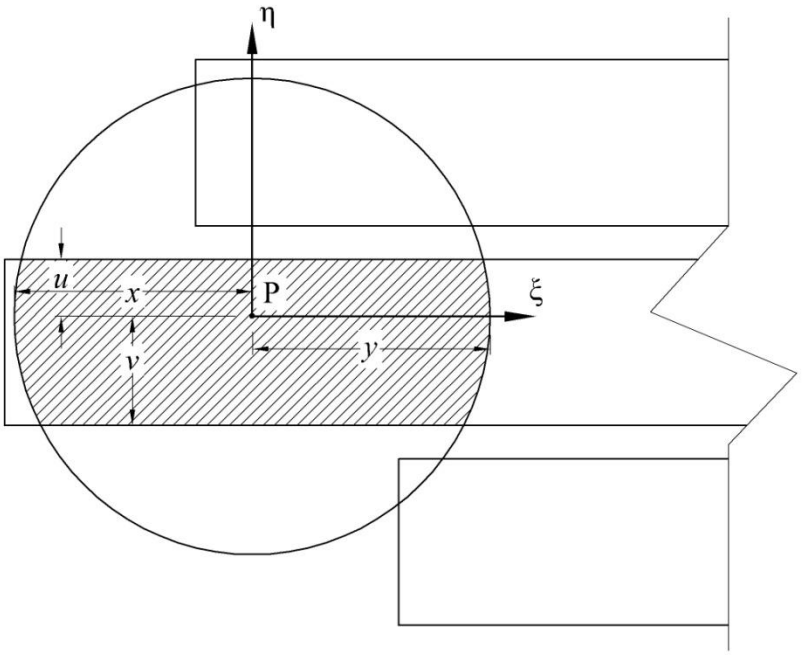

Figure 4-6 Parameters Defining Boundaries of Main Panel

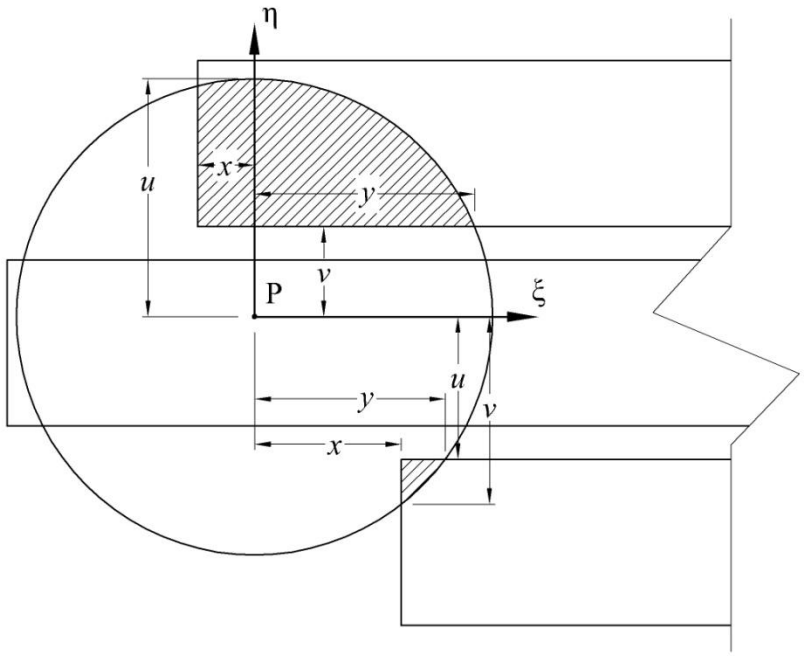

Figure 4-7 Parameters Defining Boundaries of Adjacent Panels

The parameters *u*, *v*, *x*, and *y* from Figure 4-6 and Figure 4-7 are used to subdivide each panel into "type ξ" regions, as shown in Figure 4-8. These regions, in which left and right integration limits are constants, are analogous to "type x" regions used in evaluating double integrals in Cartesian coordinates [20]. The four parameters define the distance from the point of interest to the integration boundaries. These boundaries are either the extents of the area of influence, or the edges of the longwall panel. The values of the four parameters vary from -1 to 1. Using these parameters, Equation 4-9 becomes

$$S = \int_x^a \int_{-e}^{e} \varphi + \int_a^b \int_f^g \varphi + \int_b^c \int_v^u \varphi + \int_c^d \int_f^g \varphi + \int_d^y \int_{-e}^{e} \varphi \qquad \textbf{(4-10)}$$

where

$$\varphi = P(\xi,\eta)d\eta d\xi = \frac{3}{\pi} S_{max}[1-(\xi)^2-(\eta)^2]^2 d\eta d\xi \qquad \textbf{(4-11)}$$

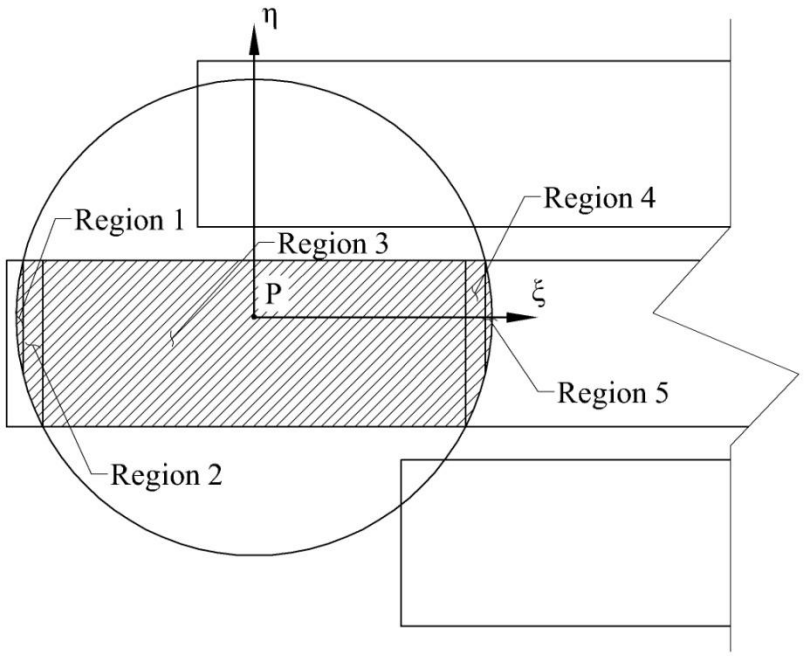

Figure 4-8 Subdivision of Main Panel into Regions

The integration limits *a*, *b*, *c*, and *d*, corresponding to the first integral of the terms in Equation 4-10, are determined as outlined in Figure 4-9. In this algorithm, α and β are the smaller and larger magnitudes respectively of u and v (e.g. if $|u| < |v|$ then $\alpha = u$ and $\beta = v$). The integration limits *e*, *f*, and *g*, corresponding to the second integrals of the terms, are defined as follows: The limit *e* is a function of ξ, as given in Equation 4-12, and the limits *f* and *g* are equal to *e*, *u*, or *v*, as determined by Equations 4-13 and 4-14.

$$e = \sqrt{1 - \xi^2} \tag{4-12}$$

$$f = \begin{cases} -e & \text{if } |u| \leq |v| \\ v & \text{if } |u| > |v| \end{cases} \tag{4-13}$$

$$g = \begin{cases} u & \text{if } |u| \leq |v| \\ e & \text{if } |u| > |v| \end{cases} \tag{4-14}$$

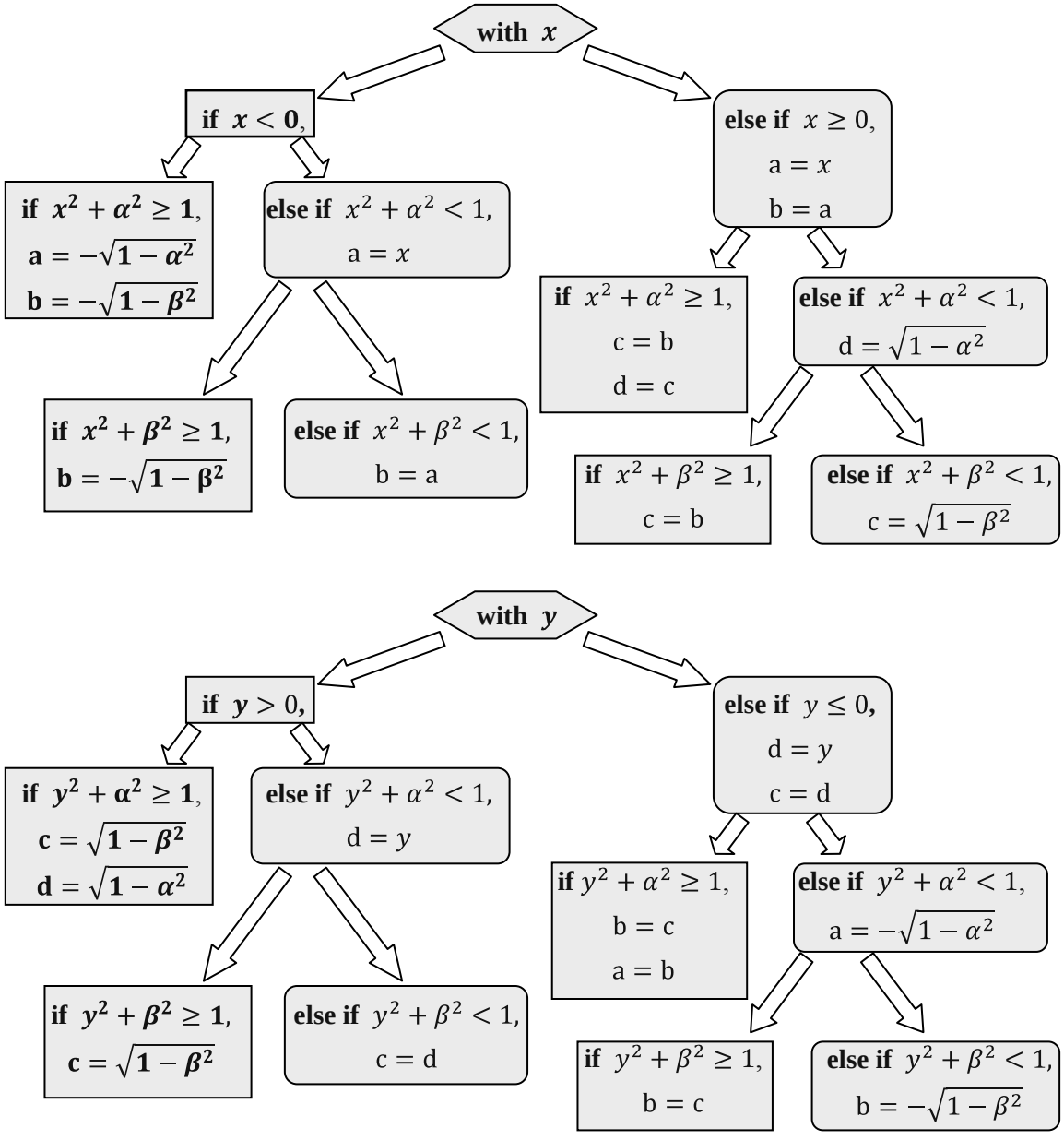

Figure 4-9 Algorithm Defining Integration Limits *a*, *b*, *c*, and *d*

As the preceding explanation implies, the integration limits of the integrals in Equation 4-10 depend upon the relative magnitudes of the four parameters shown in Figure 4-6 and Figure 4-7. The expansion of Equation 4-9 into Equation 4-10 and the creation of the algorithm in Figure 4-9 are necessary due to varying interactions of longwall panel edges and the area of influence to form the cave boundary conditions from one point to the next.

Consider the cave regions shown in Figure 4-8. These regions are formed by inputting the parameters from Figure 4-6 into the algorithm in Figure 4-9. Regions 1 to 5 correspond to the first to fifth terms, respectively, in Equation 4-10. The upper and lower bounds for Regions 1 and 5 are both functions of ξ. In contrast, the upper and lower bounds of Region 3 are constant, equal to u and v, respectively. Regions 2 and 4 have upper and lower bounds, one of which is constant and one of which is a function of ξ, which depend on the criteria given in Equation 4-13 and Equation 4-14.

In conclusion, each of the five possible regions shown in Figure 4-8 may or may not be created for a particular panel of a given point, depending on cave geometry within the area of influence. The TXI algorithm in Figure 4-9 uses the relative values of u, v, x, and y to determine which regions apply to the analysis of the panel. The algorithm is applied to each panel within each seam's area of influence, and the point's total subsidence is the superposition of the resulting subsidences.

4.3.2 TXI Method Application

The TXI method is demonstrated in this section using data provided by Deer Creek Mine, due to its high consistency and accuracy (see Chapter 3 for a description of

Deer Creek Mine characteristics). The methods described in Chapter 2 were applied to this mine to obtain subsidence and elevation plots. These plots serve three main purposes in the TXI method. The plots:

1. provide surface elevation data used to calculate overburden
2. facilitate visualization of mine workings relative to terrain
3. furnish measured subsidence profiles used as a basis for comparison

The use of subsidence and elevation plots with the TXI method is further described in the following sections.

4.3.2.1 Cross Sections

The elevation and subsidence plots were used to create four cross sections of the Deer Creek Mine. The first two cross sections are oriented west to east, parallel to the longwall lengths; the remaining two are oriented north to south, perpendicular to the longwall lengths. Both orientations have one cross section positioned in the middle of the mine workings, with the other on the edge. The locations of these four cross sections relative to the mine workings are shown in Figure 4-10.

Two sets of profiles were created along each cross section shown in Figure 4-10 using a line interpolating tool in ArcGIS. This tool creates data points which store values of either a raster or vector surface (see Section 2.2.1). The data points begin at Station zero and continue incrementally at 20 foot intervals along the line. The first profile set, shown in Figure 4-11, was created from a terrain vector surface and represents overlying ground topography. The second profile set, shown in Figure 4-12, was created from a subsidence raster surface, and represents elevation differences from 1999 to 2006.

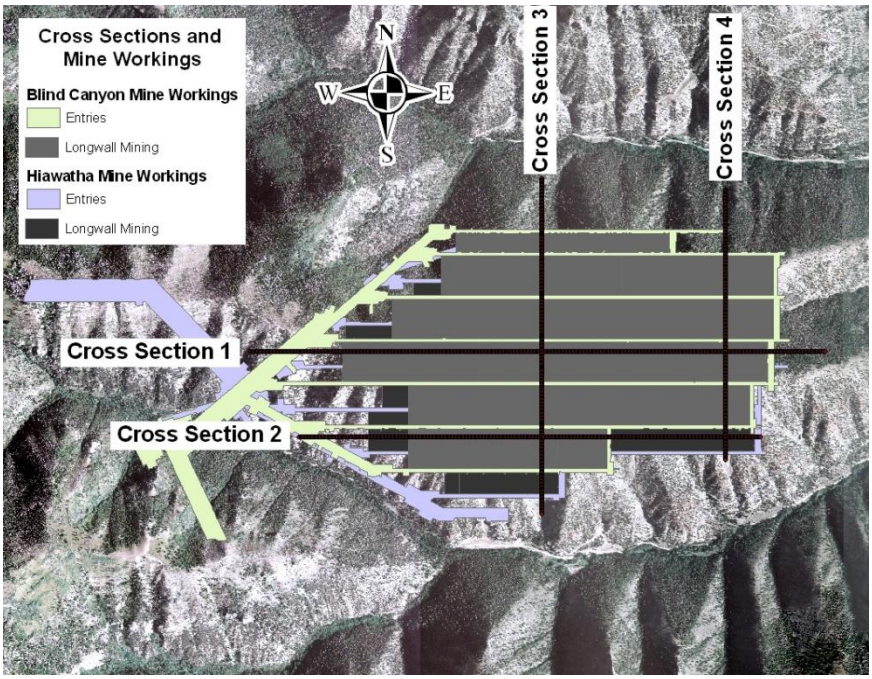

Figure 4-10 Cross Sections Relative to Mine Layout

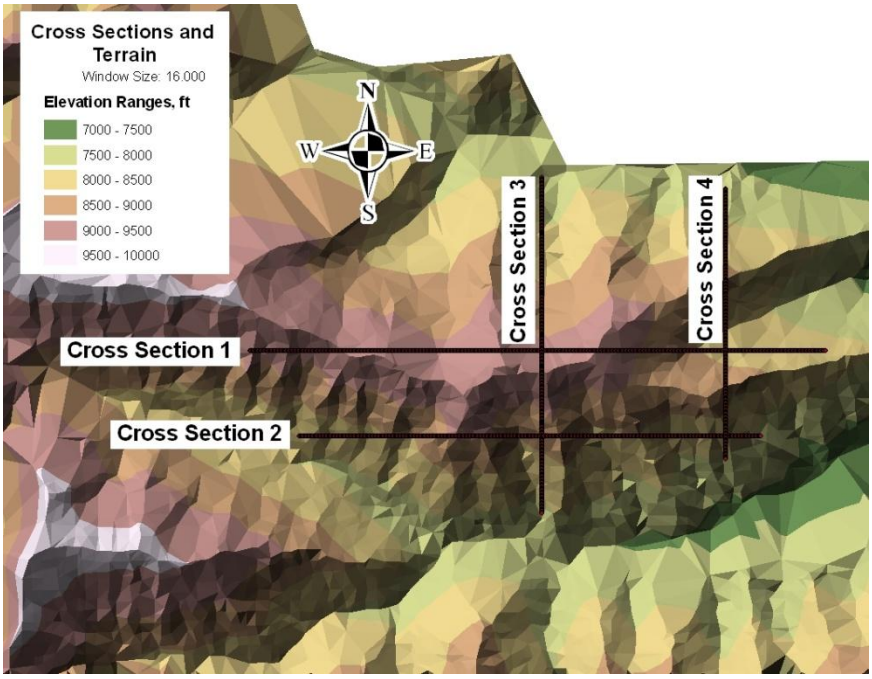

Figure 4-11 Cross Sections Relative to Terrain

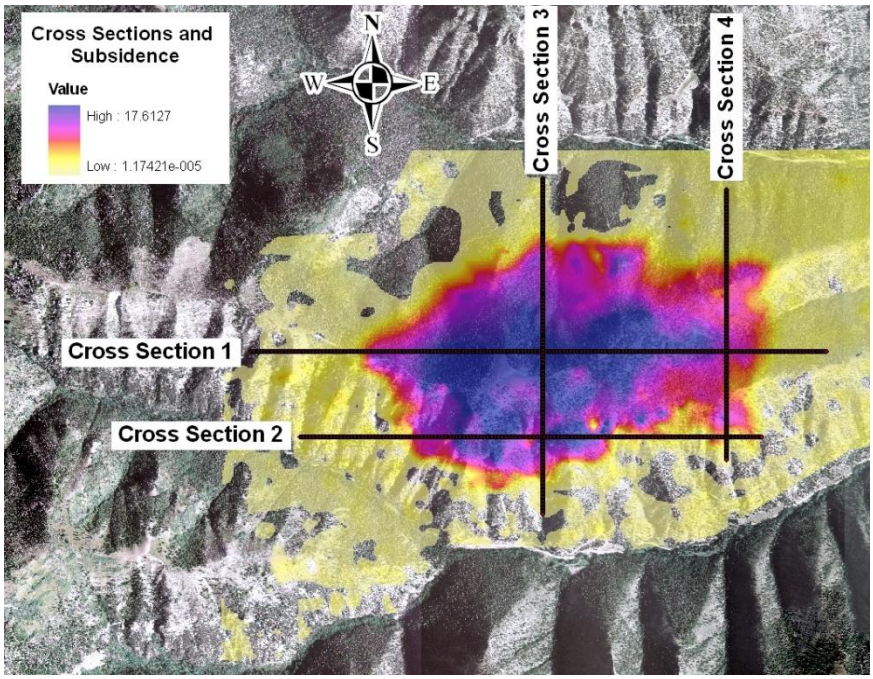

Figure 4-12 Cross Sections Relative to Subsidence

4.3.2.2 Input Parameters

The three input parameters described in Section 4.1 were first obtained for each of the four cross sections. The subsidence factor (a) was provided directly by engineers at Deer Creek Mine, and is equal to 0.9. The value for the limit angle (γ) was assumed to be 45 degrees. Both the subsidence factor and limit angle are constant for each of the four subsidence profiles created.

The overburden (h) and seam thickness (m) vary with data point locations and from one coal seam to the other. Point overburden values were calculated for each seam by subtracting the seam's constant elevation from the corresponding elevation profile values. Seam thicknesses were obtained from measurements taken by mine operators as the shear moved along the face of the longwall panel. The corresponding critical radii (B) and maximum subsidences (S_{max}) were then calculated according to Equation 4-1 and

Equation 4-2, respectively, on a point by point basis. Average B and S_{max} values were used for all points in the previous method. The elevation as well as average and extreme parameter values for each seam are given in Table 4-2.

Table 4-2. Profile Input Parameter Ranges

Coal Seam:	Hiawatha	Blind Canyon
Elevation (z):	7600 ft	7680 ft
Maximum Overburden (h_{max}):	1737 ft	1657 ft
Minimum Overburden (h_{min}):	102 ft	22 ft
Average Overburden (h_{ave}):	986 ft	906 ft
Maximum Thickness (m_{max}):	9.5 ft	9.5 ft
Minimum Thickness (m_{min}):	7.0 ft	8.2 ft
Average Thickness (m_{ave}):	7.6 ft	8.3 ft

The parameters u, v, x, and y (see Figure 4-6 and Figure 4-7) were next determined for each panel within a point's area of influence. Equation 4-10 was then applied to each corresponding set of input parameter values, (u, v, x, y, and, S_{max}). The total subsidence at a given point is the superposition of the resulting subsidence values from all longwall panels within the critical radius in each of the two coal seams.

Finally, the total subsidence values were multiplied by an additional parameter developed by the author, which is the slope factor (ζ). The slope factor is auxiliary to the TXI method, but is included in this section due to its tendency to improve the method. The rationale behind the slope factor is that subsidence is affected by the slope of the ground, in addition to the factors already discussed. The slope factor is thus proportional to the slope of the surface as shown in Equation 4-15.

$$\zeta = 1 - \frac{|z'|}{D} \qquad \textbf{(4-15)}$$

$z' =$ derivative of elevation profile at the point (slope),

$D =$ an integer determining the influence of the slope

The value of D in Equation 4-15 was determined based on a statistical analysis, which analysis compares the measured subsidence profiles with those produced from the TXI method. The D value which yields the lowest RMS error (see Section 2.2.2.3) was used for a given orientation. This value is 6 for the West-to-East profiles, and 3 for the North-to-South profiles.

4.3.2.3 Profile Plots

The following profile plots given in Figure 4-13 to Figure 4-16 show the results of the TXI and previous methods applied to the four cross sections in Figure 4-10. The calculated subsidence at each station along each cross section is plotted with the corresponding measured subsidence from aerial surveys. The ground elevations and mine workings (not to scale) are also plotted on the same graph.

Four graphs are presented in each of the following figures. The first graph provides the elevation profile plotted to scale. The remaining three graphs provide calculated subsidence profiles and the measured subsidence profile. The second graph gives the profile from the previous method. The third and fourth graphs give profiles from the TXI method, with the slope factor applied in the fourth graph. Thus, these graphs serve to map the improvements from the previous method to the TXI method, and the further improvements from applying the slope factor to the TXI method.

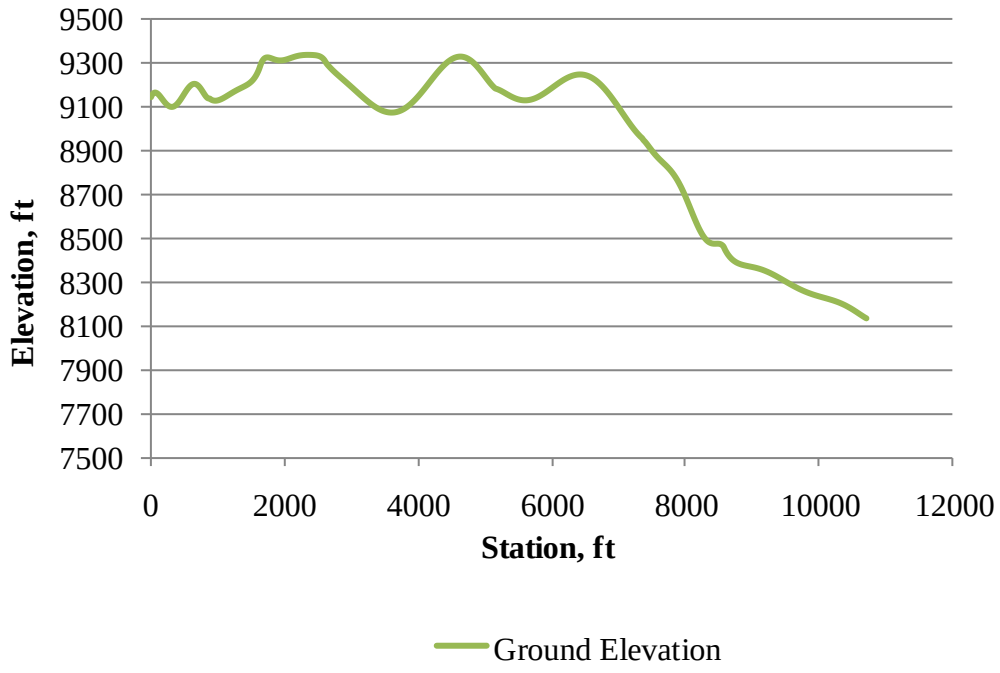

Figure 4-13a Terrain Surface Profile

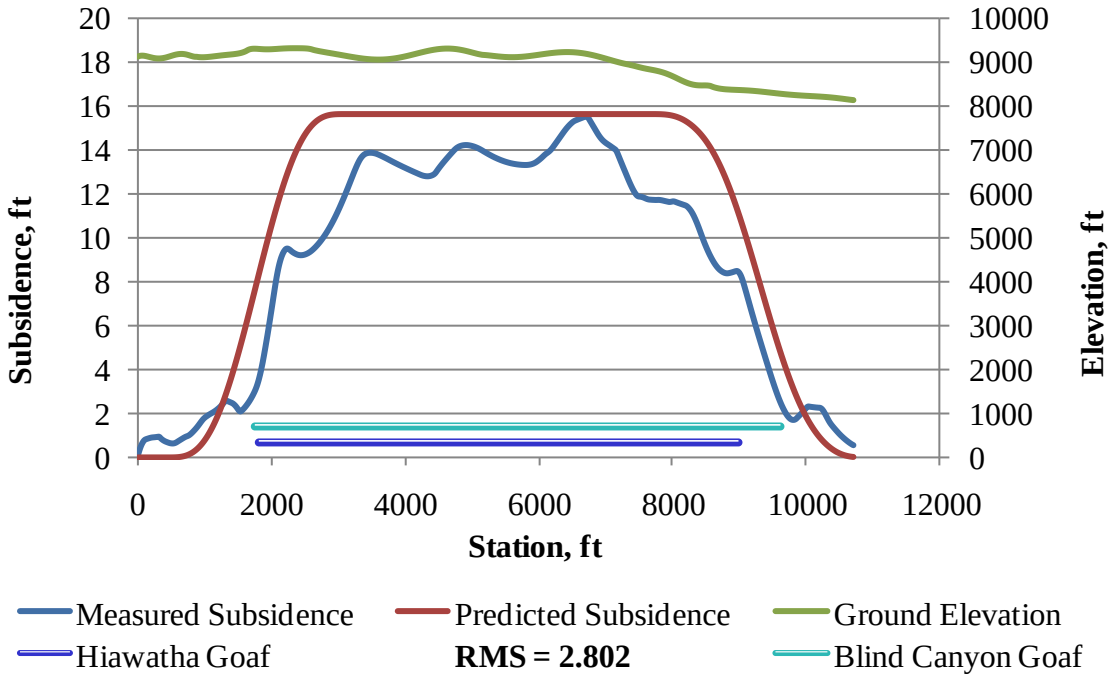

Figure 4-13b Previous Method Profile

Figure 4-13 Cross Section 1—West-to-East Middle Profiles

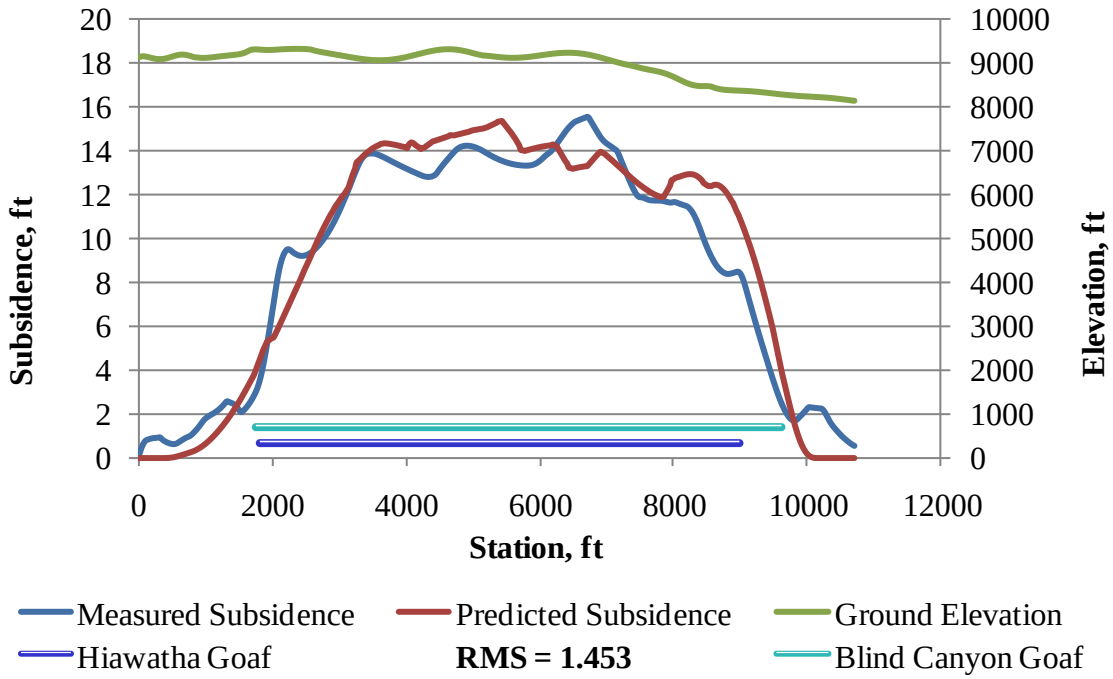

Figure 4-13c TXI Method Profile

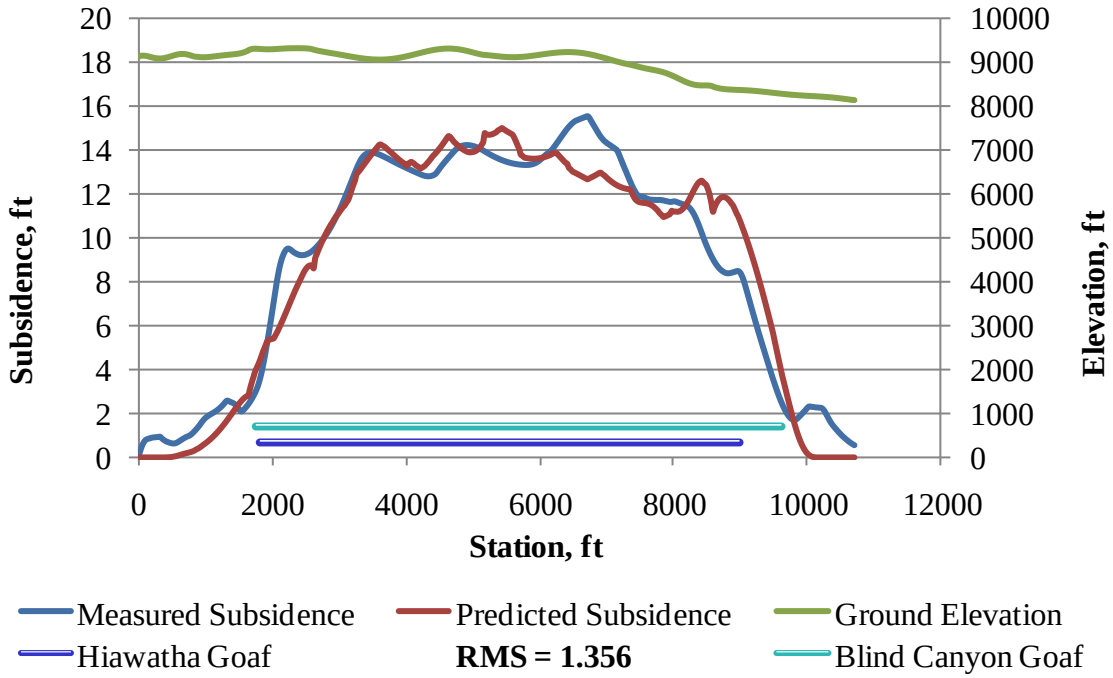

Figure 4-13d TXI Method Profile with Slope Factor

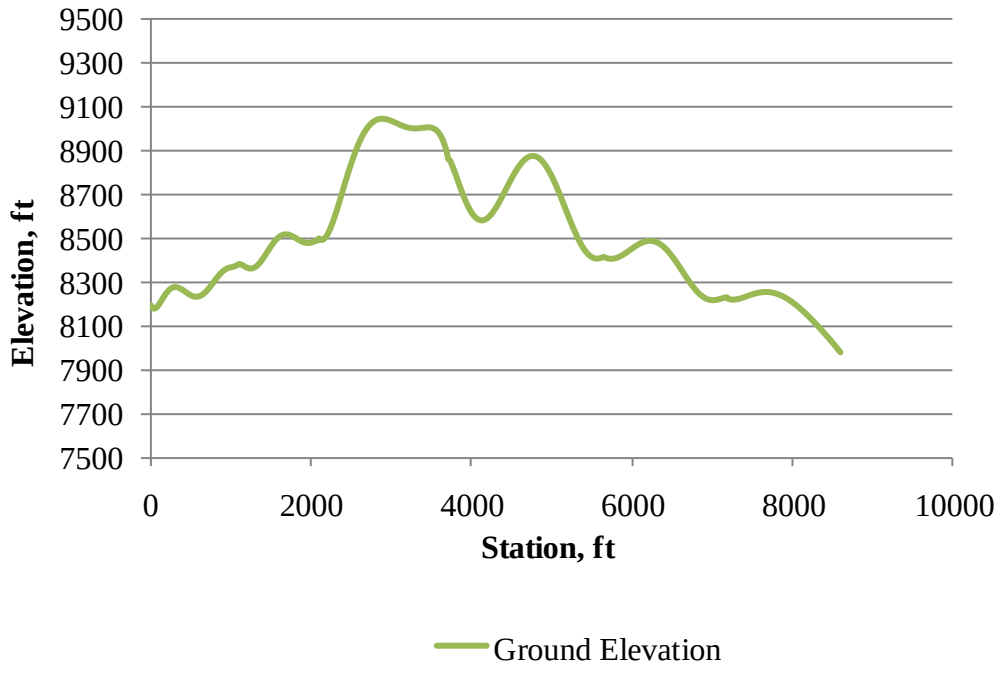

Figure 4-14a Terrain Surface Profile

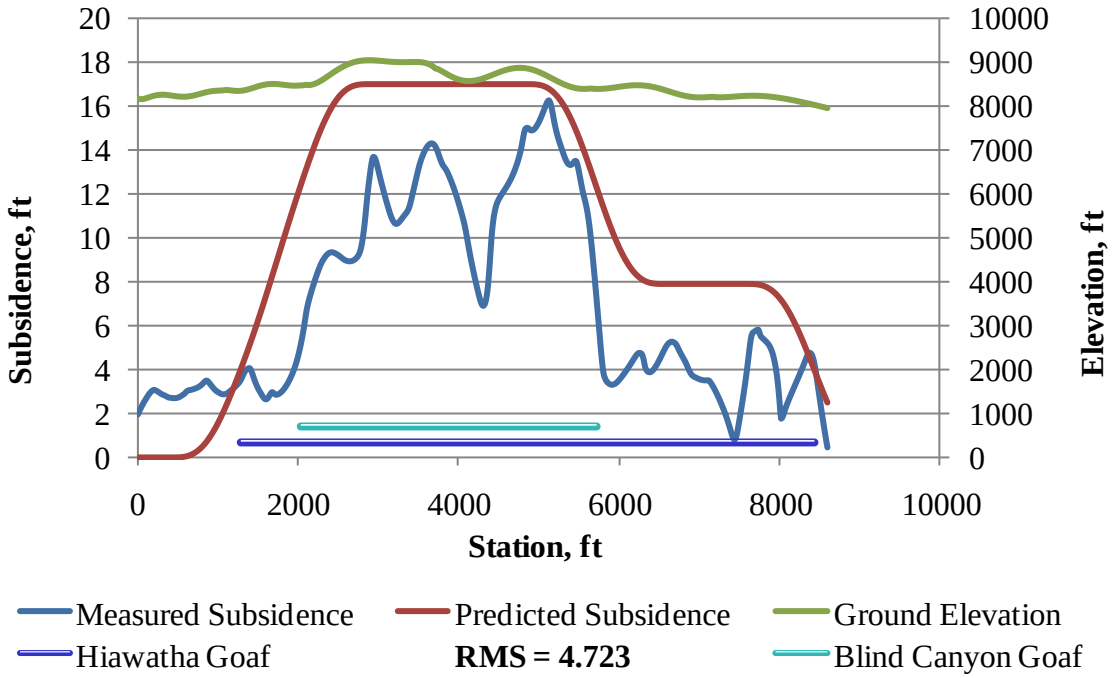

Figure 4-14b Previous Method Profile

Figure 4-14 Cross Section 2—West-to-East Edge Profiles

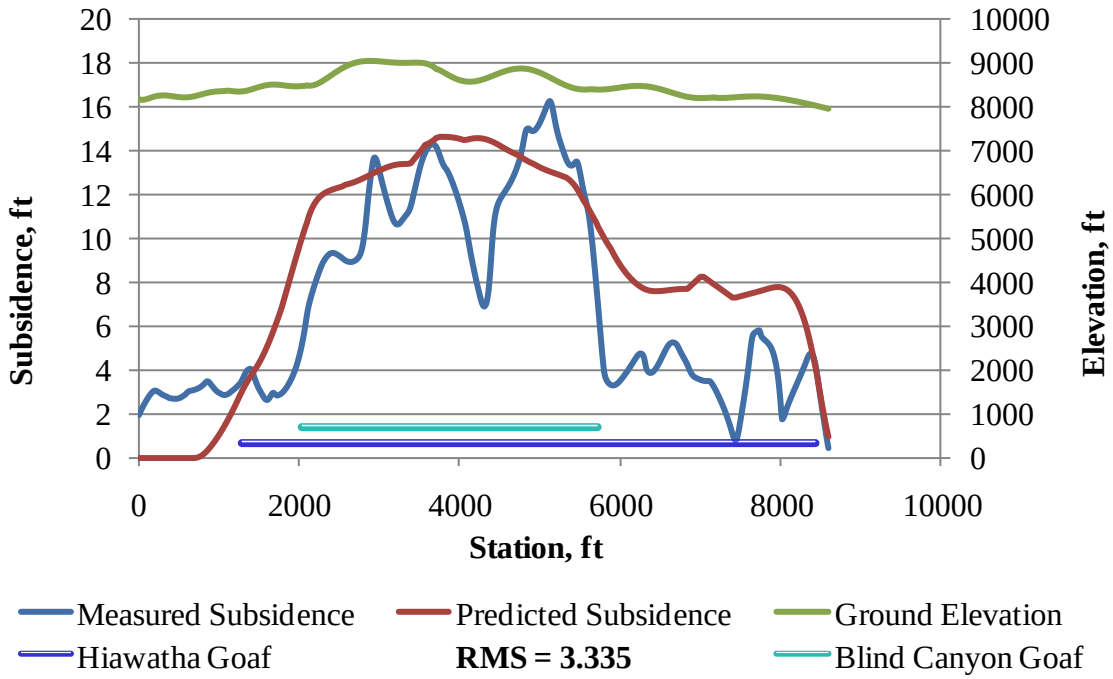

Figure 4-14c TXI Method Profile

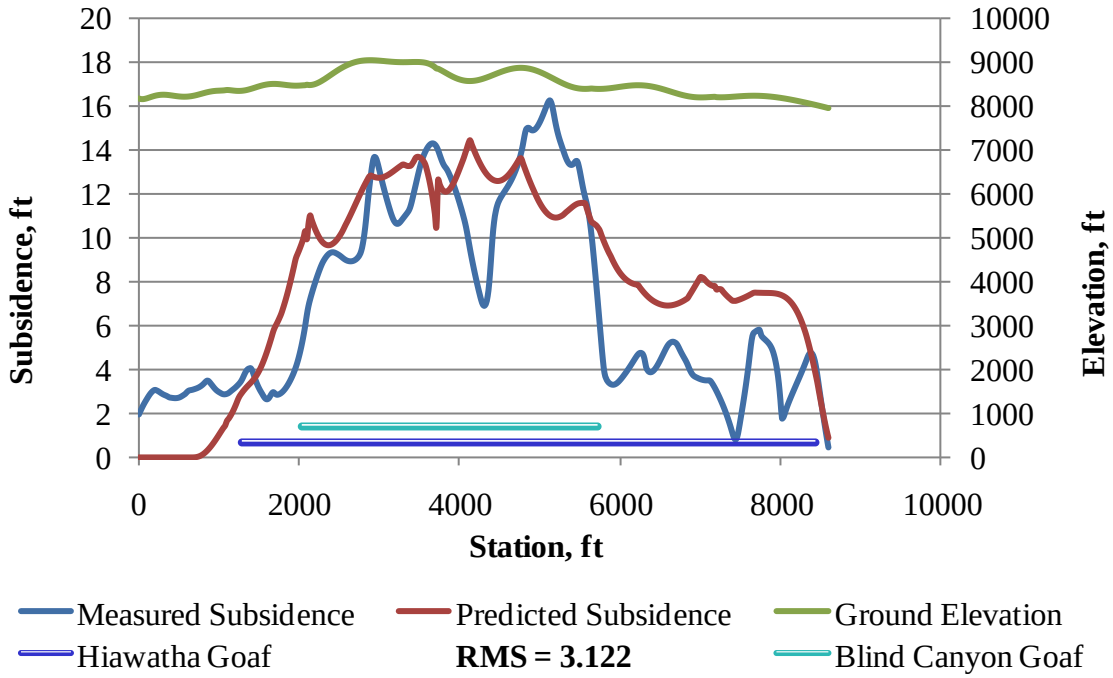

Figure 4-14d TXI Method Profile with Slope Factor

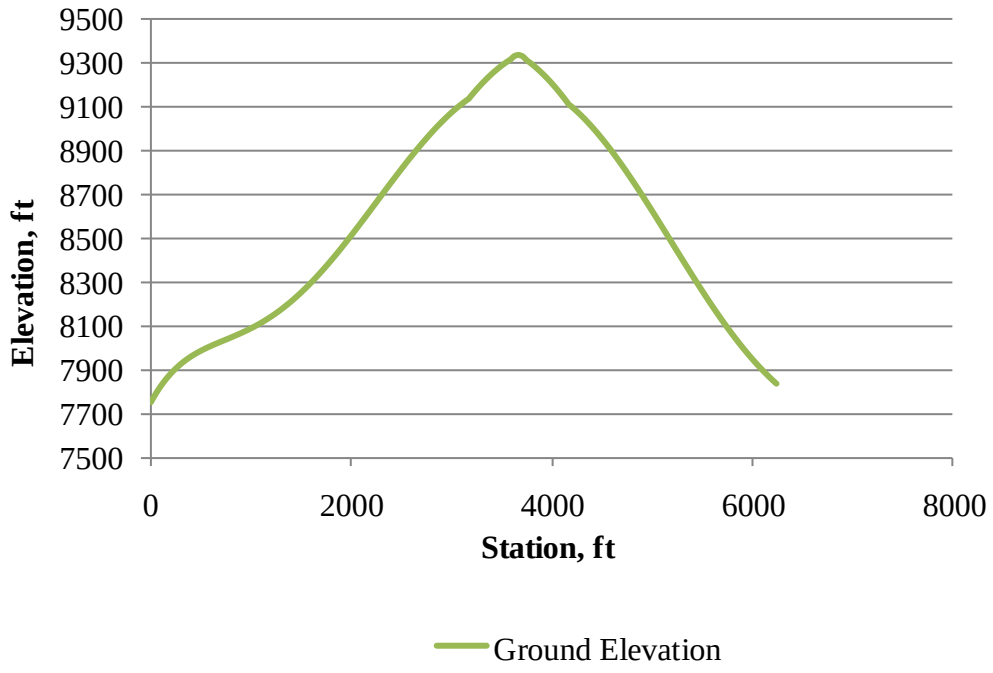

Figure 4-15a Terrain Surface Profile

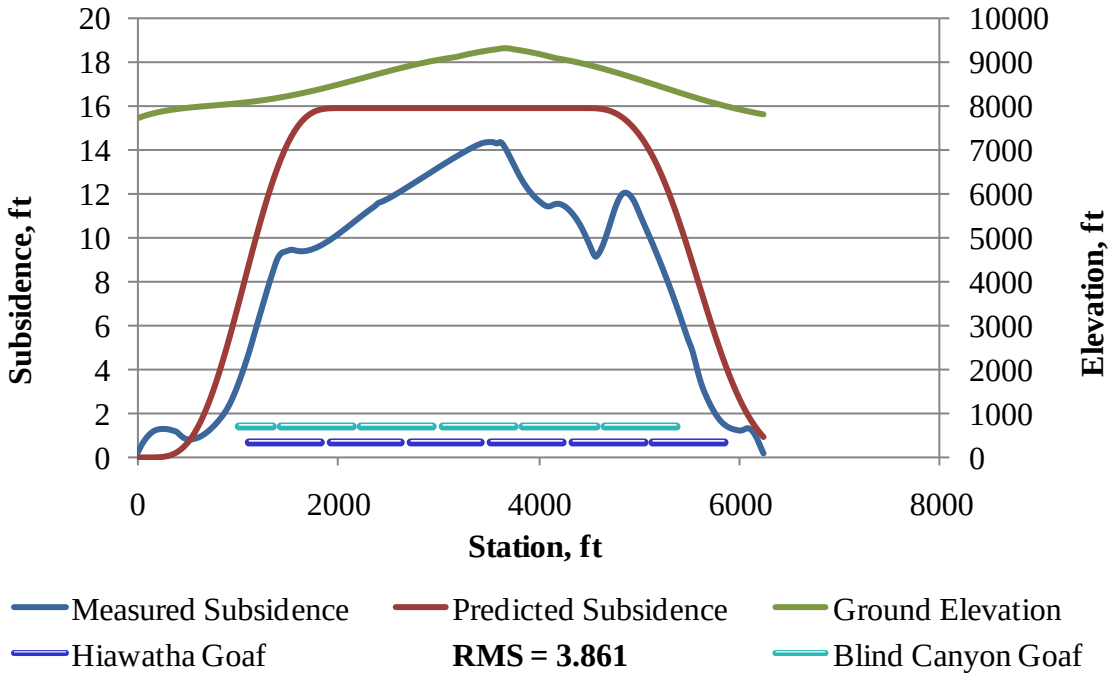

Figure 4-15b Previous Method Profile

Figure 4-15 Cross Section 3—North-to-South Middle Profiles

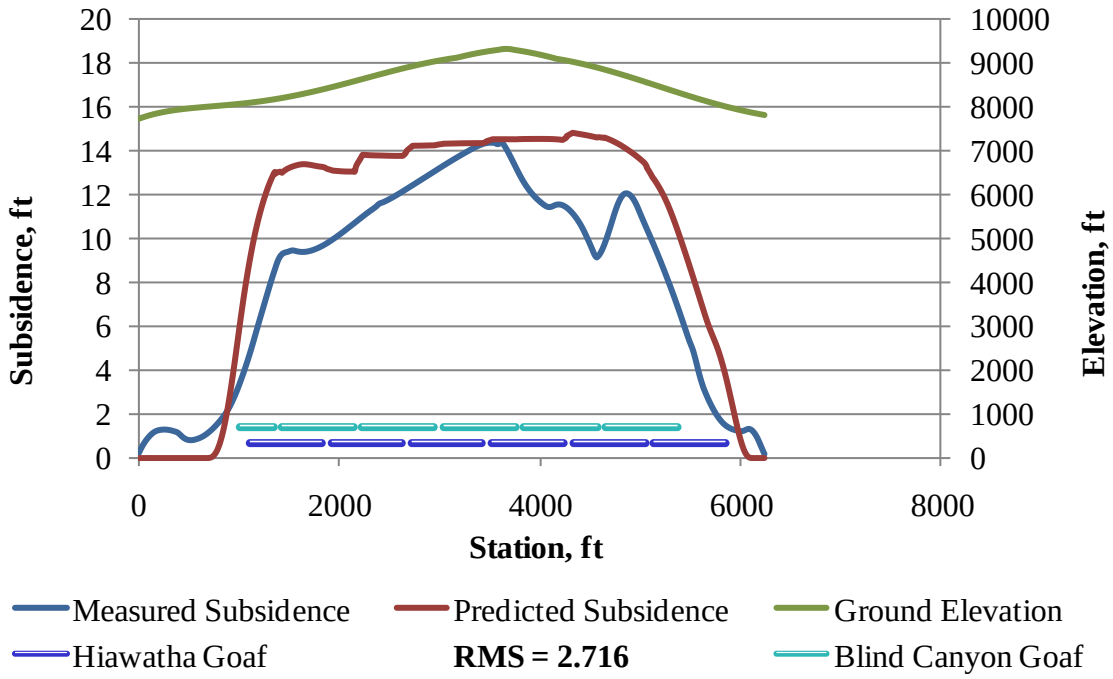

Figure 4-15c TXI Method Profile

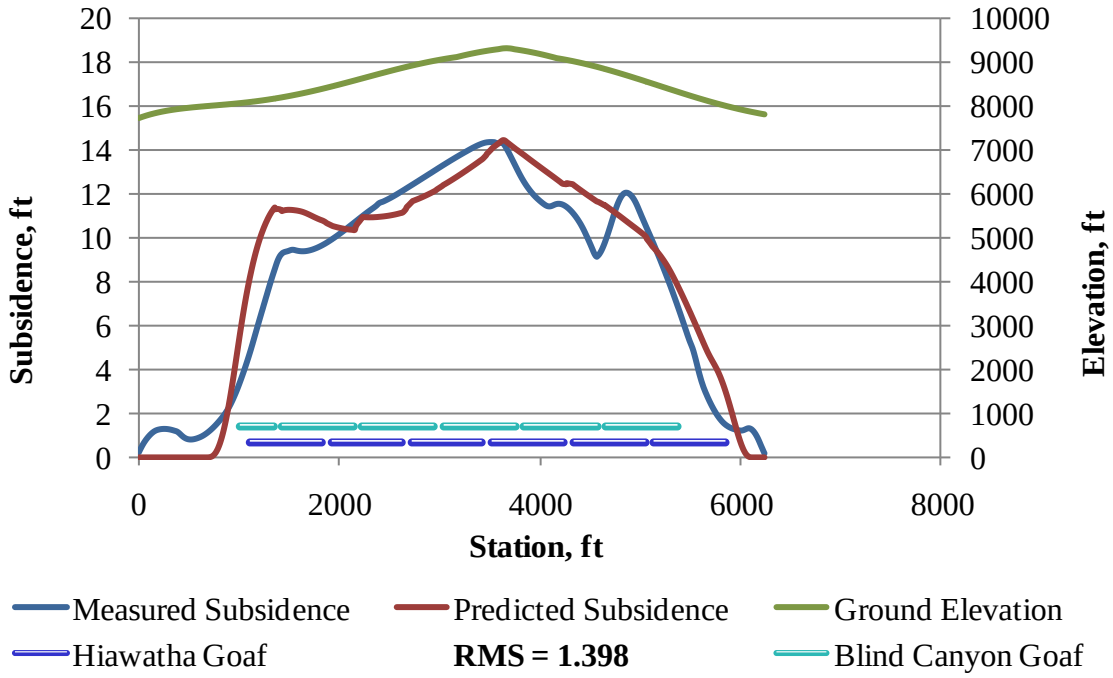

Figure 4-15d TXI Method Profile with Slope Factor

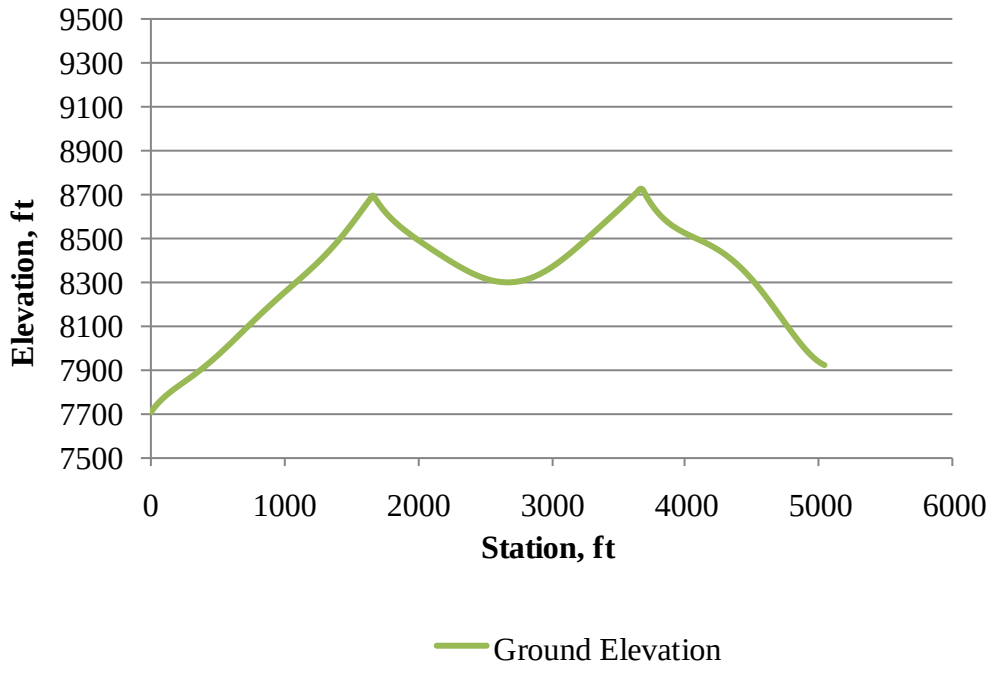

Figure 4-16a Terrain Surface Profile

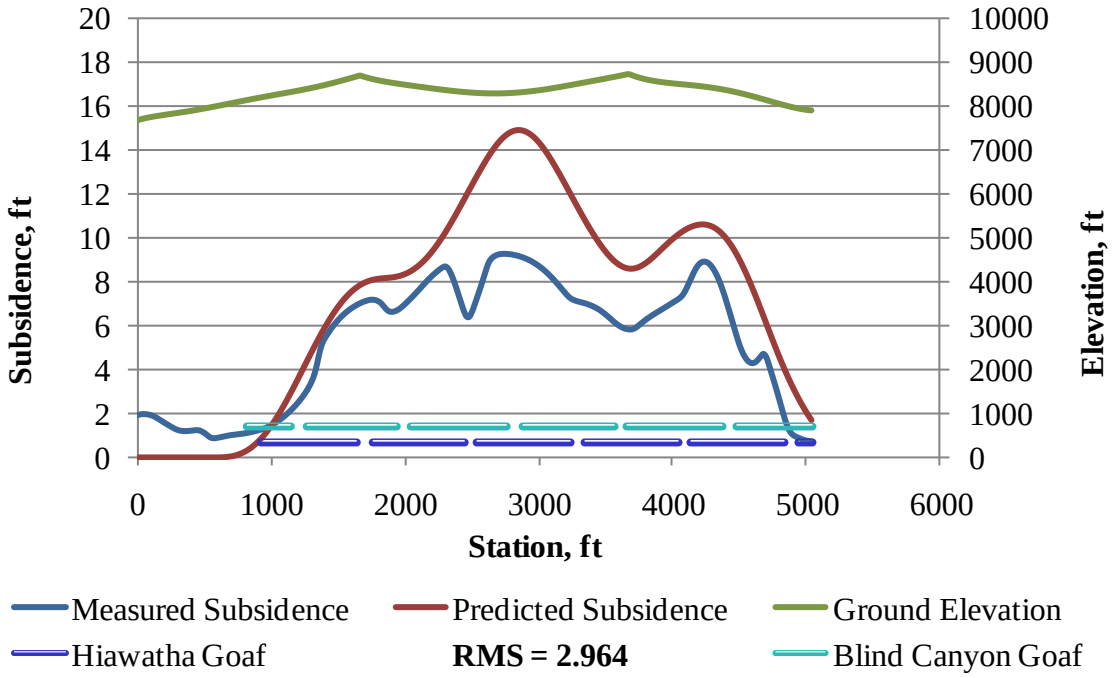

Figure 4-16b Previous Method Profile

Figure 4-16 Cross Section 4—North-to-South Edge Profiles

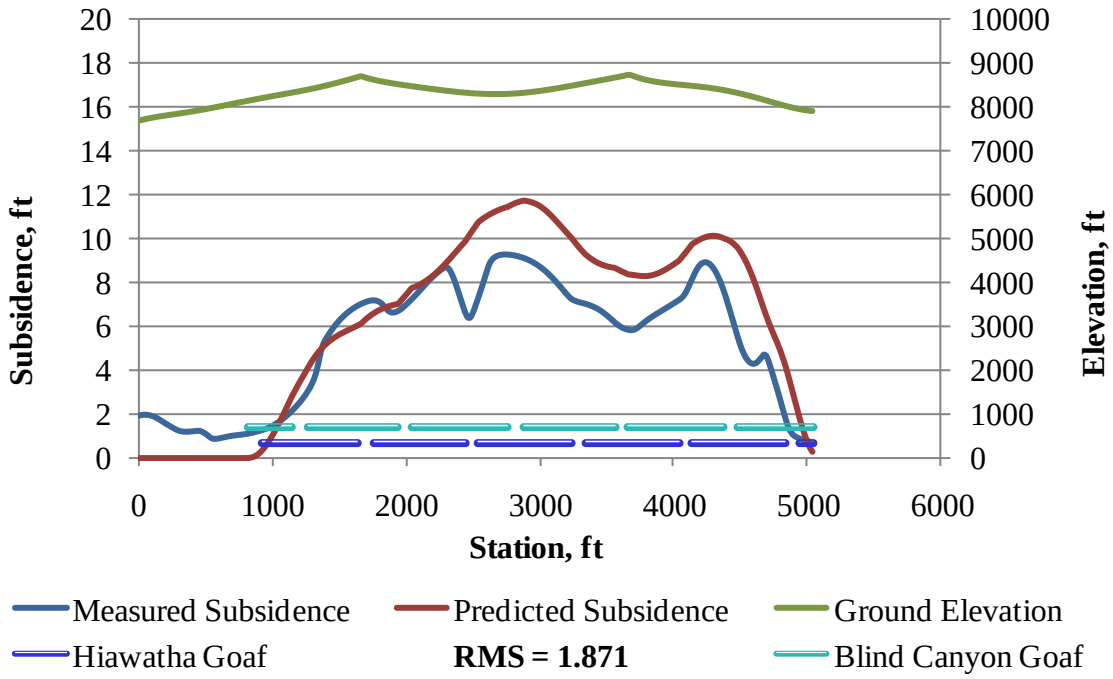

Figure 4-16c TXI Method Profile

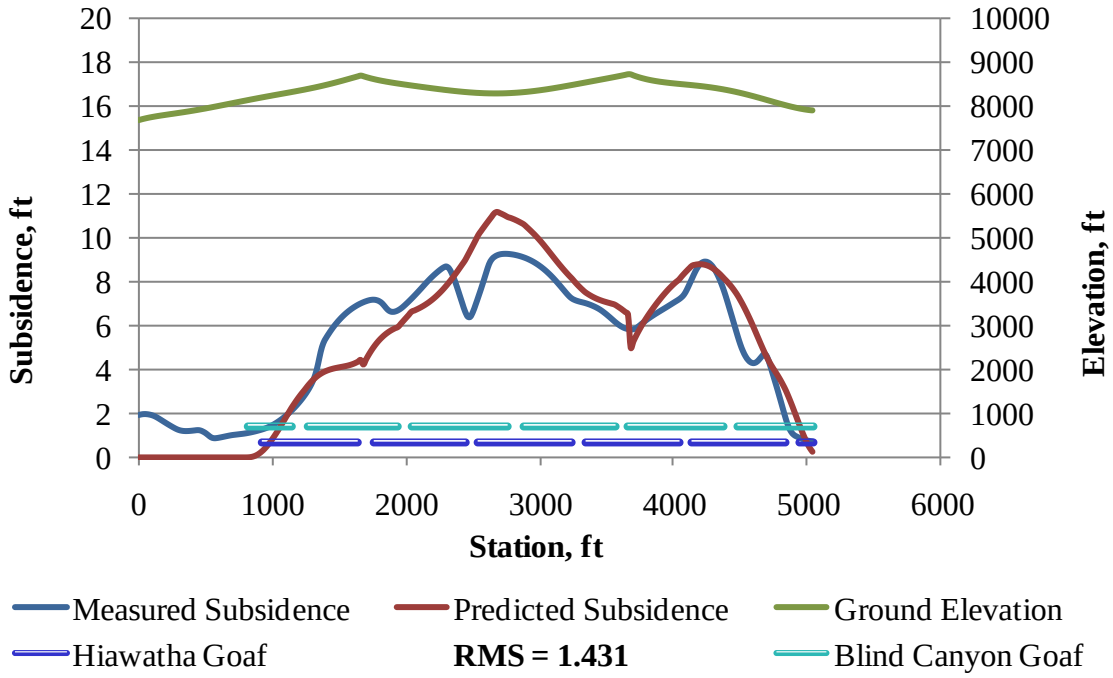

Figure 4-16d TXI Method Profile with Slope Factor

As the plots in the preceding figures indicate, the TXI method shows general improvement in subsidence profiling from the previous geometric method. The RMS error values from the previous method and from the TXI method—with and without the applied slope factor—are given in Table 4-3, along with the percent differences in RMS errors.

Table 4-3. RMS Error Values Corresponding to Various Modeling Methods

Direction:	West-to-East		North-to-South	
Cross Section:	1 – Middle	2 – Edge	3 – Middle	4 – Edge
Previous Method:	2.802	4.723	3.861	2.964
TXI Method:	1.453	3.335	2.716	1.871
Percent Difference:	**48.1%**	**29.4%**	**29.7%**	**36.9%**
TXI Method & Slope Factor:	1.356	3.122	1.398	1.431
Percent Difference:	**51.6%**	**33.9%**	**63.8%**	**51.7%**

5 Conclusions

5.1 Summary

The first main objective of this study was to design a method which uses aerial survey points to facilitate visualization of mining-induced ground subsidence. This objective was achieved using ArcGIS interpolation and map algebra tools outlined in Chapter 2. The visualization methods were applied to Deer Creek, Crandall Canyon, and Aberdeen mines to produce yearly subsidence plots. These plots were mapped with accompanying mine workings and surface topography as presented in Chapter 3. Additional subsidence plots, presented in Appendix A—printed on transparency film, were produced as separate layers of yearly subsidence, mine layout, and topography.

The second main objective was to demonstrate a method wherein:

1. data from the subsidence plots and mine geometry is incorporated into subsidence prediction models,
2. the accuracy of the previous models is improved, and
3. the improvement is quantified using statistical data.

This objective was accomplished through the development and application of the TXI method described in Chapter 4. The TXI and previous methods were applied to Deer Creek Mine data, and the resulting subsidence profiles were compared, both to each other

and to measured subsidence profiles from the aerial survey data. The RMS error values of the previous and TXI methods were computed for four cross sections of the Deer Creek Mine. The TXI method showed RMS improvements from the previous method ranging from 29.4% to 48.1%. Furthermore, the TXI method with the applied slope factors shows RMS improvements ranging from 33.9% to 63.8%.

5.2 Future Research

The technology and software currently available enables the prediction of ground subsidence with a greater degree of accuracy than previously used approximation methods. As the technology and software improve, the accuracy of available data (such as survey measurements and geological approximations) increases. This increase in accuracy in turn allows for modeling and predictive methods to improve. Further research in this area can be implemented to insure that the improvements in prediction methods keep abreast with the improvements in measuring and modeling technology.

Additionally, the TXI method may be further expanded within the current level of technology. Currently, the method produces subsidence prediction models for cross sections of the subsided surface. The method could be expanded to produce prediction models of the entire surface using ArcGIS. Also, the RMS error values from the TXI algorithm (see Section 4.3.2.3) are equivalent to those produced from error validation of the subsidence plots (see Section 3.2.2). More detailed statistical analyses of the interpolation methods could be performed to more closely ascertain their accuracy relative to the accuracy of the TXI method.

References

[1] I. Arch Coal. (2008, Annual report pursuant to section 13 or 15(d) of the securities exchange act of 1934 for the fiscal year ended December 31, 2007. United States Securities and Exchange Commission, Washington DC.

[2] C. R. Dunrud, "Some engineering geologic factors controlling coal mine subsidence in Utah and Colorado," U.S. Dept. of the Interior Geological Survey, Washington, 1976.

[3] G. Brauner, "Subsidence due to underground mining. 1. theory and practices in predicting surface deformation," United States, Tech. Rep. 1, 03, 1973.

[4] C. Y. Chen and S. S. Peng, "Underground Coal Mining and Attendant Subsidence Control: Some History, Technology, and Research," *Min Eng (Littleton Colo),* vol. 38, pp. 95-98, 1986.

[5] R. E. Gray, "Coal mine subsidence and structures." in *Mine Induced Subsidence: Effects on Engineered Structures - Proceedings.* 1988, pp. 69-86.

[6] S. C. Goel and C. H. Page, "An Empirical Method for Predicting the Probability of Chimney Cave Occurrence Over a Mining Area," *Int J Rock Mech Min Sci Geomech Abstr,* vol. 19, pp. 325-337, 1982.

[7] H. J. Siriwardane and J. Amanat. (1984, Finite element analysis and prediction of subsidence caused by underground mining. *International Journal of Mining Engineering 2(4),* pp. 271-290.

[8] C. Steed, W. F. Bawden, A. M. Coode and P. Mottahed, "Subsidence prediction for Saskatchewan potash mines." in *Research & Engineering Applications in Rock Masses, Proceedings of the 26th US Symposium on Rock Mechanics.* 1985, pp. 163-170.

[9] S. T. Wang, L. M. Galloway and G. E. Blandford, "2-d and 3-d finite element analyses of room-pillar mining systems with flat and rolling coal seams." in *Research & Engineering Applications in Rock Masses, Proceedings of the 26th US Symposium on Rock Mechanics.* 1985, pp. 231-238.

[10] L. J. Wardle and K. E. McNabb, "Comparison between predicted and measured stresses in an underground coal mine." in *Research & Engineering Applications in Rock Masses, Proceedings of the 26th US Symposium on Rock Mechanics.* 1985, pp. 531-538.

[11] E. J. Gumbel and S. B. Littauer, "Statistical control of sample extremes," United States, 02, 1967.

[12] K. Kim, S. Lee, H. Oh, J. Choi and J. Won, "Assessment of Ground Subsidence Hazard Near an Abandoned Underground Coal Mine Using GIS," *Environ. Geol.,* vol. 50, pp. 1183-1191, 2006.

[13] H. J. Siriwardane and J. Amanat, "Prediction of subsidence in hilly ground terrain using finite element method." in *Second International Conference on Stability in Underground Mining.* 1984, pp. 554-575.

[14] R. E. Bischke and P. S. Getty, "A method for assessing the potential of mine subsidence at abandoned mine sites through the assistance of finite element modeling." in *Proceedings - 25th Symposium on Rock Mechanics: Rock Mechanics in Productivity and Protection.* 1984, pp. 722-726.

[15] M. A. Trevits, R. L. King and B. V. Johnson, "Bureau of mines subsidence research program." in *Eastern Coal Mines Geomechanics, Proceedings: Bureau of Mines Technology Transfer Seminar.* 1986, pp. 57-64.

[16] F. K. Allgaier, "Surface Subsidence Over Longwall Panels in the Western United States - Final Results at the Deer Creek Mines, Utah," *Inf Circ US Bur Mines,* vol. 9194, pp. 17, 1988.

[17] US Geological Survey. (2008). The national map seamless server. *2009(4/7),*

[18] R. A. Gates, M. Gauna, T. A. Morley, J. R. J. O'Donnell, G. E. Smith, T. R. Watkins, C. A. Weaver and J. C. Zelanko. (2008), Report of investigation: Fatal underground coal burst accidents at Crandall canyon. Mine Safety and Health Administration, Available: http://www.msha.gov/Fatals/2007/CrandallCanyon/FTL07CrandallCanyon.pdf

[19] M. Vanden Berg and R. Bon. (2008). Utah coal photographic tour - Aberdeen and pinnacle mines. *2009(6/13),*

[20] L. Garner, *Multivariable Calculus.* Utah, USA: BYU Academic Publishing, 2005, pp. 171-174.

Appendix A Mine Transparencies

Appendix A contains transparency plots corresponding to the mines used in this study. The transparency plots are included for several reasons. First of all, the transparencies allow for flexibility in visualizing the subsidence and elevation plots in various combinations and overlays. Secondly, the transparencies facilitate direct examination of areas wherein subsidence from one year does not coincide with the mine workings for that year. Finally, the transparency plots can be enlarged with an overhead projector for use in presentations. The plots should be overlain such that the left edges with the white border line up, and the bottom edges line up.

The following envelopes—labeled Figure A-1, Figure A-2, and Figure A-3—contain transparencies of the Deer Creek, Crandall Canyon, and Aberdeen mines plots, respectively. The plots of Deer Creek and Crandall Canyon mines consist of mine workings, overlying ground surfaces, yearly subsidence plots, and survey points. Since aerial survey data is not associated with Aberdeen Mine, the plots of Aberdeen are similar to those of Deer Creek and Crandall Canyon, save they do not include yearly subsidence plots. In addition, the survey points in the Aberdeen mine are labeled according to station, while the Deer Creek and Crandall Canyon survey points are not labeled.

Figure A-1 Deer Creek Mine Transparency Plots: pp. 97-105

Survey Points

Blind Canyon Seam
Yearly Mining

Entries

All Years

Longwall Mining

1999

2000

2001

2002

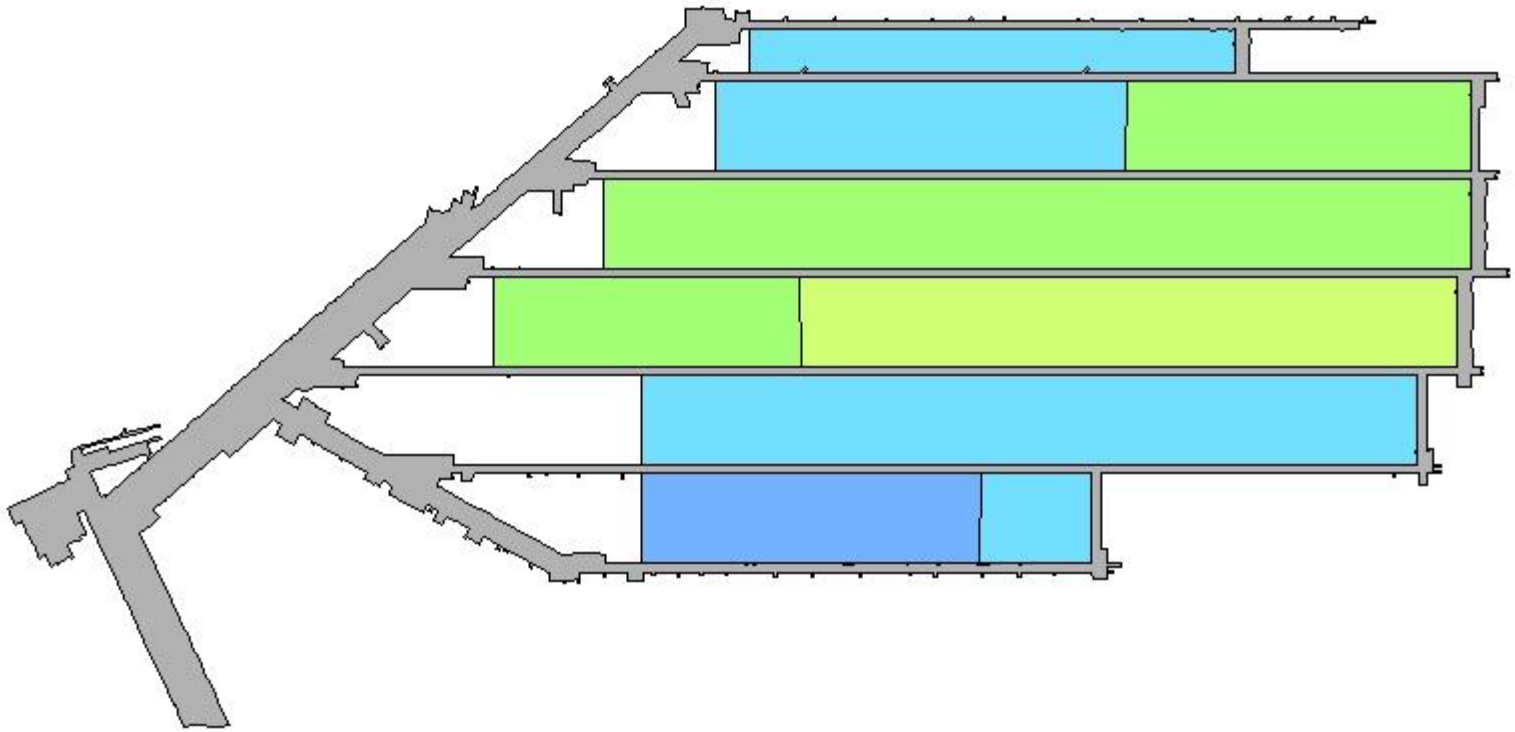

Hiawatha Seam
Yearly Mining

Entries

All Years

Longwall Mining

2002

2003

2004

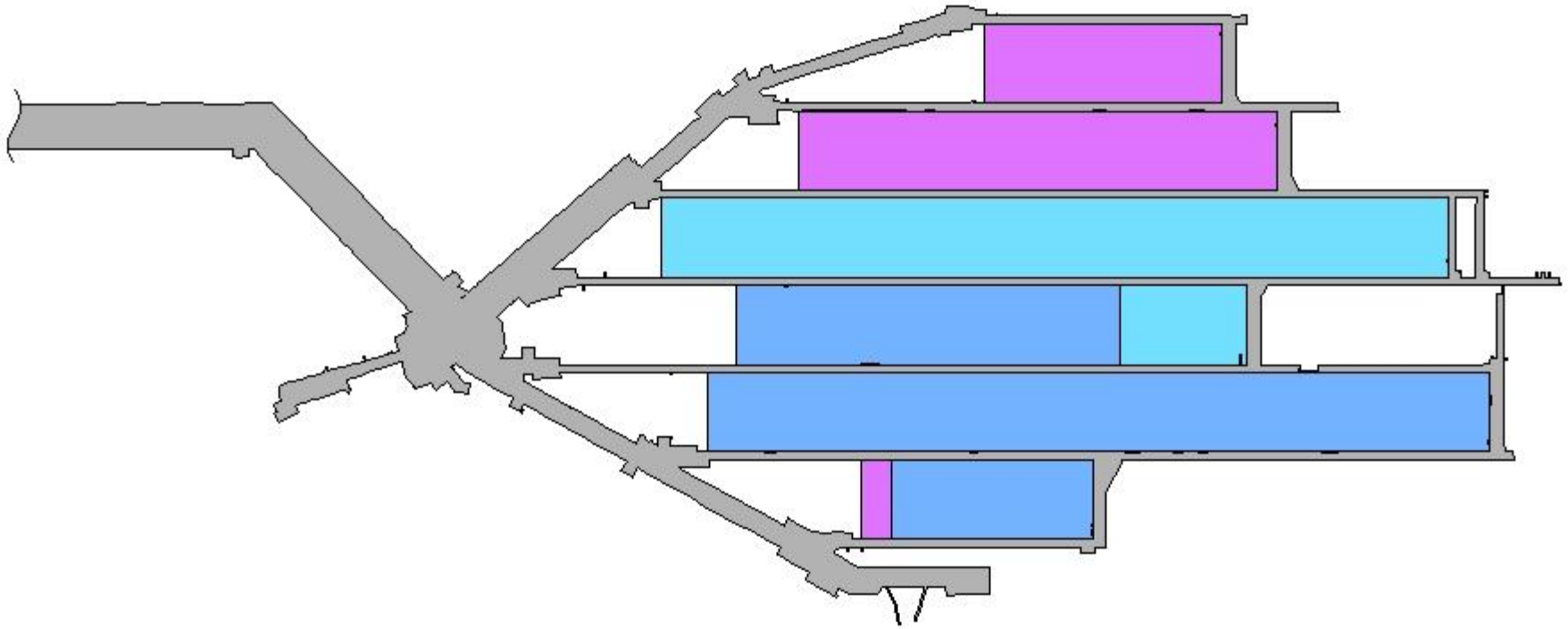

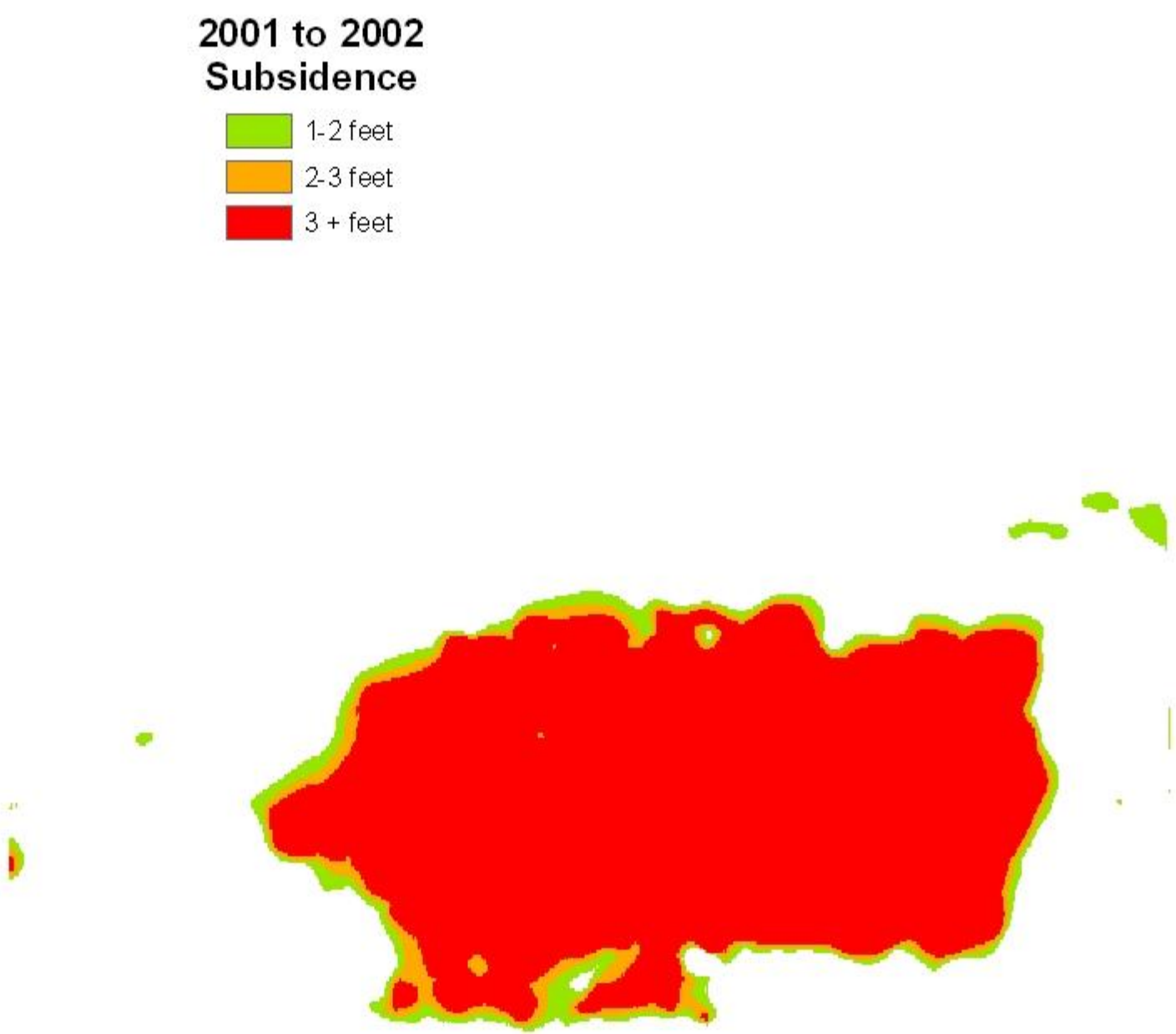
2001 to 2002
Subsidence
1-2 feet
2-3 feet
3 + feet

2002 to 2003 Subsidence

- 1-2 feet
- 2-3 feet
- 3 + feet

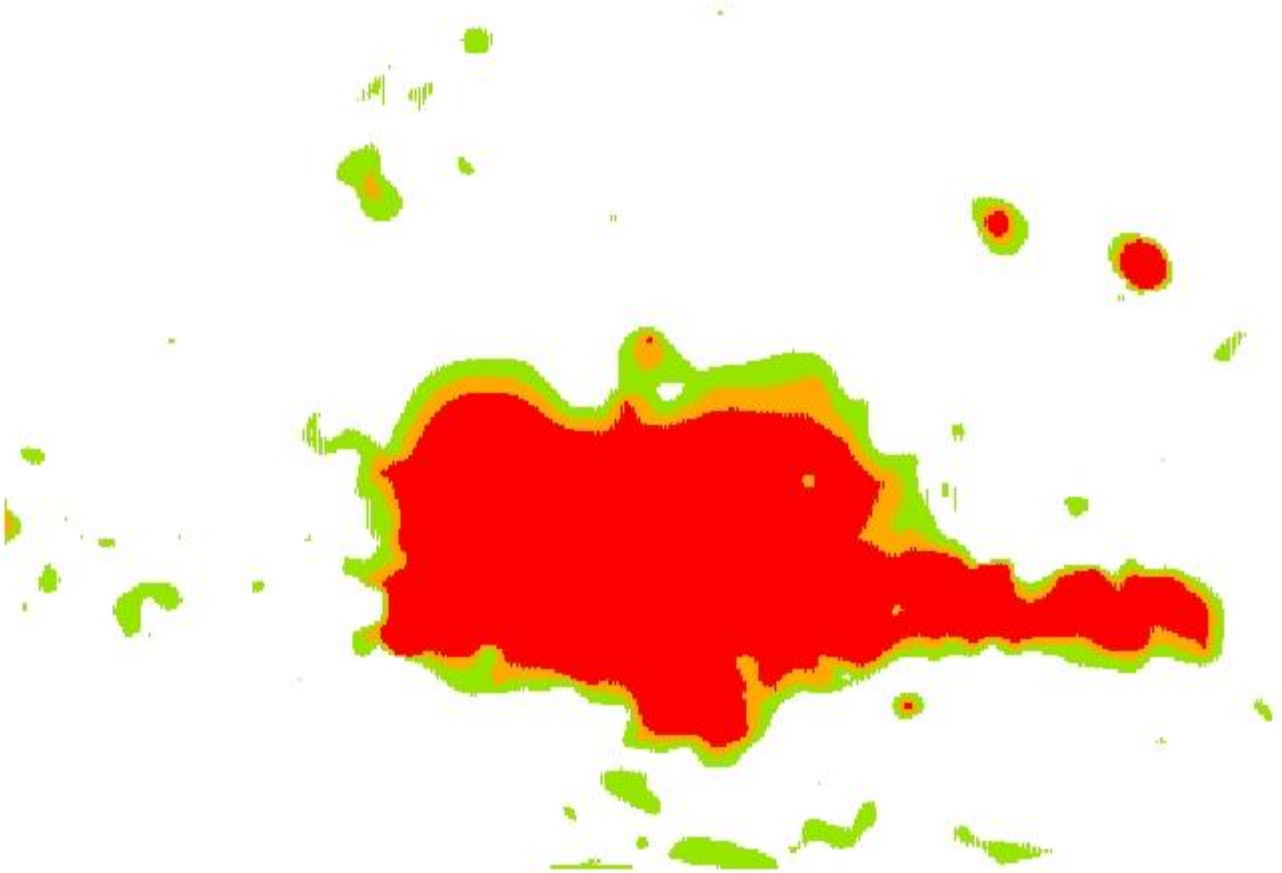

2003 to 2004 Subsidence

- 1-2 feet
- 2-3 feet
- 3 + feet

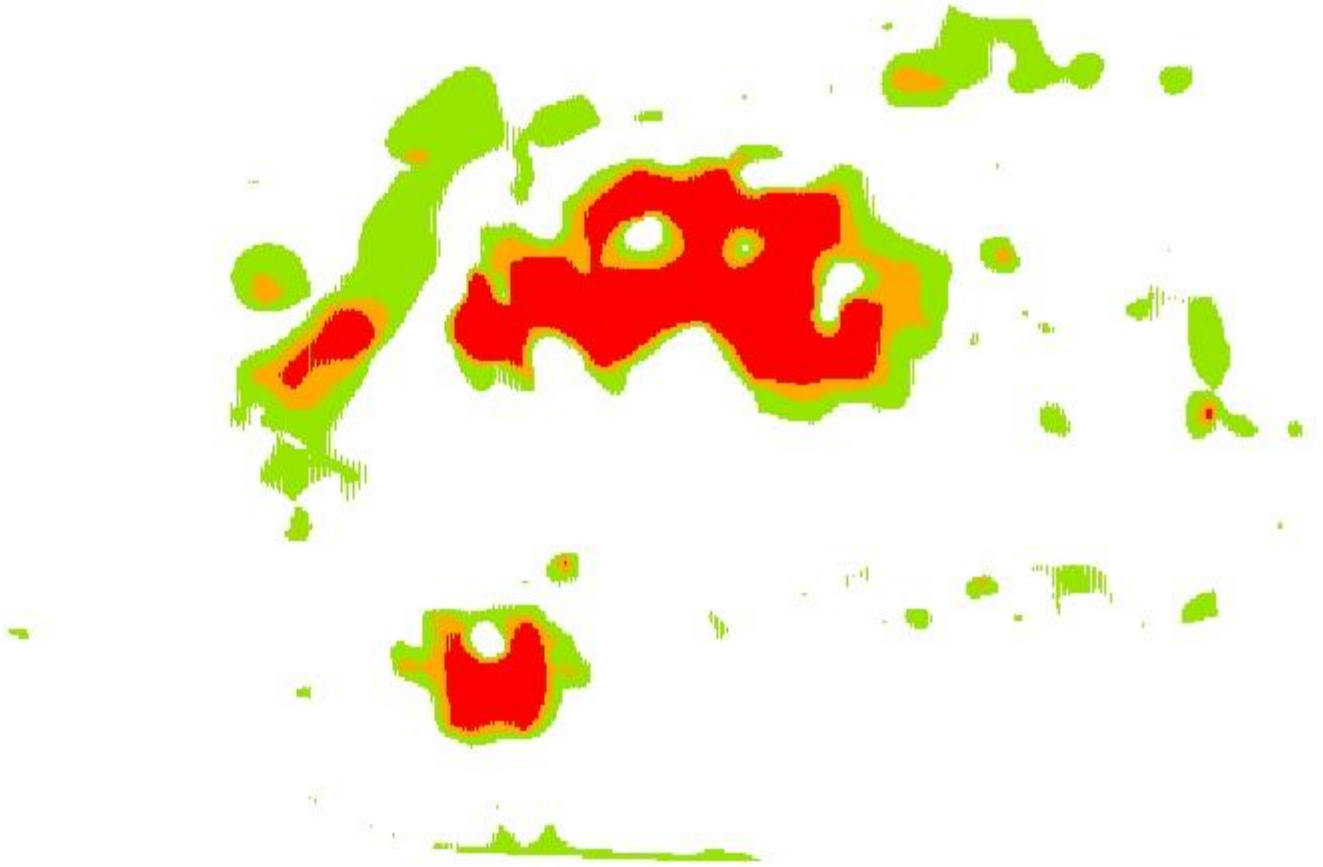

2004 to 2005 Subsidence

- 1-2 feet
- 2-3 feet
- 3 + feet

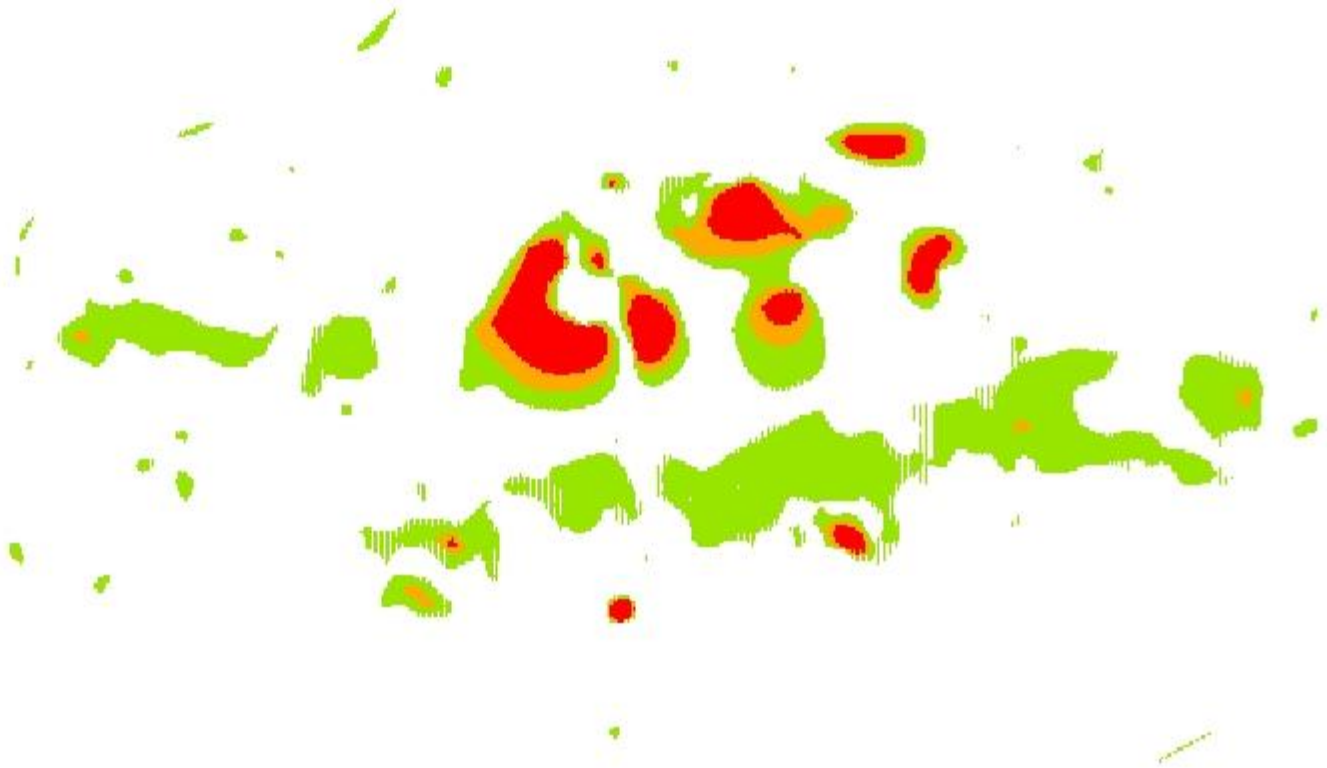

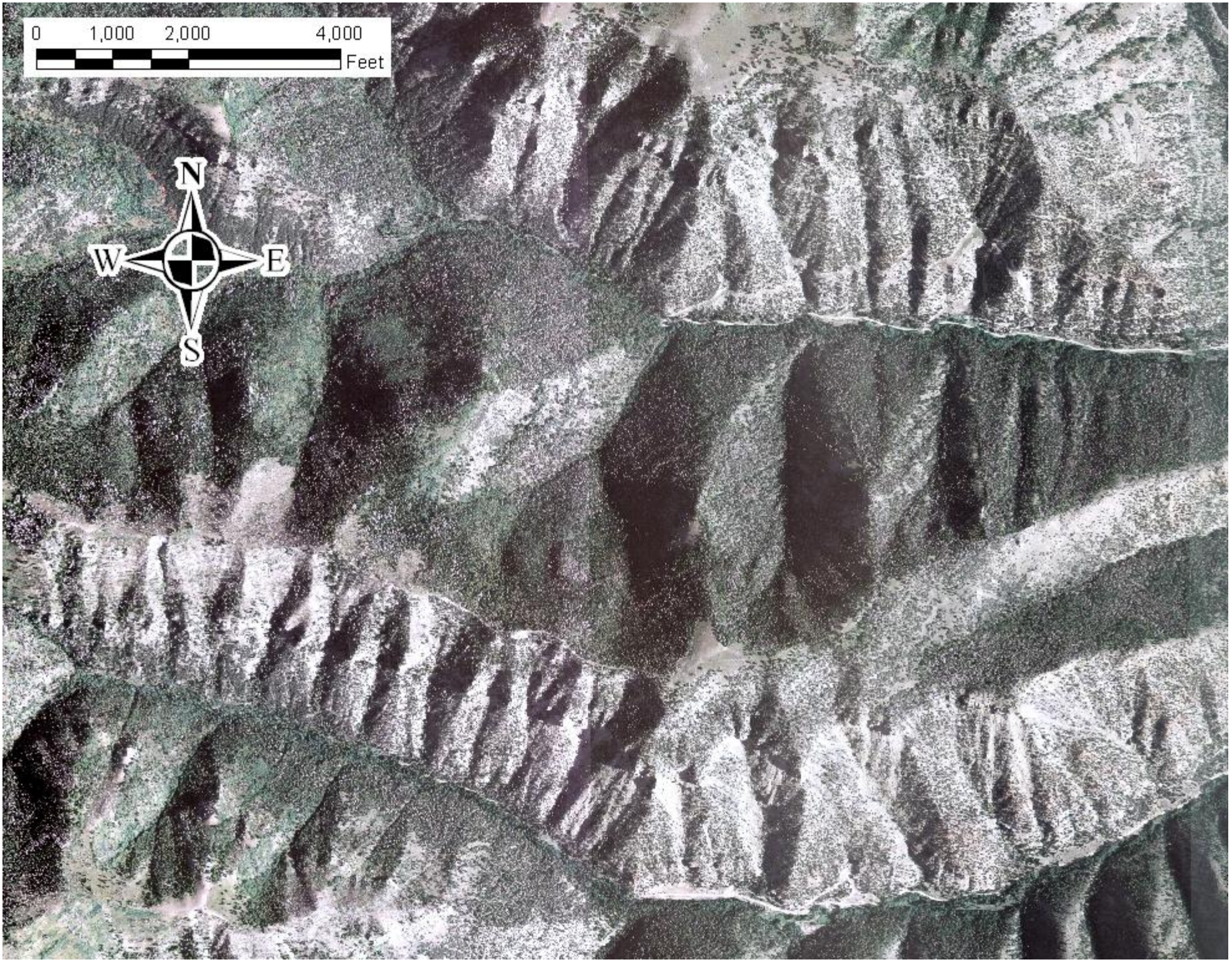
0
1,000
2,000
4,000
Feet
N
W
E
S

Figure A-2 Crandall Canyon Mine Transparency Plots: pp. 106-113

Survey Points

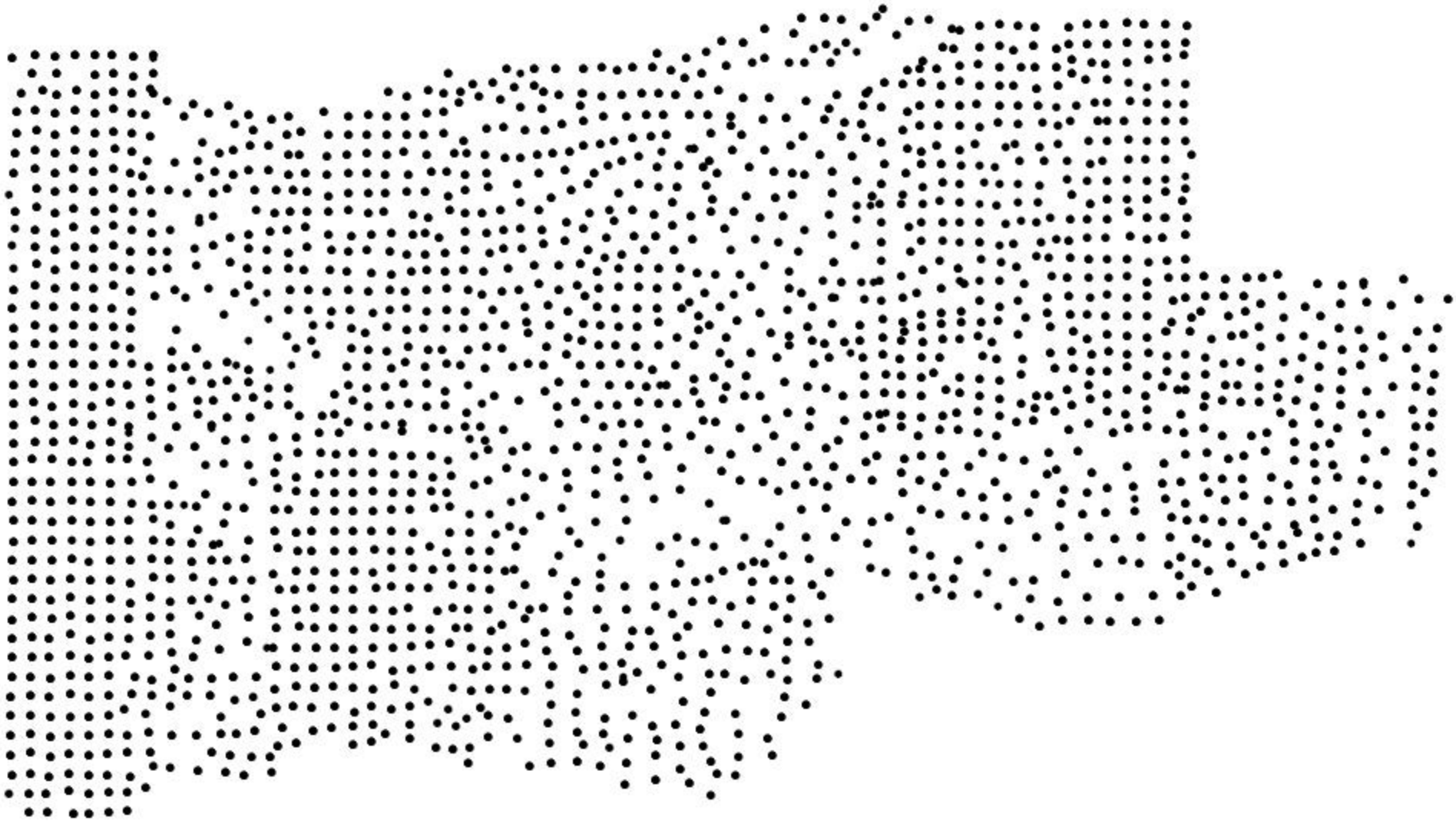

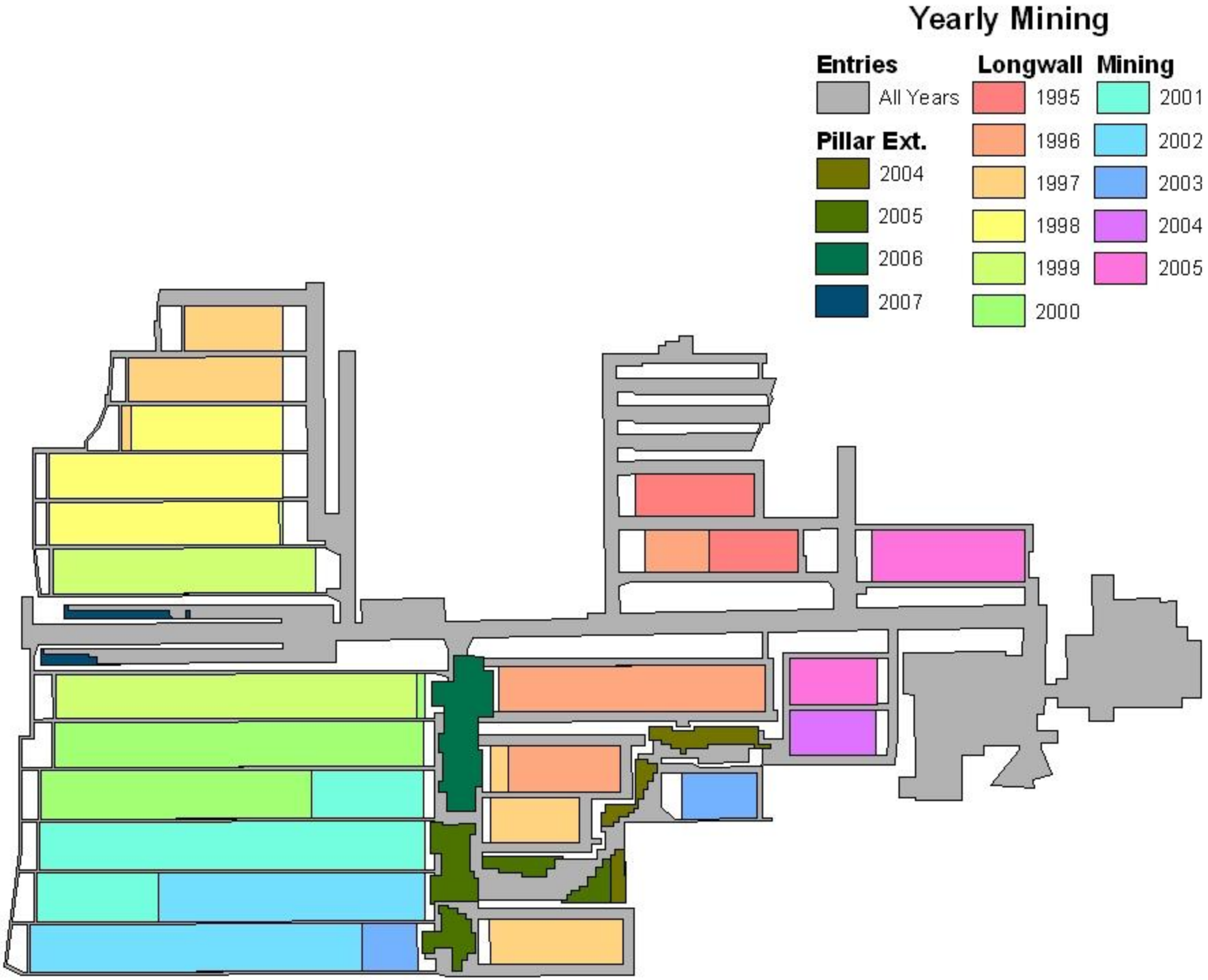
Yearly Mining
Entries
All Years
Pillar Ext.
2004
2005
2006
2007
Longwall Mining
1995
1996
1997
1998
1999
2000
2001
2002
2003
2004
2005

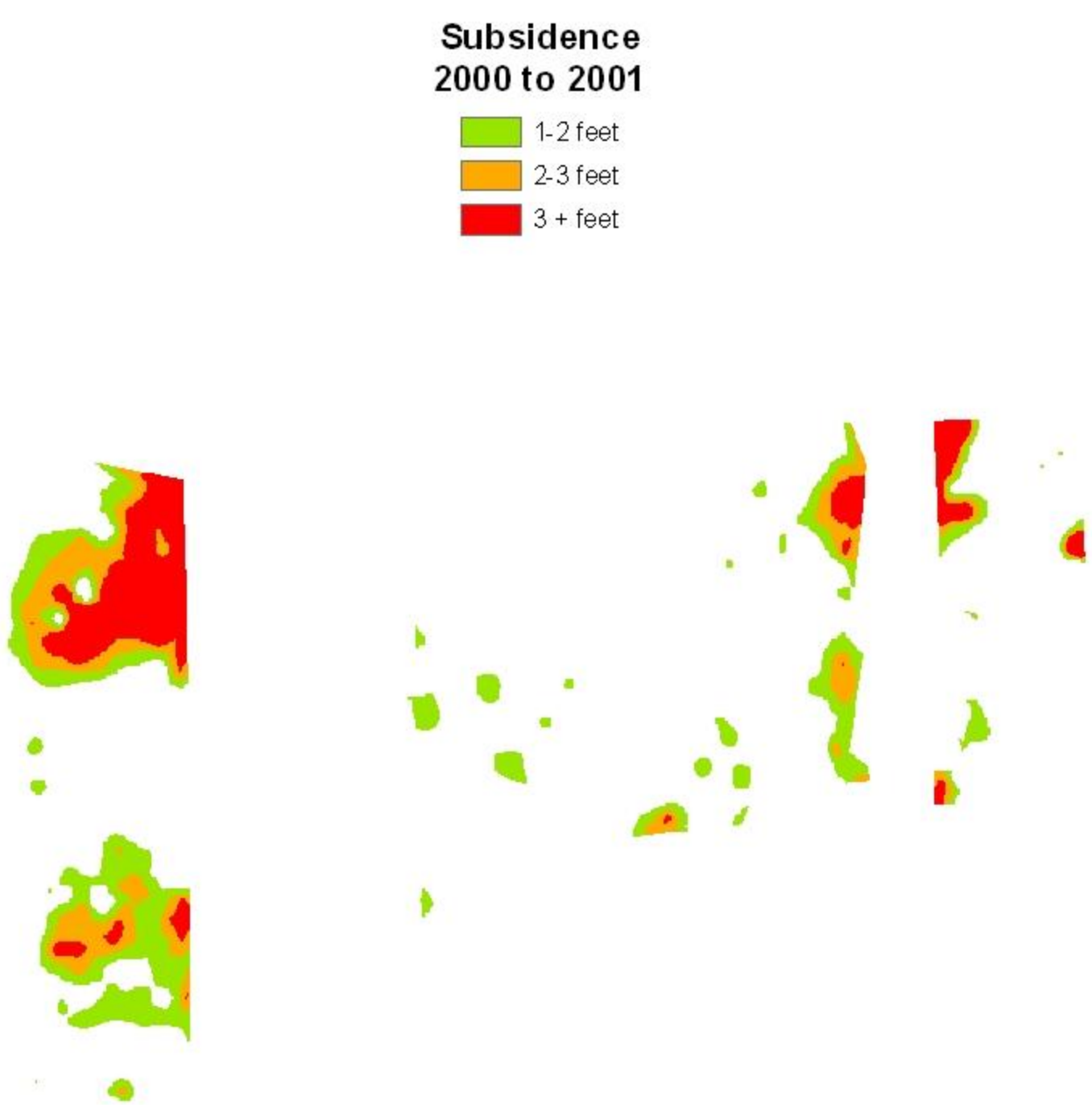
Subsidence
2000 to 2001
1-2 feet
2-3 feet
3 + feet

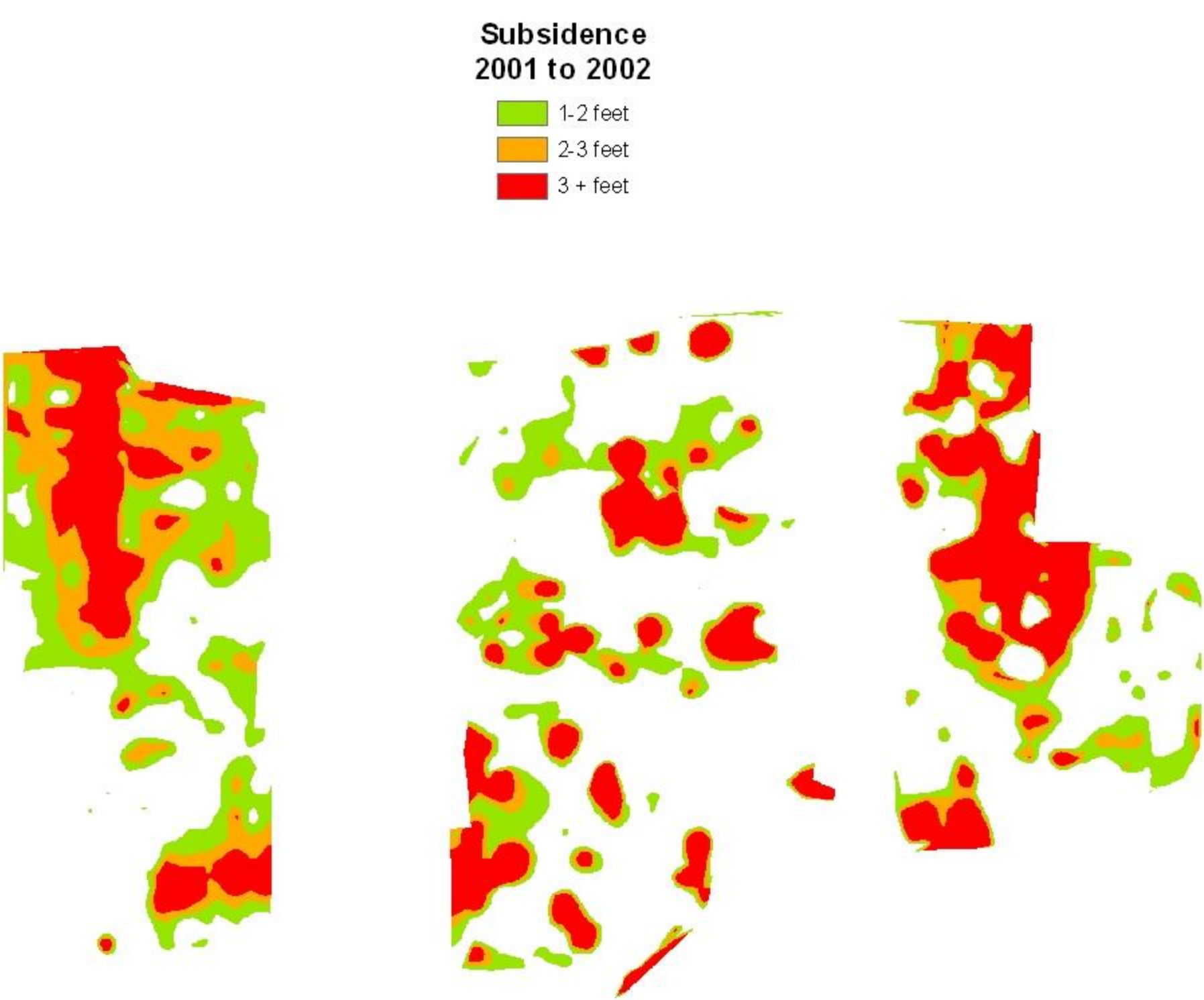
Subsidence
2001 to 2002
1-2 feet
2-3 feet
3 + feet

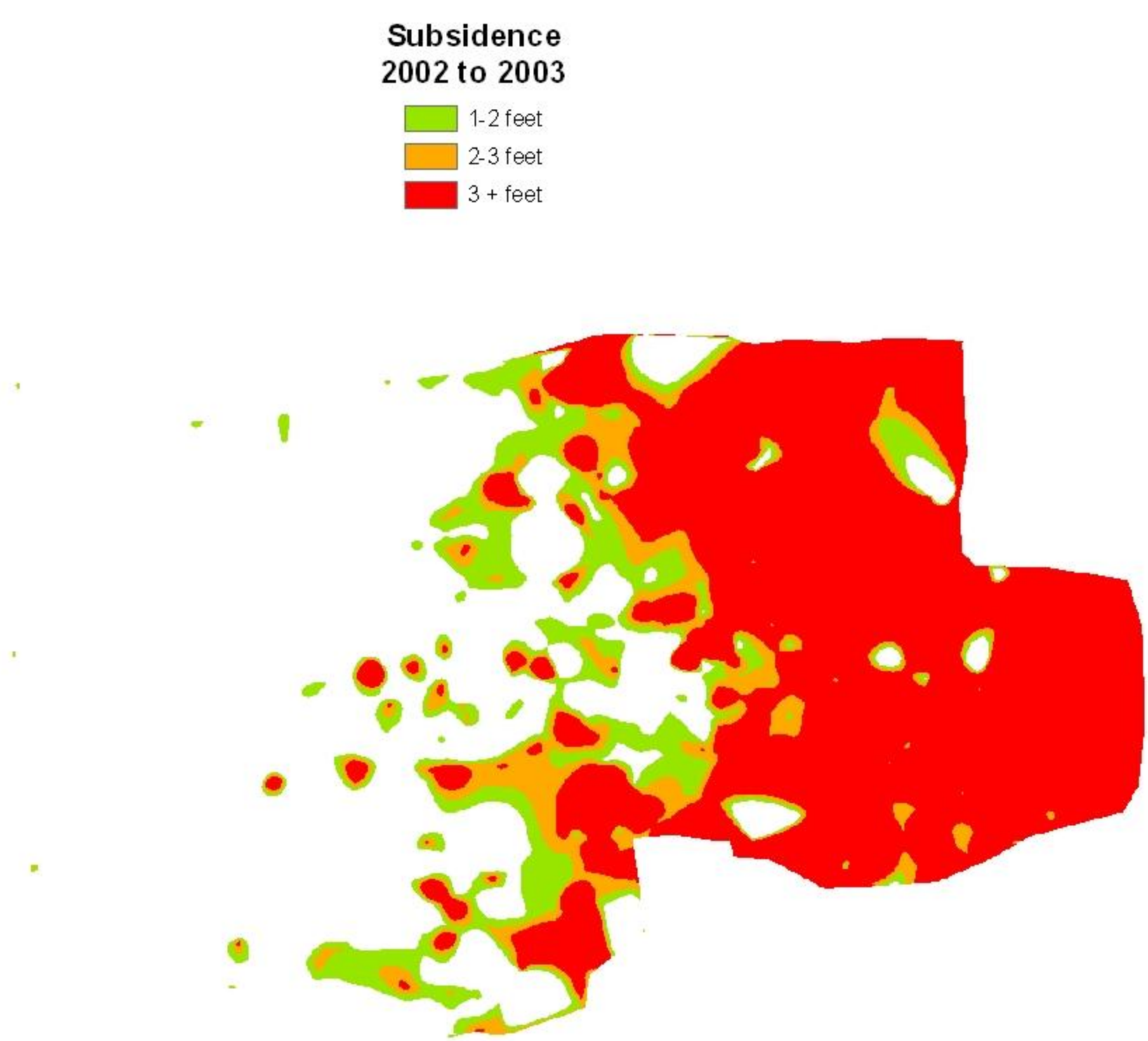
Subsidence
2002 to 2003
1-2 feet
2-3 feet
3 + feet

Subsidence
2003 to 2005

- 1-2 feet
- 2-3 feet
- 3 + feet

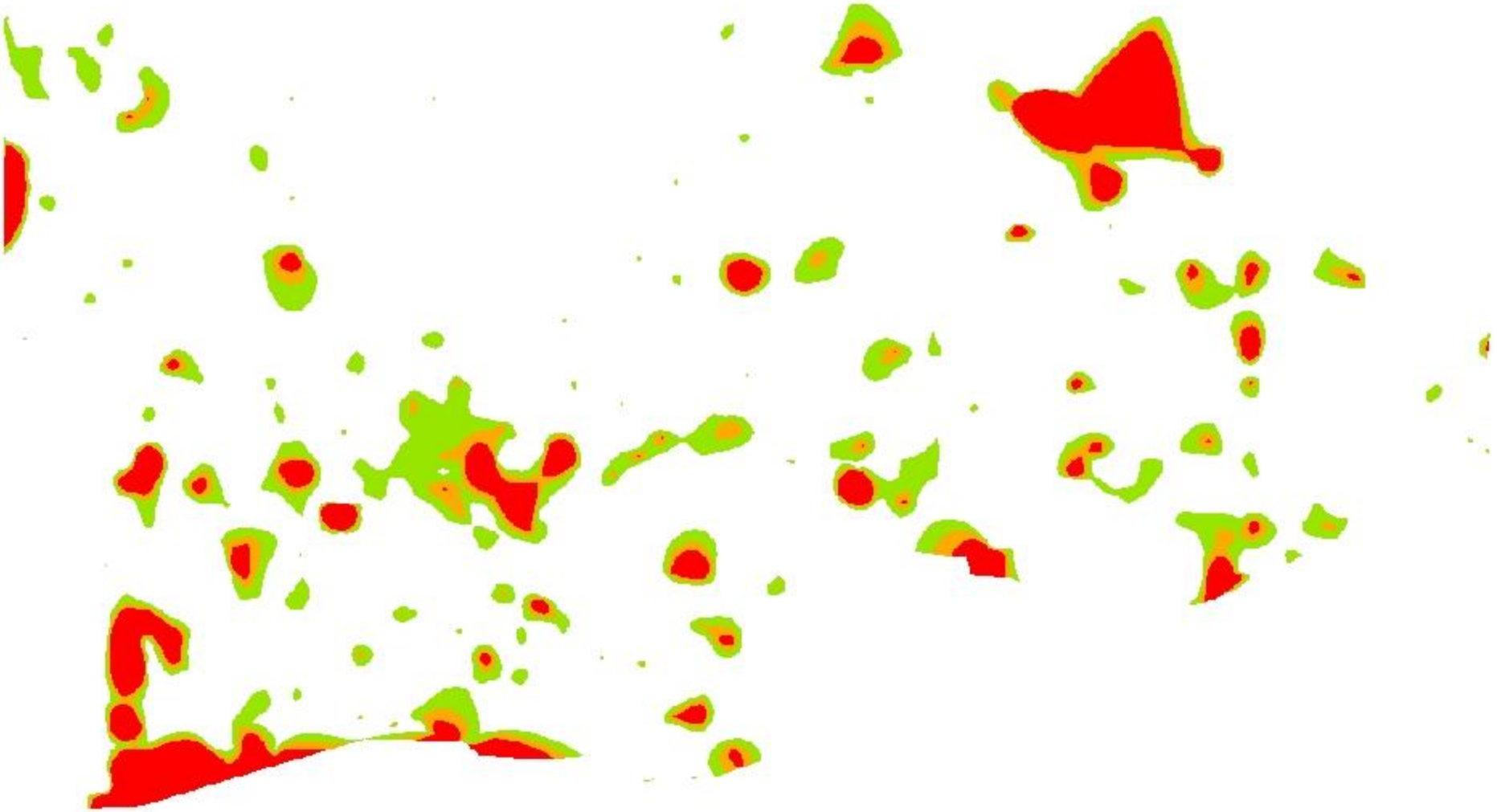

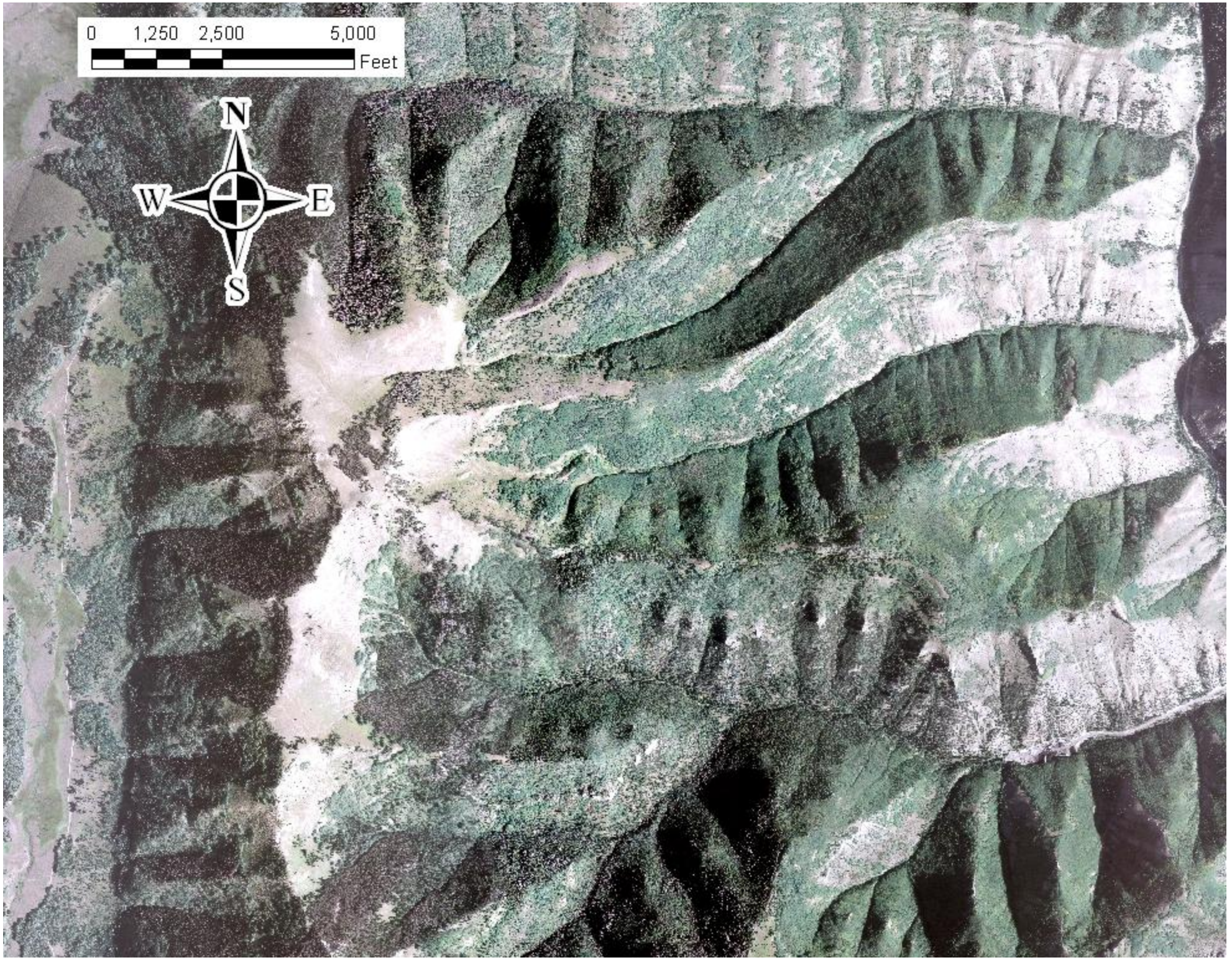
0 1,250 2,500 5,000
Feet
N
W
E
S

Figure A-3 Aberdeen Mine Transparency Plots: pp. 114-117

Survey Points

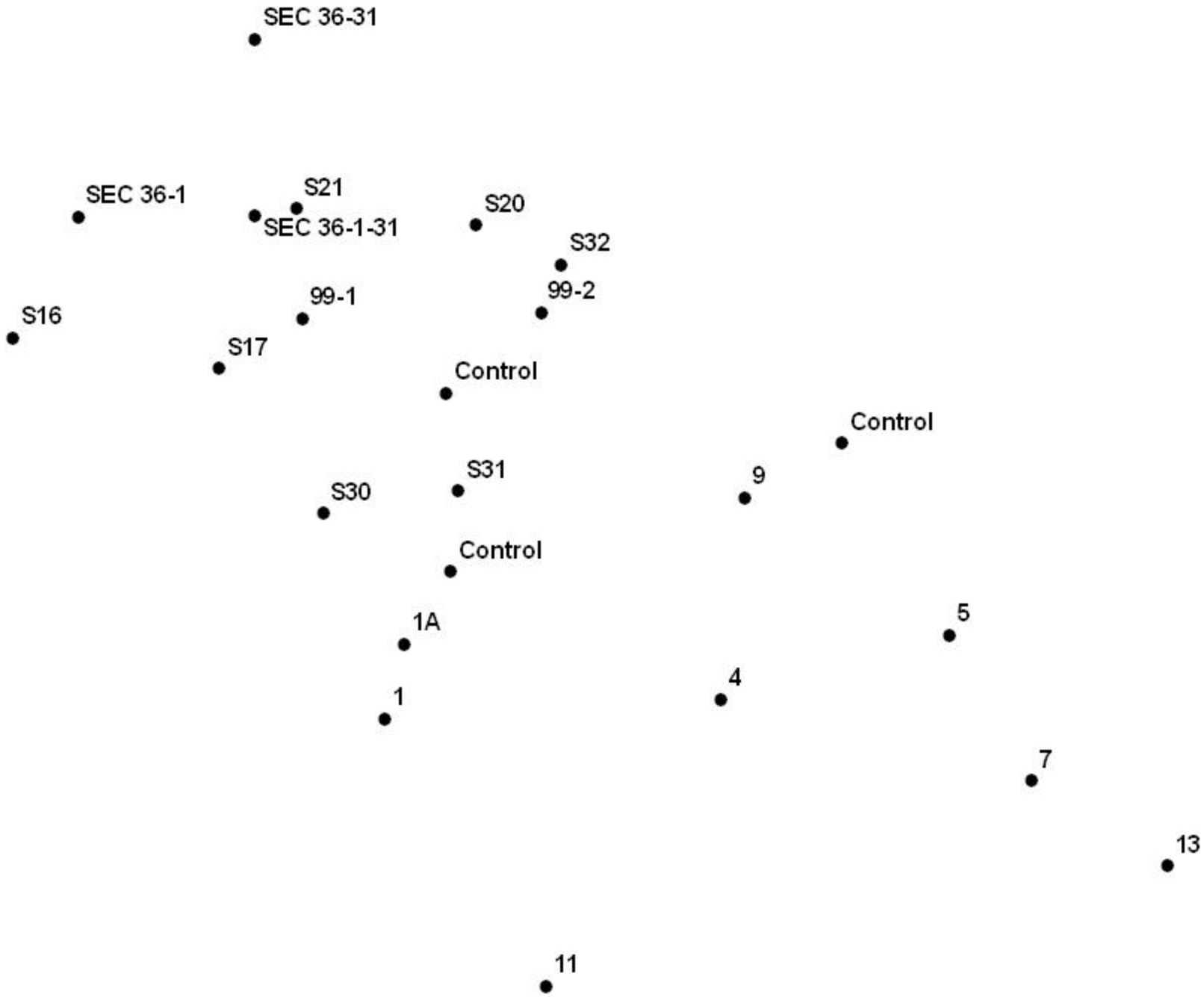

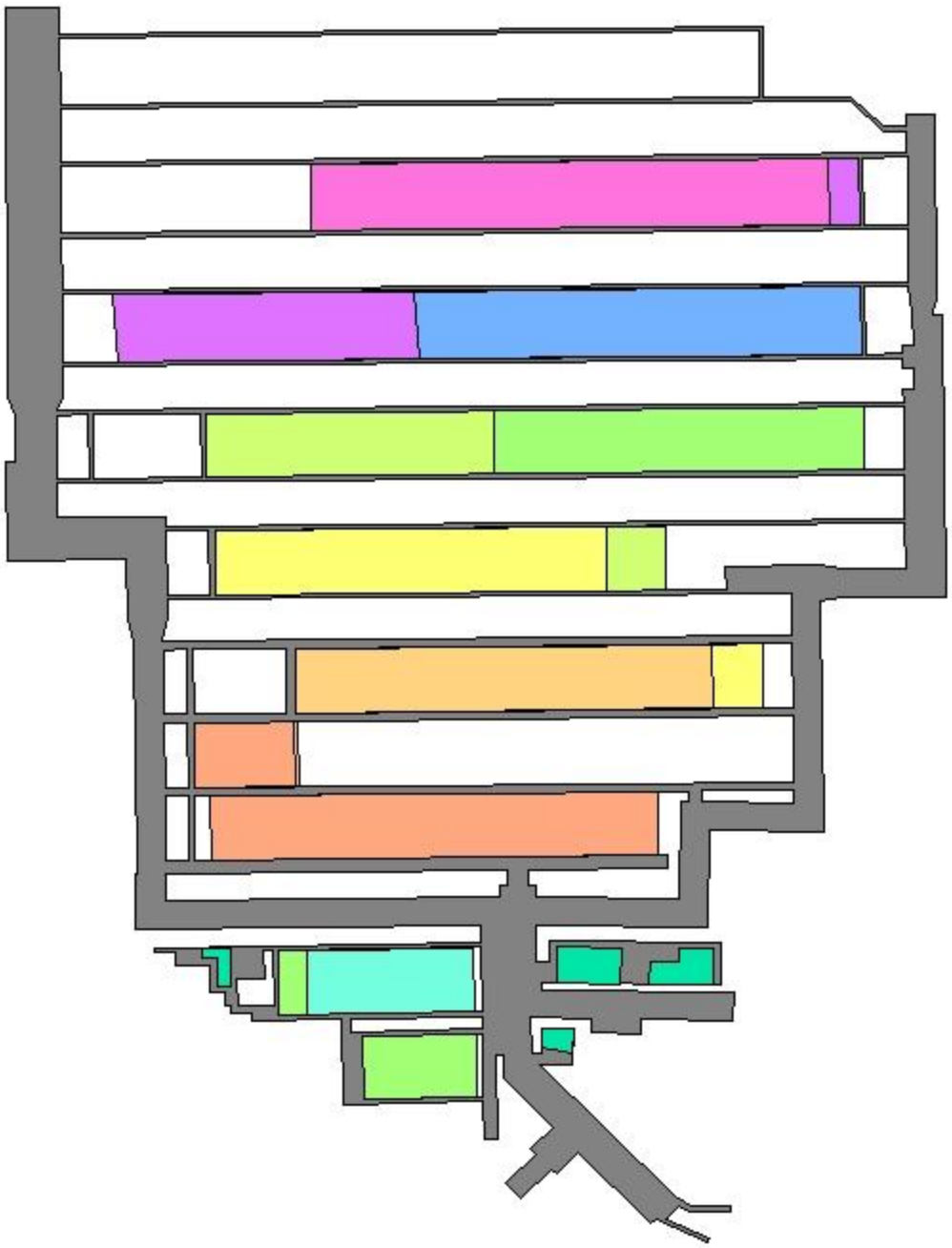

Mine Workings: Aberdeen Section 1996 to 2006

Entries

All Years

Pillar Ext

2001

Longwall Mining

1996
1997
1998
1999
2000
2001
2004
2005
2006

Mine Workings:
Pinnacle Section
1994 to 2006

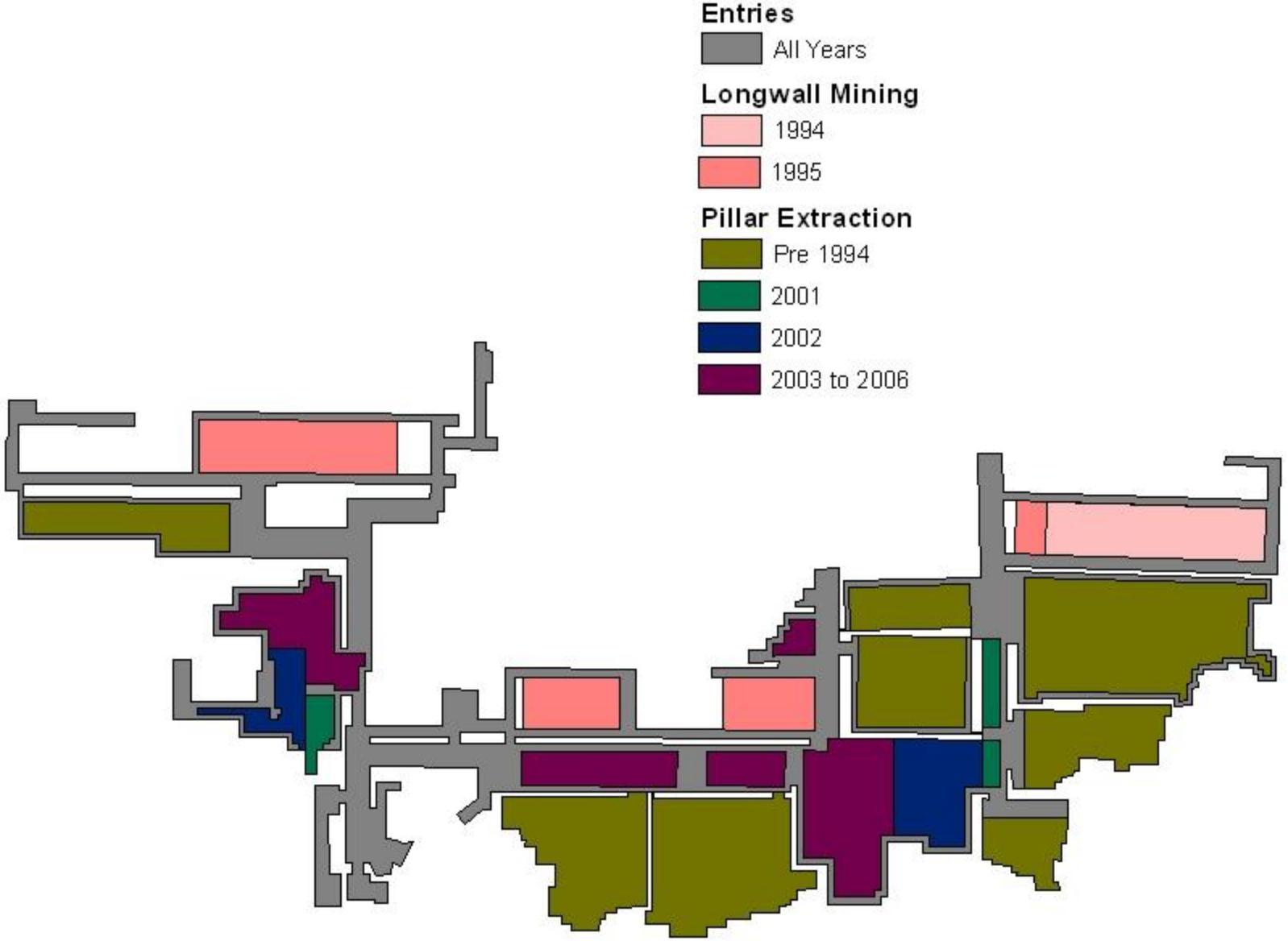

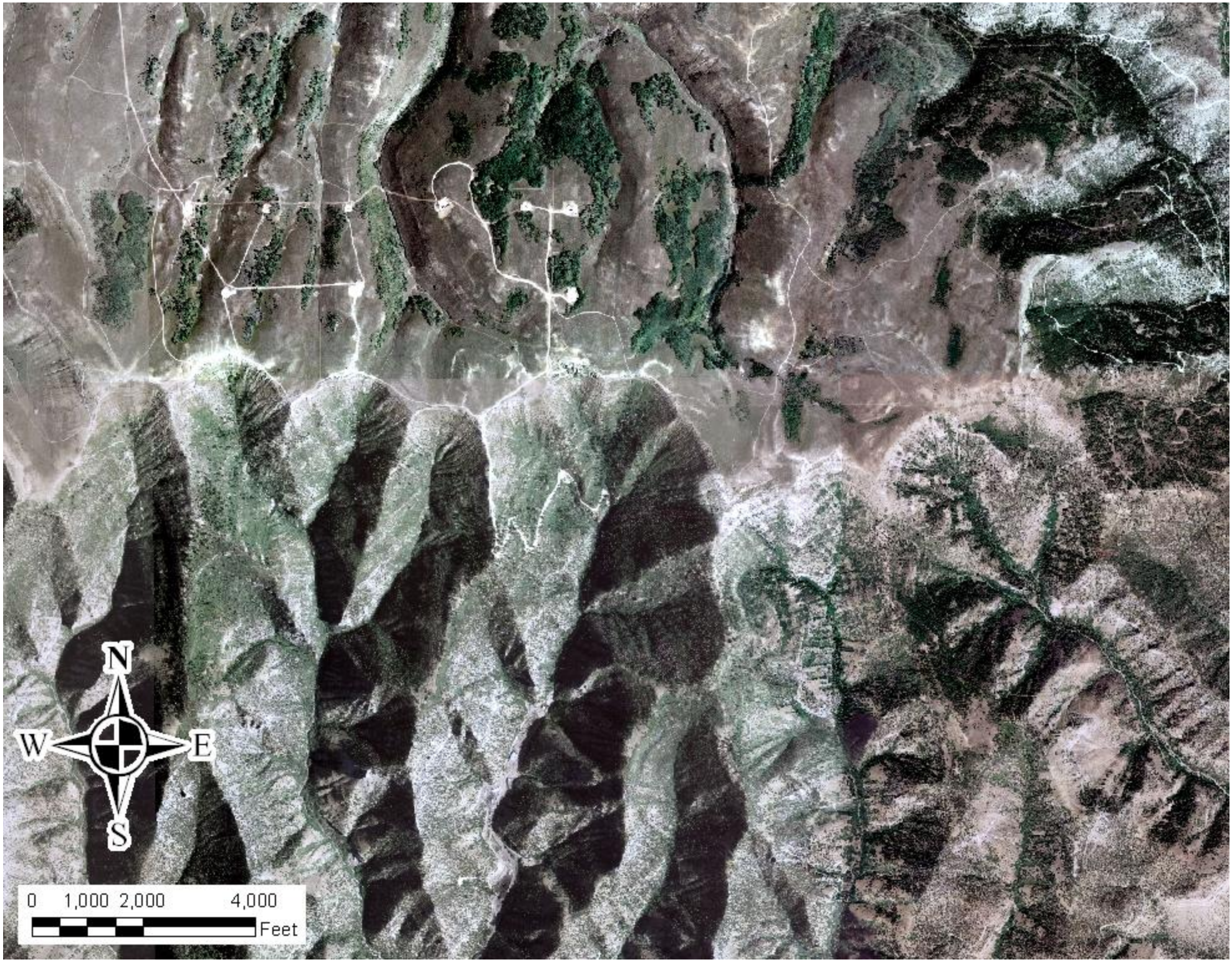
N
W
E
S
0 1,000 2,000 4,000
Feet